UNIVERSITY OF CALIFORNIA

Santa Barbara

DNA-stabilized fluorescent silver nanoclusters: A versatile nanomaterial for the specific detection of DNA

A dissertation submitted in partial satisfaction of the

requirements for the degree Doctor of Philosophy

in Mechanical Engineering

by

Jackson Travis Del Bonis-O'Donnell

Committee in charge:

Professor Sumita Pennathur, Chair

Professor Deborah K. Fygenson

Professor Kevin Plaxco

Professor Hyongsok (Tom) Soh

Professor Frédéric Gibou

March 2016

The dissertation of Jackson Travis Del Bonis-O'Donnell is approved.

_____
Deborah K. Fygenson

_____
Kevin Plaxco

_____
Hyongsok (Tom) Soh

_____
Frédéric Gibou

_____
Sumita Pennathur, Committee Chair

January 2016

DNA-Stabilized Fluorescent silver nanoclusters: A versatile nanomaterial for the specific detection of DNA

by

Jackson Travis Del Bonis-O'Donnell

ACKNOWLEDGEMENTS

I am grateful for the enormous support and guidance of my advisors, Prof. Sumita Pennathur and Prof. Deborah Fygenson. I would also like to thank the members of my doctoral committee; Prof. Elisabeth Gwinn, Dr. Danielle Schultz, Stacy Copp and Steven Swasey for their many helpful discussions; Daniel Vong, Ami Thakrar and Jeremy Wain Hirschberg for their contributions while working as undergraduate interns; David Bothman for his help keeping the lab running; the administrative and support staff of ME, ICB and CNSI; the many members, past and present, of the Nanolab at UCSB for keeping life interesting in and out of the lab; the Pacific Ocean; and the support of friends near and far. Finally, I would like to thank Daisy and my family for their endless love, encouragement and support.

VITA OF JACKSON TRAVIS DEL BONIS-O'DONNELL

December 2015

211 W Sola St Apt E, Santa Barbara, CA 93101
jtdo@engineering.ucsb.edu • (401) 864-2659

EDUCATION

2010-2016 **University of California Santa Barbara**
Ph.D. Mechanical Engineering, MEMS/Thermal Fluids, Winter 2016
Doctoral Advisors: Sumita Pennathur, Deborah K. Fygenson

2005-2009 **Brown University**
Sc.B. Physics-Mathematics, May 2009
Advisor: Derek Stein

RESEARCH

2011-2016
University of California Santa Barbara
Graduate Student Researcher
Pennathur and Fygenson Research Groups

- Synthesized and characterized DNA-templated fluorescent silver nanoclusters using microfluidics, capillary electrophoresis and fluorescence spectroscopy
- Developed novel ratiometric fluorescent probes using DNA-silver nanoclusters for specific detection of DNA and neurotransmitters
- Developed a microfluidic assay for the multiplexed detection of DNA using fluorescent silver nanocluster based probes
- Characterized the electrophoretic behavior of DNA molecules in microchannels, nanochannels and capillaries with different surface coatings in free-solution and sieving matrices

2014
California Institute of Technology
Visiting Researcher
Laboratory of Prof. Paul Rothemund, mentor Dr. Ashwin Gopinath

- Studied techniques for self-assembly and self-organization of DNA origami on surface functionalized substrates and characterization using fluid AFM

2012
Ludwig Maximillians University
Junior Nanotech Network Fellow
Center for NanoScience

- Studied techniques for characterizing biomolecules, including TEM of DNA origami and TIRF and FRET studies of tethered proteins

2009 – 2010
Brown University
Staff Research Assistant
Department of Physics

Molecular Biophysics Research Group (Prof. Derek Stein)
- Fabricated nanofluidic channels in fused silica using photolithography and wet etching
- Determined the effect of temperature on the transport and dynamics of confined DNA molecules in nanostructured fluidic channels using fluorescence microscopy
- Designed components for integrating temperature and pressure controls with nanofabricated chips using CAD software

2007 – 2009
Brown University
Undergraduate Research Assistant
Molecular Biophysics Research Group (Prof. Derek Stein)
- Performed and analyzed experiments involving DNA transport across an artificial nanotopography embedded in a nanofluidic channel culminating in first author publication
- Performed fluorescence microscopy experiments involving DNA and nanofluidic devices
- Wrote image analysis software using Matlab

AWARDS and HONORS

- Shark Tank Competition Finalist, 16th Annual UC Systemwide Bioengineering Symposium, 2015
- UCSB Graduate Division Dissertation Fellowship, 2015
- Runner up, UCSB Dept. of Mechanical Engineering "Grad Slam" Presentations, 2014
- Worster Summer Research Fellowship (mentor), Department of Physics, UCSB, 2014
- First Prize Poster, Microfluidics Division, APS Division of Fluid Dynamics, 2012
- UCSB Department of Mechanical Engineering Departmental Fellowship, 2012, 2013
- Honorable Mention, National Science Foundation Graduate Research Fellowship, 2011
- Publication selected for Best of 2009 Collection by the New Journal of Physics, 2009
- Mildred Widgoff Prize for Excellence in Thesis Preparation, 2009
- Brown University Undergraduate Teaching and Research Award, 2008

PUBLICATIONS

Peer Reviewed Journals:

1. **JT Del Bonis-O'Donnell**, S Pennathur, DK Fygenson. Changes in spectra and conformation of hairpin DNA-stabilized silver nanoclusters induced by stem sequence perturbations. *Langmuir.* DOI: 10.1021/acs.langmuir.5b03934. Published Online: December 21, 2015
2. **JT Del Bonis-O'Donnell**, DK Fygenson, S Pennathur. Fluorescent silver nanocluster DNA probes for multiplexed detection using microfluidic capillary electrophoresis. *The Analyst*, 140, 1609-1615, 2015
3. TM Wynne, C McCallum, **JT Del Bonis-O'Donnell**, P Crisalli, S Pennathur. Hybridization thermodynamics of DNA oligonucleotides during microchip capillary electrophoresis. *Analytical Chemistry*. 87, 2811-2818, 2015
4. A Russell, **JT Del Bonis-O'Donnell**, T Wynne, M Napoli, S Pennathur. Separation behavior of short single- and double- stranded DNA in 1 micron and 100 nm glass channels. *Electrophoresis*. 35, 412–418, February 2014

5. **JT Del Bonis-O'Donnell**, W Reisner, D Stein. Pressure-driven DNA Transport Across an Artificial Nanotopography. *New Journal of Physics*. 11**,** 075032 (2009) *****Selected for Best of 2009 Collection by the *New Journal of Physics*

In Preparation:

1. **JT Del Bonis-O'Donnell**, D Vong, S Pennathur, DK Fygenson. A universal design for a hairpin DNA probe providing ratiometric fluorescence detection by generation of silver nanoclusters
2. **JT Del Bonis-O'Donnell,** A Thakrar, J Wain Hirschberg, DK Fygenson, S Pennathur. DNA-stabilized silver nanoclusters for the specific detection of dopamine.
3. S Williams, P Crisalli, M Napoli, **JT Del Bonis-O'Donnell**, S Pennathur. Assessing stability, durability and protein adsorption behavior of hydrophilic silane coatings in glass microchannels.

Other Publications:

1. Co-author for ME104: Introduction to Mechatronics - Laboratory manual, UCSB, 2011
2. E Davies, L Bishop, A Lucio, JT Del Bonis-O'Donnell, S Pennathur, Y Fintschenko. *Lab-on-a-Chip Application: Field Amplified Sample Stacking (FASS) for Sample Concentration in a Nanochannel.* LabSmith Application Note. LabSmith, Inc. (2011)
3. E Davies, L Bishop, A Lucio, JT Del Bonis-O'Donnell, S Pennathur, Y Fintschenko. L*ab-On-a-Chip Application: Performing an Electrokinetic Gated Injection in a Nanochannel.* LabSmith Application Note. LabSmith, Inc. (2011)

PRESENTATIONS AND POSTERS

1. 16th Annual UC Systemwide Bioengineering Symposium, Shark Tank Competition Finalist Presentation, Santa Cruz, CA, June 2015
2. 16th Annual UC Systemwide Bioengineering Symposium, Poster, Santa Cruz, CA, June 2015
3. 2nd SoCal Microfluidics and Nanofluidics Symposium, Presentation, Pasadena, CA, June 2015
4. EMBS Micro and Nanotechnology in Medicine Conference, Poster Presentation, Oahu, HI, December 2014
5. Center for Bioengineering Happy Hour Seminar, University of California Santa Barbara, May 2014
6. NanoBioTech Montreux Conference, Poster Session, Montreux, Switzerland, November 2013
7. 17th International Conference on Miniaturized Systems for Chemistry and Life Sciences (MicroTAS), Poster Session, Freiburg, Germany, October 2013
8. American Physical Society 65th Annual Division of Fluid Dynamics Meeting, Poster Session, San Diego, CA November 2012
9. Center for Nanoscience (CeNS) - Ludwig Maximilians-Universität Workshop 2012, Poster Session, Venice, Italy, September 2012
10. University of Twente – BIOS/LabChip Group, Enschede, Netherlands, Septemeber 2012
11. Southern California Symposium on Flow Physics (6^{th}) Presentation, Santa Barbara, CA, April 2012

12. Junior Nanotech Network Wolfgang Hillen Summer School Symposium Presentation, Santa Barbara, CA, March 2012
13. Brown University Biophysics Journal Club Presentation, Providence, RI, November 2009, February 2010
14. University of Pennsylvania, Drndic Lab Presentation, Philadelphia, PA, October 2009
15. University of Gothenburg Department of Physics Seminar, Gothenburg, Sweden, June 2009
16. Brown University Prospective Science Students Tour Research Presentation, Providence, RI, Summer 2008, 2009
17. American Physical Society March Meeting Session W40: Single Molecule Biophysics, Pittsburgh, PA, March 2009
18. Brown University Department of Physics Annual Poster Session, Providence, RI, November 2008
19. Brown University Summer Research Symposium Poster Session, Providence, RI, August 2008

TEACHING/MENTORING EXPERIENCE

Teaching Assistant Experiences:
UCSB: ME104 (Mechatronics Lab), ME6 (Circuits Laboratory), ME105(x2) (Mechanical Engineering Laboratory), ME141A (Intro to Nanotechnology)
Reader/Grader: ME291A (Electricity and Magnetism), ME16 (Dynamics)
Assistant Lecturer: UCSB ME152B (Fluid Mechanics)
Mentoring:

- Jeremy Wain-Hirschberg, Ami Thakrar, Inst. for Collaborative Biotechnologies Undergraduate Research Apprenticeship Program (URAP), 2015
- Jack Kent Cooke Bridges Program for Engineering and Science Transfers, 2014
- John Devany, Worster Summer Research Fellowship, UCSB, 2014
- Matthieu Gadel, research experience for Masters student, ENSTA ParisTech, 2012
- Early Undergraduate Research and Knowledge Acquisition (EUREKA), 2011
- Adam Lucio, Research Internships in Science and Engineering (RISE), 2011
- Elizaveta Davies, Internships in Nanosystems Science, Engineering and Technology (INSET), 2011
- Research Experience for Teachers (RET) Summer 2009, 2010, 2011

PROFESSIONAL CONTRIBUTIONS

- Conference organizer, UCSB/UCLA Southern California Microfluidics Symposium, The Getty Villa, Los Angeles, CA. 2014
- Assisted reviews for *Electrophoresis*

ABSTRACT

DNA-Stabilized Fluorescent silver nanoclusters: A versatile nanomaterial for the specific detection of DNA

by

Jackson Travis Del Bonis-O'Donnell

DNA-templated silver nanoclusters (DNA-AgNCs) are fluorescent molecules containing few-atom clusters of silver stabilized by a short strand of DNA. They fluoresce at wavelengths in the visible spectrum with emission colors tuned by varying the sequence of the DNA used for their synthesis. The combination of their small size, tunable spectra and biocompatibility opens exciting, new possibilities for their use in chemical sensing, biological labeling and imaging, genetic mutation detection and the development of self-assembled DNA nanotechnologies.

A detailed understanding of the structure of DNA-AgNCs is vital for precisely engineering their properties for future applications. Specifically, changes in the arrangement and composition of bases surrounding a AgNC can strongly influence its fluorescence. Although this sensitivity has already been leveraged for the development of novel chemical sensors, a better understanding of the mechanism is needed to improve performance and broaden the applicability of DNA stabilized AgNCs. In this work, we use high-resolution microfluidic capillary electrophoresis to show that, although AgNC depend on single-

stranded DNA for their stabilization, changes made to bases in the double-stranded stem region of a DNA hairpin can perturb their structure, leading to differences in fluorescence emission.

We also explore ways in which AgNC can be robust to DNA sequence changes. We document one DNA-AgNC in which the DNA adopts different conformations, or shapes, that yield clusters with the same emission color. We also show that poly-thymidine regions, which are know to bind silver poorly,can act as convenient handles to adjust the electrophoretic mobility of DNA-AgNCs without affecting their fluorescence.

Using poly-thymidine appendages, we demonstrate a way to tune the electrophoretic mobility of a AgNC-based DNA probe for use in a microfluidic assay. These label-free probes are composed of a DNA hairpin that generates a fluorescent silver nanocluster only after binding to a specific target DNA sequence. By tuning the mobility of probes designed to bind different targets, we demonstrate a rapid microfluidic separation assay for the multiplexed fluorescent detection of nucleic acid targets for Hepatitis A, B and C.

The probe design initially used for these studies suffered from several shortcomings. Most significantly, the probe DNA failed to generate a fluorescent AgNC for some binding domain sequences. To overcome this, as well as provide added functionality, we engineer a new DNA-AgNC based sensor that supports ratiometric fluorescence measurements for the sensitive, specific and low-cost detection of DNA. Probes based on our new design generate a green emitting AgNC in its hairpin state, and a red emitting AgNC after binding their target. The ratiometric fluorescence provides a stable signal and rapid quantification of DNA concentration regardless of the choice of target, a dramatic improvement over similar turn-on fluorescent probes.

TABLE OF CONTENTS

Chapter 1

Introduction

For millennia, civilizations have recognized the beauty and value of noble metals through their use in jewelry and currency. In the last century, however, scientists' attention has shifted away from their metallurgic properties and towards their unique electronic and optical properties. In particular, small particles and clusters of noble metal atoms exhibit properties that differ from both individual atoms and bulk metals.[1,2] As the characteristic size of a noble metal nanoparticle, either spherical or rod-like, approaches the electron mean free path length (~50 nm) of their conduction electrons, interactions with particular wavelengths of light cause collective oscillations of the electrons.[3] Light scattered by these particles in solution gives them a brilliant color. However, once the particle size falls below a nanometer, or the Fermi wavelength of an electron, these nanoclusters adopt more molecule-like properties, including discrete energy states that give rise to strong fluorescence.[1] Noble metal nanoclusters were initially limited in that they could only be realized by stabilization through isolation within a low temperature noble gas matrix.[4–6] More recently, researchers have discovered ways of stabilizing highly fluorescent noble metal clusters in a solution phase, such as water, using a variety of encapsulating ligands,[1,7–9] paving the way towards their use in new applications.[10,11]

Of the different stabilizing ligands employed, single-stranded DNA oligos have attracted enormous attention for their ability to stabilize silver nanoclusters[12] with tunable properties[13] while maintaining the inherent capacity for highly specific molecular binding. The four canonical nucleobases (cysteine, guanine, adenine and thymine) bind according to Watson-

Crick base pairing (C-G, A-T) to provide one of the most specific binding modalities found in nature.[14] In addition to this well known binding behavior, the bases have a high affinity for Ag^+ with relative strengths: C>G>A>T,[15] meaning the bases drive coordination, rather than the negatively charged phosphate backbone of the DNA. This permits the surprisingly facile synthesis of few-atom silver nanoclusters in aqueous solutions. Synthetic DNA oligos ranging from 10-60 bases, typically rich in C's and G's, complex with Ag^+ ions after the introduction of $AgNO_3$. A mild reducing agent, $NaBH_4$ in a basic solution, is then added to the DNA-Ag^+ solution, chemically reducing a portion of the Ag^+ ions into elemental silver, Ag^0, producing a fluorescent silver nanocluster with a composition ranging from 10-20 atoms[16] with a rod-like structure.[17] These clusters can have exceptional optical properties such as high fluorescence quantum yields and photostability, low toxicity and synthesis cost, and excitation and emission spectra that can be tuned across the visible and near-infrared spectrum, making them viable alternatives to typical organic fluorophore dyes that are ubiquitous throughout the biological and medical sciences.[18] The many desirable properties of DNA- stabilized silver nanoclusters (DNA-AgNCs) are highly dependent on the sequence of the DNA used in their synthesis.[19] However, the relationship between the DNA sequence and the resulting AgNC is currently not well understood. Although recent work combining wellplate-level throughput with machine-learning algorithms shows promise towards more intelligently generating AgNC template sequences,[20] higher throughput techniques capable of handling larger libraries will ultimately be necessary to eliminate the guesswork. This will most likely be possible in the near future by adapting infrastructure from next-generation sequencing technologies and methodologies as well as techniques using high-throughput flow cytometry.

Despite unanswered questions regarding the details of cluster formation, the number of applications involving DNA-AgNCs have exponentially increased during the past five years. For example, bright and stable AgNCs have been used as specific labels to stain cells for a variety microscopy techniques,[21,22] and many applications have taken advantage of the inherent sensitivity of some clusters to their environment in order to create novel sensors. Specifically, small perturbations to the composition or arrangement of nearby bases can lead to dramatic changes in emission color and/or intensity.[23] Using this, DNA-AgNCs base sensors have been used to detect various ions,[24–26] proteins[27–29], microRNA,[30,31] and DNA.[23] The ability to combine a specific recognition sequence with a cluster forming sequence in a single strand provides a platform to create chemically simple sensors to detect specific DNA sequences,[32–35] as well as detect DNA mutations such as single base polymorphisms (SNPs),[36,37] which is potentially relevant for use in diagnostic assays.

Providing a better fundamental understanding of DNA-AgNC behavior and using AgNCs to develop novel probes for DNA detection forms the central focus of this dissertation. These investigations and results are presented as separate studies, divided here into chapters. In Chapter 2, we describe how the properties of AgNCs stabilized using hairpin DNA sequences change as we alter bases contained within the stem region. It is well known that even small perturbations of the DNA sequence can drastically and unpredictably disrupt or alter the fluorescence of DNA-stabilized silver nanoclusters. Understanding how the structure of the DNA affects the nanocluster it stabilizes is the key to rationalizing such effects. We approach this challenge by strategically modifying the stem sequence of a hairpin DNA that hosts a spectrally pure, red-emitting nanocluster. Most of our modifications (in base-composition, sequence orientation and loop location) reduce AgNC fluorescence in purity and shift it in

wavelength, but one modification (appending poly- thymidine to the 3' end of the stem) is inert with respect to fluorescence. Microfluidic capillary electrophoresis reveals that all the modifications induce conformational changes of the DNA and that the original, spectrally pure, nanocluster exists in two, structurally distinct conformations. Interestingly, appending five or more thymidine, despite having no effect on fluorescence, eliminates this structural degeneracy. To explain this result, we propose that the original spectrally pure cluster is stabilized by a pair of hairpins whose stems can arrange in either a *cis* or *trans* orientation. Finally, we quantify the extent to which thymidine appendages of different lengths can be used to fine-tune electrophoretic mobility of DNA-AgNC,

Chapter 3 describes the development of a microfluidic assay that uses the poly-thymidine appendages discussed in Chapter 2 with a novel AgNC-based DNA probe. By incorporating both target-binding and fluorescent-reporting sequences into a single synthetic DNA oligomer, this AgNC DNA probe eliminates the need to conjugate dye or quencher molecules. In this study, we modify a AgNC DNA probe to demonstrate single-color multiplexed detection of DNA targets. We show that appending different lengths of poly-dT to the probe sequences tunes the electrophoretic mobility of AgNC DNA probes without affecting their fluorescence spectra. We use this to introduce a set of AgNC DNA probes selective for Hepatitis A, B and C target sequences that can be processed together in a simple, single-step protocol and distinguished with a resolution of 3.47 and signal to noise ratio of 17.23 in under 10 seconds by microfluidic capillary electrophoresis.

In using the AgNC generating hairpin probes described in Chapter 3, we discovered several shortcomings of their design, including sensitivity of their fluorescence to choice of target DNA sequences and the difficulty in quantifying fluorescence of the turn-on probe.

Specifically, after binding target DNA, an AgNC-hairpin probe undergoes a conformational change that allows for the formation of an AgNC. However, as originally designed, these AgNC-hairpin probes are sensitive to the bases contained within the target binding loop, drastically limiting their utility. Because the formation and fluorescence of AgNCs are highly sensitive to the local DNA environment, adapting an AgNC-hairpin probe to an arbitrary target sequence is not trivial. We address these problems in Chapter 4, where we design a new hairpin based probe that provides a two-color ratiometric signal by generating a green emitting AgNC in its hairpin state, and a red emitting AgNC after binding target. By separating and lengthening the AgNC-stabilizing domain, we create an AgNC-hairpin probe with consistent performance for arbitrary target sequence. The new design supports ratiometric fluorescence measurements of DNA target concentration, providing a more sensitive and stable signal compared to turn-on fluorescent probes. In addition to being robust to target sequence and synthesis conditions, the redesigned probe has nM sensitivity and singe-nucleotide specificity, expanding the breadth of applicability of AgNC-hairpin probes for biomolecular detection.

Lastly, preliminary results and future directions are presented in Chapter 5. Preliminary results show that DNA-AgNCs can be employed for the specific and sensitive fluorescent detection of dopamine, an important neurotransmitter with important roles in brain function and neurodegenerative diseases. Additionally, preliminary work is presented towards understanding the relationship between sequence motifs and the structure of DNA as it relates to AgNC formation. Results show that perturbations made to sub-sequence motifs contained within a stable AgNC sequence can affect cluster fluorescence and potentially conformation, suggesting that cluster formation is dependent on secondary structures formed

through Ag+ mediated, non-Watson Crick basepairing. This preliminary work is followed by a discussion of potential future directions and projects inspired by this work and the current DNA-AgNC field.

Chapter 2

Changes in spectra and conformation of hairpin DNA-stabilized silver nanoclusters induced by stem sequence perturbations

Background

Ligand-stabilized noble metal nanoclusters are a new class of fluorophore that exhibit favorable optical properties rivaling those of organic dyes.[1,38–40] Of particular interest are few-atom silver nanoclusters stabilized by single stranded DNA oligomers, which have optical properties that can be tuned by the sequence of its nucleobases. In the decade since their invention,[12] an extensive palette of water soluble silver clusters with emission spectra ranging from the near-UV to the infrared have been synthesized using short DNA molecules as scaffolds.[13,41] The ease with which DNA molecules are designed and manufactured has enabled a growing number of applications for DNA-stabilized silver nanoclusters (DNA-AgNC) in biological labeling,[21] chemical sensing,[35,42] and genetic and molecular analysis.[30,32,37] However, engineering DNA-AgNCs for particular applications is haphazard and challenging due to the lack of fundamental understanding of how DNA sequence influences silver cluster formation and fluorescence.

Recent studies characterizing DNA-AgNCs using high performance liquid chromatography (HPLC) and mass spectrometry (MS) revealed the Ag^0 and Ag^+ composition of several clusters[16,43] and their chiral, rod-like structures encapsulated by the DNA scaffold.[17] Very little is known, however, about the structure of the scaffold. MS shows that

short, single-stranded DNA (ssDNA) oligomers often dimerize to template AgNC.[16] Circular dichroism spectroscopy (CD) suggests that specific DNA secondary structures such as i-motifs and G-quadruplexes are especially compatible with AgNC formation.[44–47] In general, however, DNA structure prediction in the presence of Ag ions and atoms, which are known to stabilize non-Watson-Crick base pairing,[48,49] is beyond the ken of current models. Studies that elucidate the structure of the DNA scaffold in DNA-AgNCs are needed if we are to eventually rationally harness the ability of small changes in DNA sequence to dramatically alter AgNC fluorescence[13].

In this study, we focused on a spectrally pure, red-emitting AgNC that forms in the presence of a DNA sequence whose secondary structure (in the absence of silver) is a hairpin with a 12-deoxycytidine (12-dC) loop and a 10 base pair (bp) stem. Previous studies have investigated hairpins with different sized poly-dC loops.[50,51] Here we maintain a constant loop and stem size to determine the effect of altering stem sequence on cluster fluorescence and conformation. We used fluorescence spectroscopy and microfluidic capillary electrophoresis (MCE) to study the spectral and conformational effects of perturbing the stem sequence. Despite the established inertness of double-stranded DNA for fluorescent AgNC formation,[19] we find these perturbations capable of altering the fluorescence of the AgNCs as well as the conformation of the DNA surrounding it. Only one perturbation, appending poly-deoxythymidine (poly-dT) to the hairpin stem, had no effect on fluorescence emission. It did, however, systematically alter the electrophoretic mobility. We quantify the utility of such poly-dT tails for fine-tuning electrophoretic mobility and leverage them to interpret the surprising observation of structurally distinct species in our original, spectrally pure, DNA-AgNC synthesis.

Materials and Methods

DNA AgNC Synthesis

DNA oligos were obtained from Integrated DNA Technologies Ltd. with standard desalting in lyophilized form without further purification and resuspended in Millipore deionized water to 500 μM and stored at -20° C until ready for use. DNA stock concentrations were measured from absorbance at 260nm using a NanoDrop ND1000 Spectrophotometer. Sodium acetate trihydrate and glacial acetic acid were purchased from Fisher Scientific. Silver nitrate (>99%) and sodium borohydride (99.99%, pellets) were purchased from Sigma Aldrich. 100 mM sodium acetate stock solution was prepared by titrating sodium acetate solution with glacial acetic acid until a pH of 4.8 was obtained. For cluster synthesis, 25 μL of 100 μM DNA oligo in water was heated to 90° C for 2 minutes then quenched in ice water to ensure hairpin formation. To determine the effect of annealing rate, we used an alternate annealing process in which the strands were slowly cooled over the course of several hours. The DNA was then combined with 50 μL of 20 mM sodium acetate buffer and 12.5 μL of 1.6 mM silver nitrate solution. After 20 minutes of incubation at room temperature in the dark, the solution was reduced by adding 12.5 μL of 0.8 mM freshly prepared sodium borohydride solution. Onset of red fluorescence was observed less than 10 minutes after reduction. Final concentrations were 25 μM DNA, 10 mM sodium acetate buffer, 200 μM silver nitrate and 100 μM sodium borohydride for a DNA:Ag^{+}:BH_4 ratio of 1:8:4. Microchip CE was performed on samples between 2 and 6 hours after synthesis.

Fluorescence, Absorbance and Circular Dichroism Spectroscopy

Absorbance and fluorescence measurements were performed on 30 μL of undiluted samples in a Corning Flat Bottom black Polystyrol 384 well plate using a Tecan infinite 200Pro. Emission spectra for clusters were obtained each hour for 5 hours after reduction and after 24 hours using 260 nm excitation and scanning the emissions. Peak excitation was determined by scanning excitation wavelengths while detecting at peak emission.

CD spectra of undiluted DNA and DNA AgNC nanocluster samples were obtained at ambient temperatures using an OLIS DSM 1000 CD spectrometer (Olis On-Line Instrument Systems, Inc.), using a 1 mm path length cuvette with an integration time of 1 s, and 75 points between 188 and 320 nm. Spectra were averaged over 3 scans and further smoothed using a Savitzky-Golay filter with a frame size of 7 and polynomial order 3.

Microfluidic Capillary Zone Electrophoresis

Custom microchannels were obtained from Dolomite Ltd (UK) and were fabricated using standard lithography techniques in borosilicate wafers and then fusion bonded to a 160 μm thick wafer. The channels were 20 μm deep by 50 μm wide with a separation channel length of 30 mm. The microfluidic chip was interfaced with an inverted microscope (Olympus IX71) using a custom machined PEEK chuck and nitrile o-rings. Voltage sequences were applied and current was recorded using a Labsmith HVS448 6000D-LC sequencer and accompanying software attached to platinum wire inserted into the reservoirs of the fluidic chuck. Fluorescence images were obtained using a LUCPlanFLN 20x/0.45NA long working distance objective (Olympus) and an Andor iXon+ back illuminted EMCCD camera with a

focused, 100 W mercury arc lamp (OSRAM HBO). The microscope (excluding Hg lamp) and camera were enclosed within a black posterboard darkbox to minimize stray light and allow high gain settings on the camera.

The electrokinetic injection and separation protocol used is described elsewhere in detail[52,53] and briefly as follows: The microchannels were filled with DI water by capillary forces and then flushed by applying voltage for 5-10 minutes for each solution in the sequence: DI, 100 mM NaOH, DI, 100 mM HCl, DI, running buffer. Running buffer solution was 10 mM sodium acetate at pH 4.8 with 1% (w/w) of polyvinylpyrrolidone (PVP) (avg. Mw= 1.3 MDa, Sigma Aldrich), which suppressed electroosmotic flow and also served as a sieving matrix[54]. Voltage schemes were modified after addition of the running buffer to account for electroosmotic flow suppression. The electric field strength for separations was calculated to be 78.8 kV/m assuming uniform channel cross section and resistance[55]. The separation channel was flushed with running buffer for at least 1 min between separations. Immediately prior to injection, sample solution containing unpurified nanoclusters was diluted with concentrated sodium acetate and PVP solution to a final buffer concentration equal to that of the running buffer with DNA concentrations ranging from 1-5 μM.

Results and Discussion

We created a family of fluorescent DNA-stabilized silver nanoclusters (DNA-AgNC) based on a hairpin DNA sequence containing a 12 base long poly-deoxycytidine (12-dC) loop and a 10 base pair (bp) stem (Figure 1), herein referred to as 12C-hp10. We chose this particular hairpin because of the bright emission and narrow spectrum of the AgNC it stabilizes. We limited our modifications to the stem sequence on the hypothesis that, being double-stranded, the stem might not interact directly with the silver[19] but would instead gently influence the loop's conformation. To check the role of sequence and orientation of stem bases on cluster formation, one variant (RevMod) reversed the 5' to 3' orientation of the sequence and substituted AT for CG in the center of a 3xCG group, disrupting a common motif in AgNC sequences.[20] To probe the effect of stem stability on cluster formation, another variant (ATrich) substituted AT for CG at multiple locations, decreasing the GC content from 70% to 40%. To decrease stability without altering base composition, a third variant (Bub10) placed the cytosine loop in the middle of the stem sequence. Finally, to determine whether thymidine, which interacts only weakly with silver ions,[56] affects cluster fluorescence, we appended different length poly-dT segments to the 3' end of the stem.

AgNCs were synthesized on the various DNA scaffolds by addition of silver nitrate and reduction with sodium borohydride (see Methods). Although Bub10 produced an exceptionally bright and stable cluster in ammonium acetate buffer at neutral pH (see SI), synthesis in a low pH environment (sodium acetate, pH 4.8) generally resulted in brighter fluorescence and shorter formation times (minutes) than synthesis in neutral or alkali buffers, so the low pH condition was used in all cases.

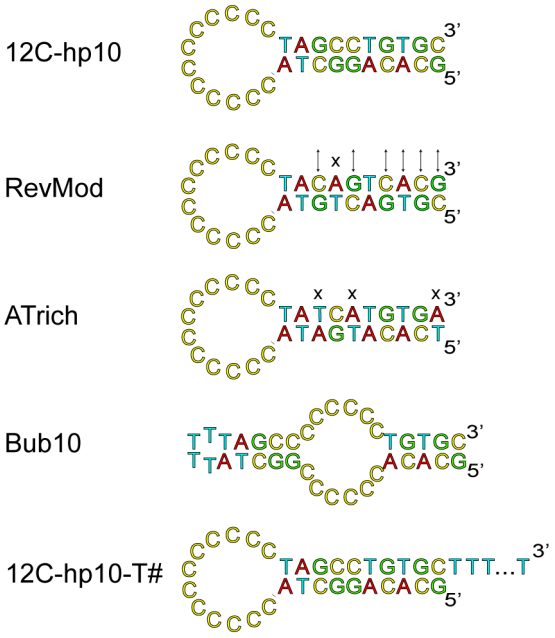

Figure 2-1 Sequence and secondary structure of the DNA strands used to template fluorescent silver nanoclusters. The original hairpin DNA (12C-hp10) consisted of a 12 dC loop with a 10 bp stem. The stem sequence was modified to produce variants that changed the stem composition, stability and size. Arrows indicate where the base pairs were flipped in orientation; 'x' indicates where a CG base pair was swapped for an AT pair.

All sequences produced AgNC with bright red fluorescence that could be excited by visible light with a characteristically large (>60 nm) Stoke's shift, as well as by 260 nm ultraviolet (UV) light (Figure 2), a universal property of DNA-AgNCs.[57] Spectra of the poly-dT variants were identical to the original, 12C-hp10 spectra (Figure 2b). Spectra of the other stem variants (Figure 2a) had a dominant emission peak near the 12C-hp10 peak and evidence of at least one other, secondary peak. Dominant peaks of ATrich and RevMod were blue-shifted relative to 12C-hp10, while the dominant peak of Bub10 was red-shifted and significantly broadened. The secondary emission peak ATrich and Bub10 were nearly identical and in the green. The RevMod spectra shows a small shoulder in the near infrared,

indicating the possible presence of an additional cluster, though it was not resolved. Peak excitation and emission wavelengths are presented in Table 1.

Peak intensity also varied among AgNCs produced by the different strands (Appendix II, Figure 1, Table 1). Relative to the original 12C-hp10, each variant exhibited lower peak emission intensity and lower total integrated intensity. Peak intensities of green species, when present, were significantly lower than red species in all cases. The Bub10 and 12C-hp10-T# produced clusters that were closest in total intensity (87% and 82%) to the original 12C-hp10 sample, while the those that contained stem mutations (RevMod, ATrich) were less than 40%.

Table 2-1 Excitation and emission maxima and relative intensity of UV-excited fluorescence from AgNC generated using poly-dC hairpin stem variants.

Sequence	*Excitation Max (nm)*	*Emission Max (nm)*	*Relative Peak Intensity (a.u.)*	*Relative Integrated Intensity*
12C-hp10	577	655	1	1
12C-hp10-T#	577	655	0.82*	-
RevMod(a)	571	637	0.38	0.38
RevMod(b)	*not resolved*	*not resolved*	-	
ATrich (a)	550	621	0.44	0.40
ATrich (b)	450	530	0.16	
Bub10 (a1)	578	665	0.36	0.87
Bub10 (a2)	600	678	0.36	
Bub10 (b)	453	534	0.18	

*averaged over all poly-dT species

High-resolution excitation and emission scans of 12C-hp10 contain a single emission peak (Figure 2c). This peak is similar in breadth (90 nm FWHM) and shape to that of a verified pure and similarly red-emitting DNA-AgNC,[16] suggesting that 12C-hp10 stabilizes

only a single AgNC emitter. By contrast, high-resolution scans of the red-shifted and broadened dominant Bub10 fluorescence, reveal two distinct peaks (Figure 2d).

To determine whether the shifts in dominant peak fluorescence were accompanied by changes in the conformation of the DNA scaffold, we performed high-resolution microfluidic capillary electrophoresis (MCE) using fluorescence detection tuned to the dominant peak.[53,58] Secondary species, dark species and free DNA were thus effectively excluded from analysis. During MCE, analytes move under an applied electric field in an electrolyte solution. The velocity of each analyte is governed by the ratio of its hydrodynamic drag to its electric charge, resulting in a separation.[58] DNA strands with significant secondary structure present a non-uniform charge density that is tightly coupled to their structure. As a result, subtle structural changes can lead to measurable changes in electrophoretic mobility and the overall shape of the electrophoretic profile.[52,59 60,61]

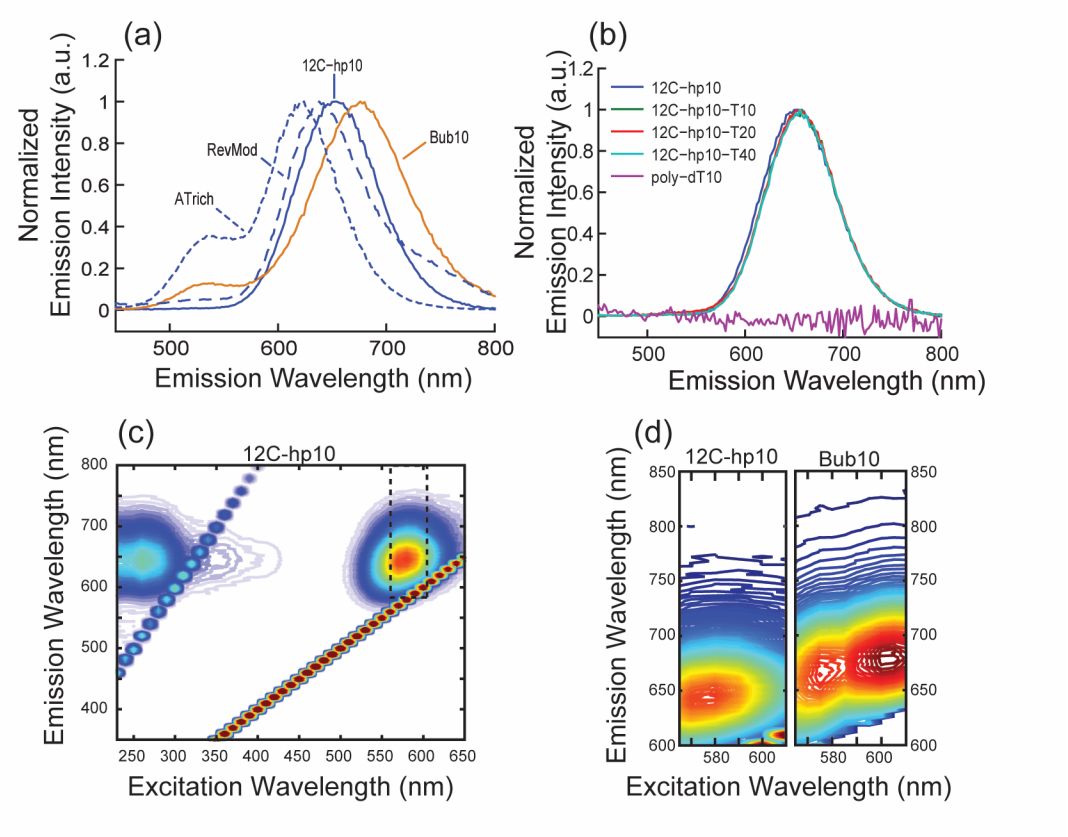

Figure 2-2 Fluorescence spectra produced by the original DNA hairpin and three variants upon reduction with $NaBH_4$ in the presence of silver ions in 10 mM sodium acetate (pH 4.8). (a) Normalized fluorescence emission under 260 nm illumination of DNA-AgNCs formed from DNA strands containing modified versions of the 12C-hp10 stem. Base pair substitutions and base pair reorientation both caused shifts in peak emission and secondary peaks. (b) Fluorescence emission of 12C-hp10 clusters with poly-dT appendages were spectrally identical. (c) Two-dimensional excitation and emission scan of the fluorescence produced by 12C-hp10 shows a single emitter that can be excited by either visible or UV light. (d) A high-resolution comparison of the dominant red fluorescence shows that Bub10 produces two distinct emission peaks while 12C-hp10 produces only one.

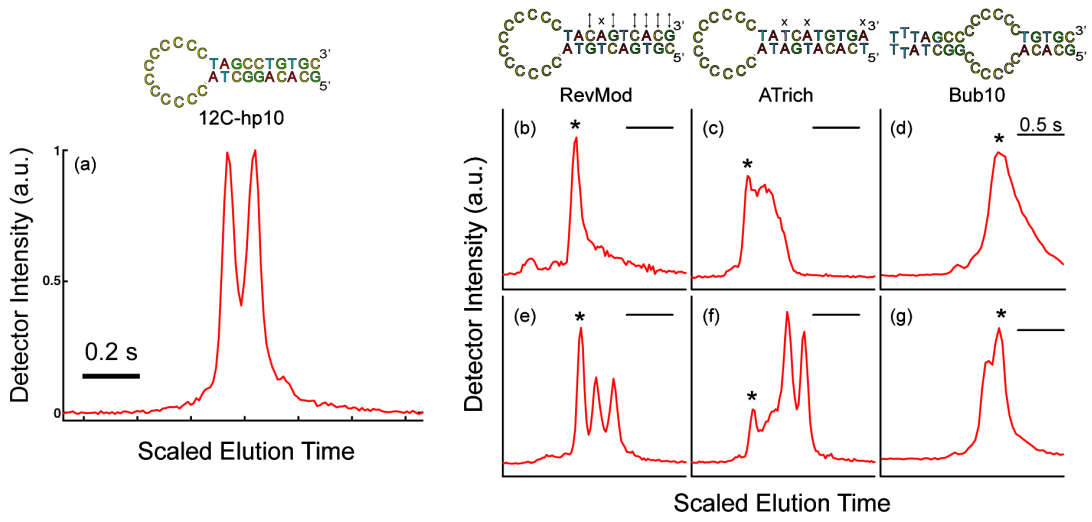

Figure 2-3 Electrophoretic separation profiles of 12C-hp10 AgNC and its stem-sequence variants collected in a 20 µm deep microchannel detecting red-emitting clusters 20 mm from the injection point. (a) 12C-hp10 produced twin elution peaks indicating the presence of two structurally distinct DNA-AgNCs. (b) RevMod produced a single, narrow peak that (e) eluted faster than the 12C-hp10 doublet. (c) ATrich produced a broad, composite peak that (f) also eluted faster than the 12C-hp10 doublet. (d) Bub10 also produced a broad, possibly composite peak, but its elution time was midway between the doublet peaks (g). An asterisk (*) labels the peak mobility produced by each variant. Fluorescence intensities were rescaled to highlight details of each separation profile.

The various DNA sequences produced AgNCs with distinct separation profiles (Figures 3 & 4). Surprisingly, the original, spectrally homogenous emitter, 12C-hp10, produced a pair of elution peaks, indicating the presence of two distinct species (Figure 3a). Of all the variants, only 12C-hp10-T5 also produced AgNCs with such a clear dimorphism (Figure 4b).

Figures 3b-d show MCE separations of the variants with stem-sequence modifications individually, while Figures 3e-g show them mixed to equivalent DNA concentrations with 12C-hp10 to reveal the relative shift in mobility. The blue-shifted emitters that formed on RevMod and ATrich had greater mobility (shorter elution times) than 12C-hp10, while the

red-shifted emitters that formed on Bub10 had a mobility in between that of the two 12C-hp10 species.

Variants with poly-dT appendages, by contrast, all had lower mobility (longer elution times) than 12C-hp10 (Figure 4). To clarify the relative mobilities, Figure 4a shows an electropherogram of a mixture of the DNA AgNC with zero, 10-, 20- and 40-dT while Figure 4b juxtaposes those with 5-, 10-, 20- and 40-dT. It is evident that increasing the length of poly-dT systematically decreases the electrophoretic mobility of the DNA-AgNCs, consistent with expectations that, given its inertness with respect to cluster fluorescence, the appendage adopts a random coil conformation and increases the hydrodynamic drag on each cluster.

Electrophoretic mobility of the slower of the two 12C-hp10 species was $-3.5\pm0.1\times10^{-8}$ $m^2/V\bullet s$, as calculated from the elution time, t, detection distance, d, and electric field strength, E, according to $\mu_{emitter}=d/tE$ and averaged over a dozen separations run on several different days and on samples from several different syntheses. The primary peak for the Bub10 samples was intermediate to the two 12C-hp10 peaks and was approximated as half the difference between the two. A plot of mobility, normalized to the slower of the two 12C-hp10 species, versus the number of thymidine appended shows the quantitative effect of the appendage (Figure 5). Specifically, 10-dT lowered the mobility by 3%, while 20-dT and 40-dT decreased mobility 4.5% and 7% respectively. A fit of the modified Ogston sieving equation[62] to the mobilities of the longest variants underestimates the mobilities of even the slower of the two 12C-hp10 and 12C-hp10-5dT species, indicating that the first few dT's have a greater proportional impact on mobility (see Appendix).

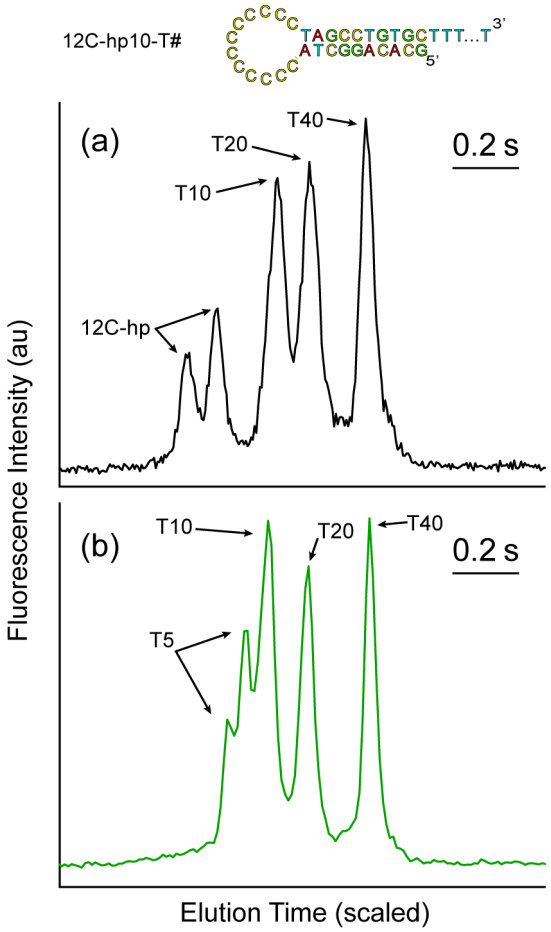

Figure 2-4 (a) Electropherogram of a mixture containing 12C-hp10, 12C-hp10-dT10, -dT20 and -dT40 fluorescent DNA-AgNCs. The dimorphism exhibited by the 12C-hp10 sequence was not evident among these poly-dT variants. The elution times of their single peaks increased with the number of thymidine. (b) Electropherogram of a mixture of 12C-hp10-dT5, -dT10, -dT20 and -dT40. The -dT5 variant exhibits dimorphism similar to the 12C-hp10, but with a longer elution time.

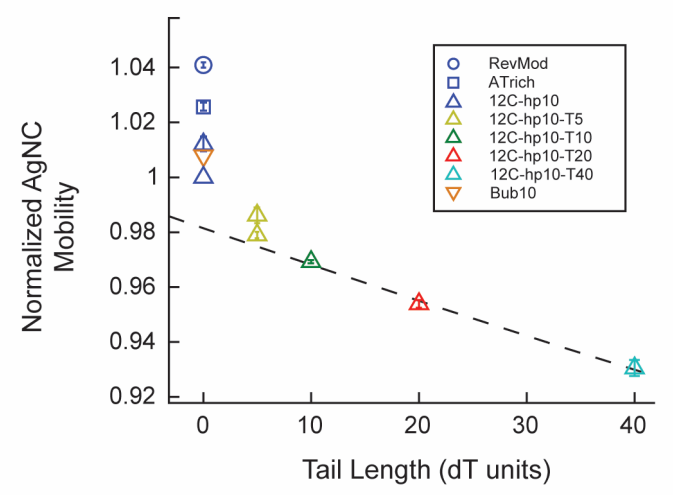

Figure 2-5 Plot of average relative mobility of DNA AgNCs as a function of the length of poly-dT appended to the 3' end of the template strand. Mobilities have been normalized to the 12C-hp10 species with the lowest mobility. Error bars indicate standard deviation of the relative mobility obtained from ten or more separation experiments. DNA AgNCs made with the Bub10 sequence have a mobility that is intermediate to the two products of the 12C-hp10 strand. The dotted line is a fit of the 12C-hp10-T10, -T20 and -T30 mobilities to the modified Ogston sieving equation.

Interpretation of the electrophoretic doublet

The presence of twin peaks in the electropherograms of 12C-hp10 and 12C-hp10-T5 is intriguing. In the case of 12C-hp10, high resolution fluorescence spectroscopy scans resolve only a single fluorescent species. Being identical in spectra as well as sequence, the two species present in the electropherograms likely contain the same Ag^0/Ag^+ composition, the same overall charge and the same silver-base interactions.[16] Therefore, we conclude that the species present in the two peaks must differ in the secondary structure of the surrounding DNA. To the best of our knowledge, this is the first evidence that markedly different conformations of the same DNA sequence can provide identical environments for a silver nanocluster.

One possibility is that the peaks represent clusters comprised of multimers containing different numbers of DNA strands. However, the relative intensity of the peaks did not correlate with the rate at which the DNA strands were annealed prior to synthesis (data not shown), suggesting that the two structures involve the same number of DNA strands. Furthermore, the 1% difference in their electrophoretic mobility is much subtler than differences typically observed between (i) ssDNA and dsDNA (~5% mobility difference),[63] (ii): between 10 and 20 nucleotide ssDNA (~50% difference) (see Supporting Information), and (iii) between self-dimer and hairpin DNA structures.[30] Mobility shifts of one or few percent are often attributed to subtle differences in DNA conformation.[60,61]

A compelling scenario is that the species in the doublet are different configurations of a hairpin dimer. First, red-emitting AgNCs formed on non-complementary DNA homodimers have been observed before.[17,30] Second, the absolute electrophoretic mobilities of the species in question are large compared to those of single stranded 10 and 20 base ssDNA under the same separation conditions (see Supporting Information), suggesting that they are compact. Third, at low pH, hairpin DNA with poly-dC loops have been shown to form two distinct dimerized structures,[64] in which the cytosine loops are hemi-protonated and adopt an i-motif configuration with their stem regions either (i) adjacent to (*cis)* (Figure 6a) or (ii) opposite each other (*trans*) (Figure 6b). Finally, the lack of a doublet in electropherograms of AgNC formed on 12C-hp10 with 10 or more dT appended is consistent with the *cis* dimer being destabilized[60] by the entropic cost of anchoring two disordered polymers next to each other. Therefore, we expect the single peak observed in electropherogram of long-tailed variants is comprised entirely of *trans* dimers.

The absence of doublets in the electropherograms of stem-sequence variants RevMod, ATrich and Bub10 emphasizes the influence that bases in the stem region have on overall structure and ultimately fluorescence of AgNCs. The Bub10 variant contains two C-tracts within its sequence, which could easily result in an intramolecular or intermolecular i-motif structure. However, because the two regions on either side of the C-tract for Bub10 have the same length, dimer formation via C-tract binding would not be asymmetric as it is in the case of 12C-hp10.

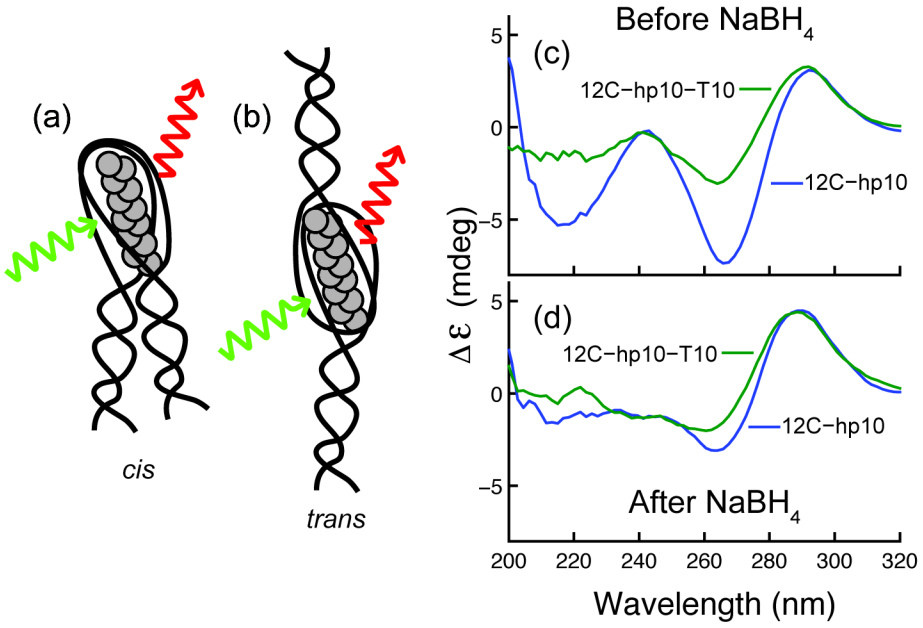

Figure 2-6 Left: Schematic representation of the two possible dimer conformations stabilizing DNA AgNCs on 12C-hp10: (a) *cis* and (b) *trans*. Right: Circular dichroism (CD) spectra of ssDNA templates 12C-hp10 and 12C-hp10-T10 with 0.2 mM $AgNO_3$ in 10 mM sodium acetate (pH 4.8) (c) before and (d) after reduction with $NaBH_4$ (0.15 mM final concentration). 12C-hp10-T10 shows little change upon reduction, whereas 12C-hp10 loses two well-defined minima upon reduction, to become similar to 12C-hp10-T10. Both display the 290 nm peak characteristic of a cytosine mediated i-motif throughout.

The presence of an i-motif in single-stranded DNA, poly-dC hairpin dimers, and DNA AgNCs has been correlated with a peak in circular dichroism (CD) at 290 nm.[44,60,65] This

peak is present in CD spectra of both 12C-hp10 and 12C-hp10-T10 with silver nitrate in sodium acetate buffer (pH 4.8) both before (Figure 6C) and after (Figure 6D) reduction with $NaBH_4$, lending support to the hypothesis that an i-motif region serves as the nanocluster formation site.

Another striking feature of the CD spectra is a pair of strongly negative peaks at 215 nm and 265 nm that are seen only in 12C-hp10 before reduction. The origin of the 215 nm peak is not obvious but, for DNA, a negative peak around 265 nm is characteristic of antiparallel strands in a quadruplex.[65] The absence of this peak in the T10 variant suggests that it is the stems of the cis-dimer that form a quadruplex. That this stem-based quadruplex disappears upon reduction with $NaBH_4$ suggests that the emissive AgNC constrains the relative positions of the cis-stems to an angle incompatible with quadruplex formation.

It should be noted, however, that these spectra may be biased, or even overwhelmed, by non-emissive species because CD measurements are not specific to emissive structures. This severely limits the utility of CD spectroscopy for the analysis of unpurified DNA AgNC solutions and highlights one advantage of microchip CE.

Shifts in fluorescence and mobility are consistent with the gain/loss of one or two Ag^+

Data from Schultz *et al*.[16] indicates that addition or removal of a single Ag atom/ion can increase or decrease the peak emission wavelength of an AgNC by ~ 20 nm. Spectral shifts between related DNA-AgNC can therefore be expected to correlate with changes in their size and, possibly, effective charge, with blue shifts corresponding to smaller, more negatively

charged clusters (decreased electrophoretic mobility), and red shifts to larger, more positively charged clusters (increased electrophoretic mobility).

The magnitudes of the blue shifts in peak emissions of RevMod (-18 nm) and ATrich (-34 nm) suggest their AgNC have one and two fewer Ag/Ag^+, respectively.[16] Accordingly, these emitters had shorter elution times than the 12C-hp10 species. The elution peak of RevMod was narrow and almost twice as bright as the 12C-hp10 peaks, suggesting that its dominant fluorescence comes from a single emitter with a unique charge composition and DNA conformation. In contrast, ATrich, produced a broad elution profile with a small, but discernible peak at the front, which was less than half as bright as either of the 12C-hp10 peaks. This broad profile suggests either the presence of multiple emitters or that the DNA has an unstable secondary structure. The latter is consistent with the reduced thermal stability of the AT-rich stem (AT-rich: Tm = 53.6°C, 12C-hp10: Tm = 64.0°C).[66] More frequent fluctuations in conformation of the stabilizing DNA would also explain the relatively low fluorescence of the ATrich solution if, for example, cluster emissivity is sensitive to details of scaffold conformation.

Of the two red emitters that formed from Bub10, the one that is only 10 nm red-shifted relative to the 12C-hp10 emission probably comes from a cluster with the same number of Ag/Ag^+ and only slightly modified secondary structure, consistent with their having similar mobility. The other emitter, which is at least 20 nm red-shifted suggests the presence of a cluster with one additional Ag/Ag^+, consistent with the lower mobility tail in the electropherogram.

Bases contained within the stem can interact with AgNCs

In isolation, short, fully-complementary duplexes are incapable of hosting fluorescent AgNCs.[19] How then to explain the observed effect of stem base sequence and orientation on the AgNC hosted by a hairpin DNA?

One possibility is that, in the presence of Ag^+, hydrogen bonding between Watson-Crick base pairs in the stem is interrupted[49] such that "stem" bases are available to bind Ag/Ag^+ much like "loop" bases. However, if the stem bases were directly binding the cluster, one would expect a variant like AT-Rich, which lacks Ag-binding bases in its stem, to result in the greatest spectral shifts and mobility changes. Instead, we find that variant RevMod, with its subtle rearrangement of stem bases and minor composition change, differed most from 12C-hp10 in both spectra and mobility.

Another possibility is that, in the context of a hairpin, the AgNC is positioned to interact with both single and double stranded bases at the same time. This could happen if, for example, the loop folds back over the stem. Although the base nitrogens most likely to bind silver are the same ones involved in hydrogen bonding in standard Watson-Crick base pairs, Hoogstein base-pairing, a low-energy excitation of duplex DNA structure that makes ring nitrogens on guanidine and adenosine available for binding in the major groove, could support direct interaction between stem bases and silver atoms/ions.[67] Given the considerations discussed in the previous section, it seems unlikely that the 12C-hp10 DNA-AgNC hairpin adopts such a conformation. And, again, since neither the mobility shifts nor the spectral shifts are very large, it seems more plausible that all the variants are hairpin dimers as well.

We suspect that the stem bases' influence the AgNC in a less direct manner. The sequence of the stem, particularly closest to the loop, determines how tightly the loop is clamped, thereby adjusting the range of conformations available to the loop bases. Loop conformation can directly influence base-Ag interactions and cluster formation. Weakly clamped loops would explain the formation of two nearly identical AgNC emitters on Bub10, whose two 5-basepair stem regions are less strongly hybridized than the original's 10-basepair stem.

Stem mutations generally diminished fluorescence intensity from the resulting AgNC samples (Table 1). The reduction in intensity could be due to reduced quantum yield or lower overall chemical yield of the clusters. Low chemical yield is likely to explain most of the loss in integrated intensity of RevMod and ATrich samples because synthesis of their different-sized clusters may be optimized at a different silver-DNA stoichiometry. Bub10 stabilizes multiple clusters with spectra and electrophoretic mobility that suggest it is similar in size to 12C-hp10. Competition for silver among these various clusters may also reduce chemical yield. We note, however, that in addition to synthesis conditions, low chemical yield could result from diminished photostability or increased susceptibility to oxidation.[50] In the case of AgNCs generated from 12C-hp10-dT# variants, lower quantum yield is a more likely explanation. Reduced overall intensity when excited in the UV is expected due to the UV absorbance of the poly-dT appendage, which is not in direct contact with the cluster and does not effectively transfer energy.[57]

Appending poly-dT provides a convenient means for tuning AgNC mobility

The spectra and mobilities of poly-dT variants (Figures 2 and 4) were consistent with expectations that the appendage does not interact with the AgNC and simply increases the effective size of the DNA-AgNC by adopting a random coil conformation. Under our separation conditions the decrease in mobility per unit poly-dT length for long overhangs was 0.13% per dT. This is comparable to the proportionate decrease in mobility per dT appended observed using linear polyacrylamide coated capillaries and FITC-labeled poly-dT in the range of 16 to 100 nucleotides, albeit under different separation conditions.[68] Appending poly-dT to the DNA scaffold of an AgNC can thus provide a convenient set of tunable mobility markers for high-resolution separation assays such as isotachophoresis, where focusing and separation of analytes is highly dependent on mobility.[69,70]

Conclusions

We have shown that sequence variations to the stem region of a hairpin DNA template affect both fluorescence emission, the final DNA conformation and the electrophoretic mobility of the AgNC species. A single red-emissive DNA AgNC that formed on one hairpin template had a structural dichotomy, which disappeared when 10 or more thymidine were appended. We attribute this dimorphism to two distinct i-motif dimerizations of the hairpin loop, one of which is destabilized in the presence of long overhangs. Clusters formed on a variant hairpin DNA did not share this dimorphism. A hairpin DNA in which the poly-dC region was in the middle of the stem, rather than looped at the end, formed two fluorescently distinct clusters, of indistinguishable mobility. We conclude that, although the poly-dC loop

is likely to be the primary site of dimerization and nanocluster stabilization, the bases contained within the stem affect cluster formation, either through direction interaction with the cluster or by inducing change in the DNA conformation.

The electrophoretic mobility of a DNA encapsulated silver nanocluster can be finely tuned without altering its optical properties. Specifically, the mobility of our DNA-AgNC derived from a hairpin DNA sequence decreased between 1% and 7% upon appending poly-dT of lengths ranging from 5 to 40 units to the 3' end of the hairpin stem. The poly-dT overhangs did not affect the resulting fluorescence spectra or yield.

We found the electrophoretic mobility of all Ag-DNA variants to be consistent with the structural properties implied by differences in their emission properties. Our results highlight the subtleties involved in directly engineering fluorescent DNA AgNC, as well as their potential as flexible standards for separation assays. Microfluidic capillary zone electrophoresis provides a sensitive and informative platform for the analysis of detailed DNA-AgNC structure using unpurified samples that complements bulk fluorescence characterization.

Supporting Information: Fluorescence emission of samples synthesized in NH_4OAc buffer, absorbance spectra of 12C-hp10 and poly-dT variants, details on curve fitting, electropherograms of 10 and 20 base ssDNA, and fluorescence intensity of 12C-hp10 over time at different storage temperatures can be found in the Appendix.

Chapter 3

Fluorescent silver nanocluster DNA probes for multiplexed detection using microfluidic capillary electrophoresis

Background

The growing need for highly specific and sensitive molecular probes for nucleic acids has led to research and development of fluorescent probes that take advantage of the inherent selectivity of short synthetic DNA oligos.[71] For example, mole- cular beacons (MBs) are a popular nucleic acid based probe for DNA detection composed of a synthetic hairpin DNA covalently labeled with an organic fluorophore and a quencher molecule.[72,73] MBs rely on the probe undergoing a conformational change upon binding to its DNA target. This confor- mational change increases the distance separating the fluorophore and quencher to produce an increase of fluorescence signal. However, these probes often suffer from high background fluorescence and issues with binding as a result of interactions between bound dyes and target.[74] Furthermore, conjugating two different molecules to each MB requires purification steps that result in high costs with low yields com- pared to unmodified DNA synthesis. (A standard molecular beacon can cost $500 for a guaranteed yield of 10 nmol.)

Additionally, for applications that require multiplexing, a multi color approach using MBs with fluorophores of distinct emission spectra adds potentially unwanted complexity to optical detection hardware.

As an alternative to using fluorophores and quenchers for nucleic acid probes, the facility of using fluorescent silver nanoclusters has recently been demonstrated. Fluorescent silver nanoclusters (AgNC-DNA) self-assemble on single stranded DNA template strands and can have photophysical properties rivaling those of MBs.[30,32,34,35,75] AgNC-DNA are few-atom silver clusters stabilized by the nucleobases of a synthetic DNA host strand.[12,76] They are easily synthesized and can be tuned to exhibit bright fluorescence emission across the visible spec- trum via the nucleotide sequence of the host DNA, making them ideal candidates as novel fluorophores.[19,41] The prospect of incorporating sequences for both AgNC stabilization and DNA target binding selectivity into a single oligomer has led to a growing number of novel detection strategies.[23] Some methods of DNA detection using AgNCs rely on spectral shifts,[37,77] while others produce 'turn-on' probes,[32,34,35] providing a simple and robust method for fluorescence based DNA detection.

Many of these approaches are intended to produce modular probes, where the target binding portion of the sequence can easily be substituted. The standard approach to multiplexing involves distinguishing between probes by color.[78,79] For the case of AgNC-DNA probes, this means changing both the target binding sequence and the AgNC forming sequence.[31] Although there exists a varied palette of AgNC-DNAs to choose from,[41] their synthesis conditions and formation times are often just as varied and can change spectra once incorporated into a larger probe strand often with a reduction in color variation.[31] Recent advances have shown that machine learning algorithms combined with batch processing of oligomers can aid in the discovery of new sequences that stabilize AgNCs,[20] but many have similar emission spectra, presenting a challenge for colorimetric multiplexing.[43] Therefore,

an alternative to color differences between the AgNC-DNA probes is needed for robust multiplexing.

To address this need, we show that by appending poly-dTs to probe sequences, it is possible to easily and rapidly separate and identify different AgNC-DNA probes for nucleic acid targets. These poly-dT regions are easily appended to probes during oligo synthesis and do not require the additional steps, purifications or cost required of a base or end label modification, making this approach particularly well suited for several AgNC based probes.[32,34] The strategy of appending poly-dT is not well suited to typical, end-labeled MBs because it would increase the distance between fluorophore and quencher, resulting in higher background fluorescence levels. Our separation-based approach of AgNC-DNA probes dramatically increases the potential degree of multiplexing by demonstrating an alternative to typical multi-color methods. Multi- color multiplexing is limited by the finite bandwidth resulting from wide emission spectra and the increasing complexity of filter sets needed to distinguish overlapping spectra. Our approach can be easily extended to multiplex tens of species with a high resolution CE separation by simply appending poly-dTs. The DNA oligos for these probes cost $60 for a guar- anteed yield of 30 nmol, making them an affordable alternative to multiplexing using spectrally distinct MBs or trying to adapt the approach to MBs using base modifications as opposed to end-tagged strands. In this proof-of-principle work, we have generated single-color probes to detect DNA targets for Hepatitis A, B and C from a single sample, a formidable task using standard PCR techniques.[80] We then identify these probes from a pre-mixed sample using microfluidic capillary electrophoresis (mCE).

Results and Discussion

Probe design and synthesis

To demonstrate a multiplexed approach towards using luminescent AgNC-DNA probes we modify a hairpin DNA that was previously characterized for nucleic acid detection of a Hepatitis B surface antigen gene[34] (HBV) to create turn-on probes for two additional nucleic acid targets: Hepatitis A (HAV) and Hepatitis C (HCV). This hairpin based AgNC probe was previously characterized and revealed to have a superior signal to background ratio, linear fluorescence response to target DNA concentration and a limit-of-detection of 3 nM.[34] We chose this probe design because of its simple, single-stranded, modular design, which we hoped would translate into a straightforward process of adapting it to different target DNA sequences without having to optimize the AgNC forming sequence for each probe. Each probe consists of a length of synthetic DNA divided into 4 sequence regions: (i) a fluorescent AgNC nucleation region (12 bases), (ii) a probe region (30 bases), (iii) a AgNC-blocking region (7 bases), and (iv) a mobility modifying region (10–20 bases). The structure and behavior of the probes are outlined schematically in Fig. 1. In the native 'off' state, the AgNC nucleation region hybridizes to the blocking region of the probe. While it is hybridized, the silver is unable to access the fluorescence-inducing sequence[19] and formation of the AgNC is inhibited. When the probe hybridizes to its target, the hairpin opens and exposes the AgNC-stabilizing region of the probe. Silver ions bind to the newly exposed nucleobases and become fluorescent nanoclusters upon chemical reduction with sodium borohydride. The exposed blocking region is short and not expected to stabilize a fluorescent AgNC.[34]

Tailoring a probe to different targets involves replacing the 30 base probe region with a sequence complementary to the desired target. For the HAV and HCV probes, we replaced the probe region with sequences complimentary to conserved 30 base regions in the 5′UTR of the HAV and HCV genome,[81,82] which are commonly used for detection.[83,84] For optimal function of the AgNC-DNA probe, neither probe nor target sequences should form fluorescent AgNCs themselves. Since AgNC-DNA typically form on cytosine rich strands, especially those with significant secondary structures,[47] we selected probe-target sequences with few cytosine and guanine repeats, and little or no secondary structure within the probe region sequence because secondary structure in either probe or target sequences could also have a negative impact on probe-target hybridization.

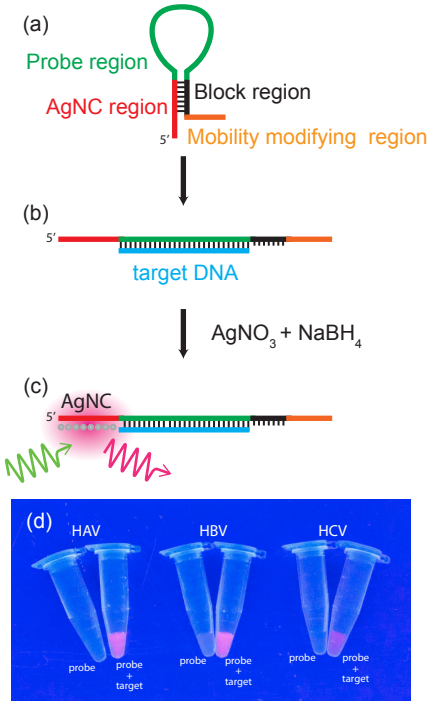

Figure 3-1 Schematic representation of AgNC-DNA probe. (a) The DNA adopts a hairpin conformation in its native state. Regions of the DNA sequence are labeled according to their function. (b) When the probe region binds to the target DNA, the hairpin opens, exposing the

bases in the AgNC region. (c) A fluorescent silver nanocluster forms upon addition of silver nitrate and reduction by sodium borohydride. (d) Photograph of AgNC-DNA probes on a UV transilluminator.

Using this strategy, we found sequences that produced viable fluorescent probes for HAV and HCV that were spectrally similar to the original HBV probe (see Appendix). Each probe has a stable predicted hairpin conformation with melting temperatures above 45 °C that opens in the presence of complimentary target with an estimated melting temperature above 50 °C as expected[85,86] (see Appendix).

However, despite adhering to this design strategy, we had to try several HCV probe sequences before finding one that produced a viable probe. These unsuitable sequences were complementary to various regions of the HCV's 5′ UTR but yielded poor probes that either did not fluoresce upon hybridization or produced fluorescent clusters in their native hairpin state (see Appendix) The predicted secondary structures of these problematic probes contain some secondary structure within their hairpin loops (See Appendix), which may contribute to why some of the probes themselves stabilized fluorescent AgNCs, however, their lower melting temperatures suggests that the structures within the loop should not be very stable. Once hybridized to target, these non-functional probes have estimated melting temperatures comparable to the functional probes. We conclude that the ability of a probe to stabilize a fluorescent AgNC is sensitive not only to the AgNC region sequence, but also to interactions with bases contained in the probe region, a phenomenon common to other AgNC probe designs.[30,32] We also note that rational design strategies are limited because free energy models for predicting secondary structure neglect the effect of Ag+ on mediating non-Watson–Crick base pairing.[48,87] Ag-mediated base-pairing can lead to the formation of

unpredicted mismatched self-dimers and hairpins and have previously been shown to stabilize fluorescent AgNCs.[30] Our CE results, discussed below, provide further evidence for the presence of unexpected silver-mediated conformations that yield multiple, spectrally similar AgNCs from the HBV probe-target duplex. Taken together, these results highlight the inherent difficulty of trying to tailor even seemingly straightforward AgNC probes for different target sequences.

To tune the mobility of our functional probes for multiplexing, we altered their mobility modifier regions by appending differing lengths of poly-dT at the 3′ end of the hairpin sequence. The poly-dT region decreases the electrophoretic mobility of the probe, allowing for multiple probes with the same fluorescence spectra to be screened from a single sample.[88] This approach reduces the complexity of multiplexing by eliminating the need to devise new sequences or optimize synthesis conditions to create bright, stable AgNCs with distinguishable spectra. Additionally, eliminating the need for spectrally distinct probes minimizes the number of filter sets and excitation sources required for typical multicolor assays. Thymine bases were chosen for the mobility modifying region because long stretches of thymine (i) have little to no secondary structure, making the mobility shift a simple function of their length; (ii) have a low affinity for silver ions compared to other bases[56] and thus do not dramatically affect stoichiometry; and (iii) have a low propensity for forming fluorescent AgNCs at neutral pH.[19] The AgNC DNA probes presented here were all prepared using the same procedure and produced bright red-emitting clusters in the presence of their respective DNA targets.

Fluorescence characterization

Samples containing a single probe type were mixed with equimolar amounts of their respective target DNA in buffer and briefly annealed prior to synthesis and incubation. Emission spectra were first characterized using UV illumination at 260 nm, which universally excites the AgNCs,[57] to determine peak emission wavelengths. Emission spectra of each probe with and without target are shown in Fig. 2a. The fluorescence emission peak for the HAV and HBV probe + target complexes under UV illumination was centered at 603 nm with comparable intensities, but would red-shift over the course of several hours by as much as 10 nm. The HCV probe + target complex produced a significantly brighter AgNC solution with a redder emission peak centered at 624 nm. This difference in the emission spectrum of the HCV AgNC indicates that the probe design scheme is not perfectly modular, as previously discussed. We suspect the greater fluorescence intensity of the HCV probe + target sample is due to a greater chemical or quantum yield rather than a greater binding affinity because chemical and quantum yields are highly variable amongst different AgNCs.[16,41] Additionally, the UV-excited spectra are asymmetric, indicating the presence of a heterogeneous mixture of AgNCs formed during the synthesis.[16]

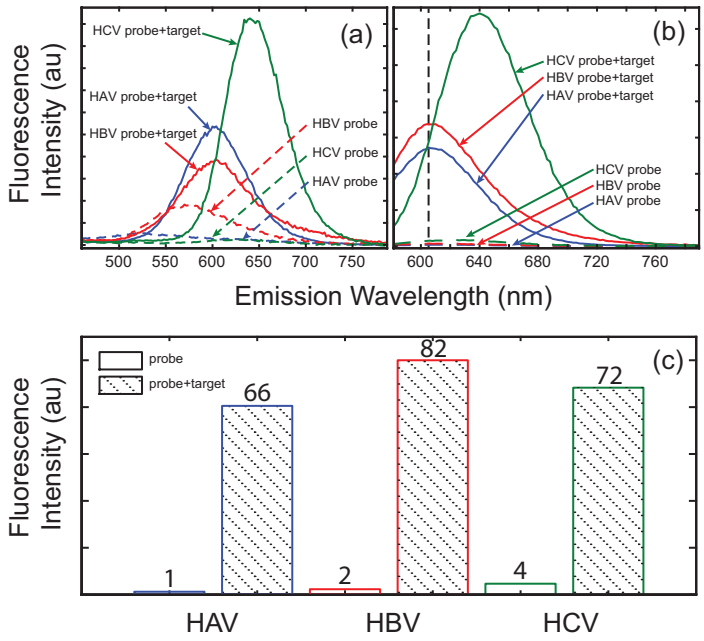

Figure 3-2 Fluorescence spectra of AgNC-DNA probes in their native states and bound to target DNA. (a) Fluorescence emission spectra under 260 nm illumination, which universally excites different AgNC-DNAs.34 (b) Fluorescence emission spectra under 550 nm excitation. Spectra in (a) and (b) are normalized to their brightest peaks. (c) Emission intensity at 606 nm of each probe with and without target under 550 nm excitation. Intensities are normalized to the fluorescence of the HAV probe without target.

Each probe + target complex could also be excited by light in the visible spectrum. An excitation scan was performed to determine the visible excitation peak for each probe (see Appendix from which a universal visible excitation wavelength of 550 nm was selected. At this wavelength, the probes had emission spectra that peaked at 608 nm, 608 nm and 643 nm respectively (Fig. 2b). Exciting the probes at 550 nm selectively eliminated the weak fluorescence emitted by the HBV probe without target (Fig. 2a). Excitation in the visible spectrum minimizes absorption of excitation light by non-fluorescent species in the sample, resulting in higher intensity fluorescence emission (see Appendix). Given the comparable fluo- rescence emission wavelengths and intensities, as well as the similar hairpin design and

binding free energy, we assume the HAV and HCV probes we present have a comparable limit of detection to that of the HBV probe.[34]

The spectra of the AgNCs produced by the different probes were similar enough to allow all to be excited and detected simultaneously. Fig. 2c compares the emission intensity at 606 nm for each probe and probe + target complex when excited at 550 nm. The fluorescence enhancement, $E = (I_{probe+target} - I_{probe})/I_{probe}$, for probes hybridized to their respective targets was 65, 40 and 17 for HAV, HBV and HCV with probe and target concentrations of 34 μM each. To ensure that each probe was selective for its intended target, we tested each probe in the presence of each of the three target DNA strands. Each probe created a bright fluorescent silver cluster only in the presence of its respective target (Fig. 3). Solutions containing a probe with mismatched DNA target exhibited minimal fluorescent signal indicating that the probe did not hybridize with the target DNA and thus did not open its hairpin conformation to produce a fluorescent AgNC.

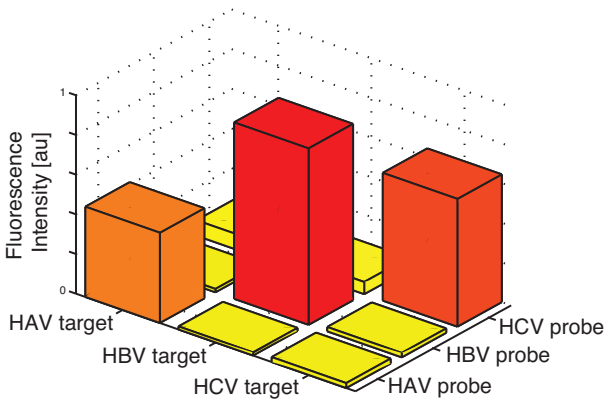

Figure 3-3 Fluorescence emission of AgNC DNA probes for HAV, HBV and HCV in the presence of each of the three DNA target strands. Fluorescence emission was monitored at

625 nm under 550 nm excitation. The probes are selective for their respective targets as indicated by the bright fluorescence enhancements.

Next, we evaluated the effect of adding poly-dT to the mobility modifying regions of the probes. To distinguish HAV, HCV and HBV, we added different lengths of poly-dT to the HAV and HCV probes, leaving the HBV mobility unchanged. The poly-dT versions of the probes produced AgNCs with spectra indistinguishable from their original versions when hybridized to target DNAs. Fig. 4 compares the emission spectrum of AgNCs formed by the original HAV and HCV probes to an HAV probe containing a 20 T region and an HCV with a 10 T region. As expected, the poly-dT region did not yield a fluorescent AgNC when each probe is in its native hairpin state, nor it affect the fluorescence of the AgNC that forms on the 5′ region of the probes when bound to their respective targets. There was no discernible shift in peak emission and the relative emission intensities were comparable. The observed increase in emission intensity upon adding poly-dT to the HAV and HCV probes (≈20% and ≈11% respectively), although negligible for our purposes, is too large to attribute solely to pipetting uncertainty. It is more likely due to a change in quantum efficiency or structural stability imparted by the poly-dT.

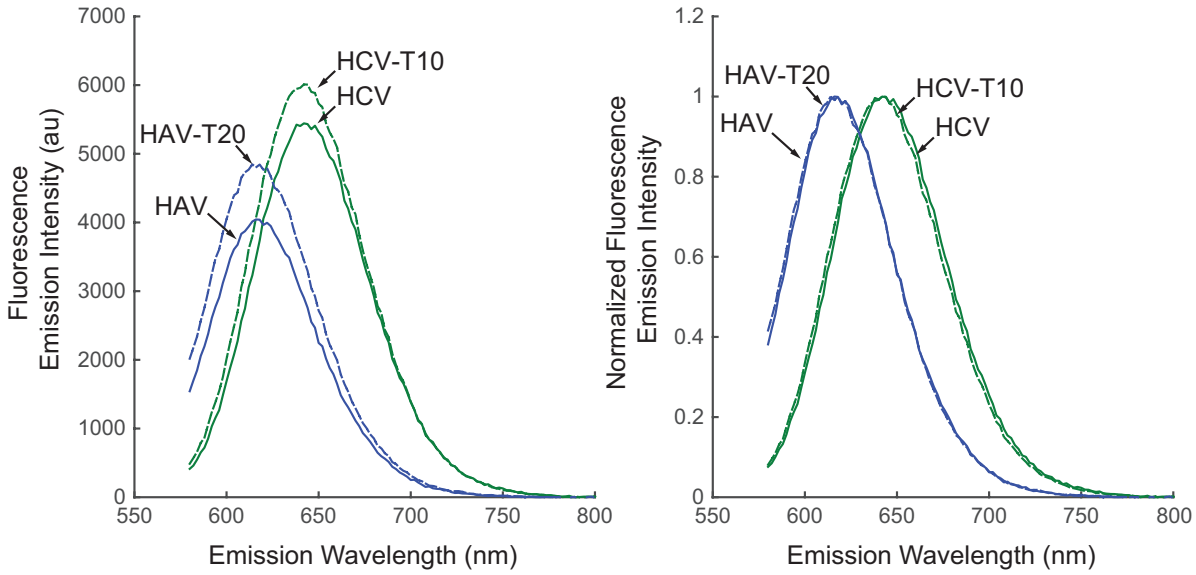

Figure 3-4 Fluorescence spectra of the AgNCs formed by the HAV-20T HCV-10T probes bound to their respective targets compared to versions without the poly-dT mobility modified regions. Samples were excited at 550 nm. Left plot shows absolute emission intensities and the right plot shows normalized intensities. Adding poly-dT to the sequences did not affect the emission spectra or function of either probe.

Multiplexing using mCE

To demonstrate multiplexed detection using these probes, we prepared a mixture of equimolar amounts of HAV-20 T, HBV and HCV-10 T probes to create a mixed probe solution. Each of the three target DNAs were added to the probe mixture and the standard AgNC synthesis was performed. After synthesis, the sample containing the probe mixture and target DNA produced fluorescent nanoclusters with emission spectra comparable to samples containing only a single probe. The mixed target sample produced an emission peak at 628 nm (see Appendix), falling between the peaks produced by the HAV, HBV and HCV probes alone, indicating the presence of AgNCs produced by the different probes.

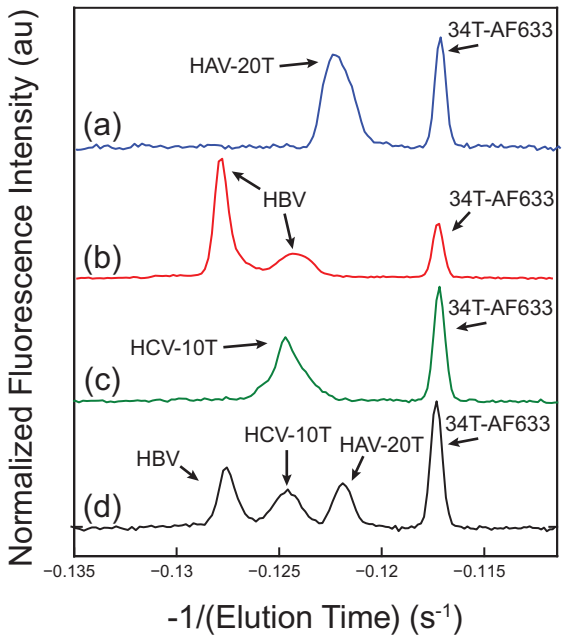

Figure 3-5 Separations of fluorescent AgNC-DNA probes and an Alex- afluor633 labeled poly-dT DNA (34T-AF644) by microfluidic capillary electrophoresis (mCE). (a)–(c) Probe mixtures containing only a single target DNA produced peaks with elution times modified by the size of the poly-dT mobility modifying region of probe-target complex. (d) A probe mixture containing all the DNA targets separates into 3 fluorescent peaks, easily confirming the presence of the different targets.

To distinguish between targets in a mixed sample, we exploit each probe's mobility modifying region by performing a mobility shift assay using mCE. Samples containing probe mix and different DNA targets were electrophoretically separated and detected in under 10 seconds using a custom built apparatus.[52] An in situ fluorescent standard was added to samples during mCE separation: a DNA strand composed of 34 dT with an Alexafluor633 dye conjugated to the 5′ end, which helped correlate separation behavior from run to run. To confirm the identity of the fluorescent species identified by mCE, we prepared AgNC probe samples containing only a single target DNA and compared their elution times to that of the reference poly-dT34-AF, as shown by the electropherograms presented in Fig. 5. Fig. 5

clearly shows that each DNA probe has a distinct mobility, which depends on the size of their respective poly-dT regions; the longer the poly-dT region, the longer the species takes to elute through the polymer matrix within the channel. Fig. 5d shows a sample containing all three DNA targets. The probe mixture is clearly separated into three distinct peaks enabling easy identification.

We quantify the separation resolution, R using $R = \Delta t/\sigma$ where Δt is the time separating the two least separated peaks, and σ is the half-width half-max of the broadest peak. Additionally, we define our signal to noise ratio, SNR as L_0/N where L_0 is peak height above the average noise level and N is the characteristic noise width, which we take as twice the standard deviation of the background signal. We successfully resolved all of our probes from a single mixed sample with a minimum resolution of R = 3.47 and SNR = 17.23 in under 10 seconds. Our separation is characterized by a large Peclet number (approx. 107), implying that we can assume a pure advection limit where the shapes of the peaks are dictated by the following: initial plug shape prior to separation, the mixing of multiple species, or the kinetics of binding among species contained within the plug.[89] This technique should be readily adaptable to the most sensitive CE and mCE setups available. For example, recent work using isotachophoretic sample concentration in microfluidic chips has achieved limits of detection down to 100 pM using MBs for nucleic acid detection, which could easily be coupled to capillary zone electrophoresis to concentrate and separate samples on chip in a single run.[90,91]

The electropherogram for the HBV probe (Fig. 5b) exhibited two elution peaks in the presence of only HBV target. This smaller, secondary peak eluted at a later time, comparable

to the HCV probe containing a 10 T modifying region, which could potentially lead to a false-positive detection of the HCV target. The species contained in the second elution peak is likely due to an additional, unpredicted conformation or dimerization of the AgNC-DNA probe resulting from Ag+ mediated base pairing. mCE measurements of an HBV-T10 probe with target revealed that the mobility of both peaks shifts and that the slower of the two overlaps with the HAV-T20 peak. Overlapping peaks can be eliminated in practice either by tuning the lengths of the poly-dT regions or improving sep- aration resolution by increasing separation length or modifying the sieving matrix. Alternatively, the probe can be redesigned with a different recognition sequence to try and eliminate the additional structure. The unpredictable structure of DNA in the presence of Ag+ emphasizes the difficulty of designing AgNC-DNA probes that rely on structural changes upon binding target.

Experimental methods

AgNC-DNA synthesis

Synthetic DNA oligos were purchased from Integrated DNA Technologies, Inc. (Coralville, Iowa, USA) with standard desalting, with exception of the poly-dT34 containing a 5′ modified Alexafluor633, which was purified by HPLC. Sequences were checked for secondary structures using the NUPACK web server.[92] DNA strands were rehydrated using 18.2 MΩ cm de-ionized water (DI, MilliQ, Millipore), stored at 100–500 μM at −20 °C and thawed at room temperature as needed. Sodium phosphate buffer was prepared as a 10× stock at a concentration of 200 mM and pH of 7.1 by combining solutions of sodium

phosphate monobasic and sodium phosphate dibasic (Fisher Scientific, ACS certified) in DI. pH was verified using an Oakton pH 11 series meter and dual junction electrode.

AgNC-DNA probe solutions were prepared by combining 32.2 μL of 20 mM sodium phosphate buffer with 3 μL of 500 μM DNA probe and 3 μL of 500 μM DNA target (or 3μM of DI for target-free samples) and then placed in a dry block at 85 °C for 15 min and then at room temperature for 15 min. To prepare fluorescent clusters, 0.9 μL of 10 mM silver nitrate (Sigma Ultra) was added to the samples and were left for 20 min at room temperature in the dark. Lastly, 4.5 μL of freshly prepared 2 mM sodium borohydride (Aldrich 99.99%, pellets) was added to each sample and vortexed before incubating at room temperature in the dark for 2–5 hours until fluorimetric and mCE analysis. For samples containing a mixture of probes, the volume of each reagent was 48.3 μL of buffer, (3×) 1.5 μL of probe DNA, (3×) 1.5 μL of target DNA (or DI), 1.35 μL of 10 mM silver nitrate, and 7.75 μL of 2 mM sodium borohydride.

Fluorimetry

Fluorescence measurements were performed between 1 and 4 hours after synthesis using a plate reader (Tecan infinite 200Pro with Tecan i-control software, Tecan Group Ltd.). 30 μL of each sample was placed into a 384 well microplate (Part 3540, Corning, Inc.). The emission wavelength step size was set to 2 nm and bandwidth to 20 nm. The excitation band-width was 5–10 nm. Gain was manually adjusted to maximize intensity for the brightest species and then held constant over all spectra measurements. The gain was re-optimized to maxi- mize signal for single wavelength detection measurements. Emission spectra were fit to Gaussian curves to determine peak wavelengths using the Matlab (The Mathworks, Inc.)

function fit(). Images of tubes containing fluorescent probes (Fig. 1d) were obtained on a UV transilluminator (Fisher Scientific).

Microfluidic capillary electrophoresis

Microfluidic capillary electrophoresis was performed using borosilicate chips (Dolomite Ltd UK) containing 20 μL deep by 50 μL wide isotropically etched microchannels arranged in a cross pattern (three 1 cm long channels and a 3 cm long separ- ation channel). The channels were pretreated by vacuum flushing the following solutions for 10 min each: (i) deionized water, (ii) 100 mM NaOH, (iii) 1 M HCl, (iv) run buffer. The run buffer contained 20 mM sodium phosphate pH 7.1 with 1% (w/w) polyvinylpyrrolidone (PVP, 1.5 MDa avg. mol. wt. Sigma Aldrich) and 0.6% (w/w) hydroxyethyl cellulose (HEC, 90 kDa avg. mol. wt. Sigma Aldrich). PVP served to reduce electroosmotic (bulk) flow to allow for faster elution times while the HEC acted as a sieving matrix to improve separation resolution between DNA probes of different sizes.

The microfluidic chip was mounted to an inverted microscope (IX71, Olympus) outfitted with a controllable stage (Proscan II, Prior Scientific) using a custom made aluminum and polyetheretherketone (PEEK) chuck. Electrophoretic separ- ations were performed using a HVS448LC 6000 (Labsmith, Inc.) high voltage sequencer with platinum wire as electrodes. We performed pinched injection separations as described in detail elsewhere.[52,53] A sample plug of approximately 50 μL in length was electrokinetically driven down the separation channel under an applied electric field of 75 kV m^{-1}. Excitation light from a mercury arc lamp (U-HGLGPS, Olympus) passed through a filter cube (31002 TRITC/Rhodamine, Chroma Technology Corp.) and 20× microscope objective (CUCPlan FLN 20×/0.45,

Olympus) positioned 20 mm down the separation channel where emission light was collected using a back illuminated EMCCD camera (iXon+, Andor Technology). Tiff images from the EMCCD were processed using custom Matlab scripts to generate electropherograms. Sample plugs typically took between 5 and 10 seconds to reach the detection point.

Conclusions

Modifying the electrophoretic mobility of AgNC-DNA probes provides a simple, inexpensive method for multiplexed detection of nucleic acids. By modifying the target binding sequence, we were able to adapt a single probe to different target sequences, though not all target-binding sequences yielded viable probes. Appending poly-dT to AgNC DNA hairpin probes reduces their electrophoretic mobility as measured by microfluidic capillary electrophoresis. Poly-dT tails tuned mobility without affecting fluorescence emission or probe specificity for the detection of DNA targets for HAV, HBV and HCV from a single mixed sample. Electrophoretic separations also revealed that some probes yielded multiple species, which could cause a false-positive detection, emphasizing the difficulty in designing AgNC-DNA probes when little is known about their structure. Mobility-adjusted AgNC DNA probes allow for easy integration into microfluidic-based total analysis systems because they require only a single excitation/detection channel and a single-step sample preparation. The probes are made from unmodified, unpurified synthetic DNA strands, making this rapid, single-color multiplexing approach a potential low cost method for detecting multiple DNA targets simultaneously.

Chapter 3 and Appendix III are reproduced with permission from JT Del Bonis-O'Donnell, DK Fygenson, S Pennathur, Fluorescent silver nanocluster DNA probes for

multiplexed detection using microfluidic capillary electrophoresis. *Analyst*. **2015,** *140*, 1609-1615. Copyright 2015 Royal Society of Chemistry.

Chapter 4

A universal design for a hairpin DNA probe providing ratiometric fluorescence detection by generation of silver nanoclusters

Background

Nucleic acid detection and quantification is a critical tool for molecular biology and clinical diagnostics as it can provide important genetic and regulatory information without the need for expensive and time consuming sequencing. Synthetic nucleic acids containing conjugated fluorescent dyes are among the most widely used probes owing to their availability, customizability and ease of use. Fluorescence provides high sensitivity while sequence-dependent hybridization provides specific, separation-free detection.

Molecular beacons (MBs) are a well-known example of hybridization-based fluorescence probes for specific nucleic acid detection. MBs consist of a short oligonucleotide with fluorophore and quencher moieties conjugated to opposite ends.[73,93] In its native state, the probe adopts a stem-loop structure with the fluorophore and quencher held in close proximity by the stem, quenching fluorescence emission. After the loop hybridizes with its complementary target DNA, the oligonucleotide adopts an extended conformation, separating the fluorophore and quencher, and increasing the fluorescent signal. Among the drawbacks of MBs are high background fluorescence and susceptibility of their organic fluorophores to photobleaching. Additionally, the bulky dyes can interfere with target

hybridization and the two conjugations require multiple steps of purification and ultimately low yields at a high production cost.[32,72,94,95]

One approach to overcome these limitations is utilizing DNA-stabilized fluorescent silver nanoclusters (DNA-AgNCs) as an alternative to the dye-quencher conjugation in MBs.[34,96] DNA-AgNCs are a new class of fluorophore composed of few-atom silver clusters stabilized by a short DNA oligo,[12,23] some of which exhibit bright emission, good photostability, high quantum efficiencies and biocompatibility. The low-cost and facility of their synthesis makes them an attractive alternative to common fluorophores such as organic dyes and quantum dots, motivating an assortment of novel DNA probes.[123,32,37,97] Incorporating AgNC stabilizing sequences into a hairpin DNA, AgNC generating MBs have been shown to be a simple and flexible method for label-free, turn-on fluorescent detection of DNA.[34,96] Like an MB, the probe contains a target binding domain within the hairpin loop. A 12-base sequence that stabilizes a fluorescent AgNC is contained within the hybridized stem, where base-pairing competes with silver ion binding,[19] preventing the cluster from forming. Once the probe hybridizes with its target and unfolds, the AgNC sequence is freed from the stem and generates a fluorescent AgNC. Low production costs, owing to the absence of conjugation and purification steps, make these elegant fluorescent probes an attractive alternative to classical MBs.

Sensitive and specific detection of Hepatitis B DNA and thrombin protein were recently accomplished using AgNC generating MB hairpin probes. However, attempts to apply the design to other binding sequences were not successful.[96] Ideally, exchanging the binding sequence to tailor the probe for different targets should not affect the probes basic function.

In this work, we identify interactions between the AgNC and binding domains as the cause for inconsistent performance of the original AgNC-MB design for different targets. We improve upon the original AgNC-MB design by eliminating target-dependent performance and introducing ratiometric functionality[98] by redesigning the stem domains. Our new ratiometric fluorescent probe design exhibits high sensitivity and signal stability. Lastly, we demonstrate that our new probe is robust to changes of the target-binding domain by creating probes for a variety of clinically relevant DNA targets as well as demonstrating its specificy by discriminating between targets containing a single nucleotide polymorphism (SNP). These results highlight key concepts to better understand and engineer the behavior of AgNC-based probes for molecular detection.

Results and Discussion

Motivated by our earlier study, we sought to understand why the hairpin design of Xiao *et al.* failed to produce consistent AgNCs for different target sequences in order to create a more universal probe. At first glance, there is no obvious reason replacing the sequence in the loop region should impact the probe's ability to produce a cluster. These probes consist of a synthetic DNA oligomer with three sequence domains (Figure 1): i) a AgNC domain comprised of 12 bases previously shown to independently stabilize a red emitting AgNC,[13,34] ii) a 30 base loop domain complementary to DNA targets, and iii) a 7 base 'blocking' domain. In its hairpin state, the AgNC domain is hybridized with the blocking domain, inhibiting cluster formation ('off' state). Conversely, the probe produces a cluster after hybridization with target DNA liberates the AgNC domain from the stem ('on' state). Like a MB, changing the binding sequence contained in the loop should not affect target binding or

the conformational change provided the sequences have similar length and GC content.[93] As long as the 12-base AgNC region is left the same, the cluster produced is not expected to change. However, our previous work involving multiplexing this probe design for a separation based assay proved otherwise. We revisit these probes in our current work to better understand their mode of failure. We replace the 30 base loop region for HBV target binding to produce probes with sequences complementary to a common sequence targets for Hepatitis A (HAV) as well as four different regions of a common domain for Hepatitis C (HCV1, HCV2, HCV3, HCV4).[81–84,96]

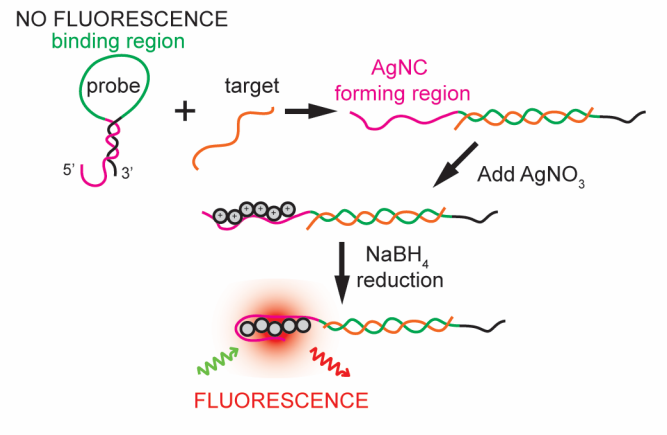

Figure 4-1 Schematic representation of DNA detection via AgNC formation on a hairpin DNA.

We find that the probes containing binding regions for HAV and HCV, both with and without target present, exhibit markedly different fluorescence behavior than the original probe for HBV. Fluorescence emission scans (Figure 2) of samples containing the different probes under 260 nm illumination[57] reveal that although the HBV probe produces strong red fluorescence after binding target, as reported previously, only 2 of the other 5 NC12 probes

produce clusters with sufficient fluorescence after binding (red solid lines). Of these, HAV produces clusters with a similar 600 nm peak emission as the HBV, whereas the HCV3 probe produces clusters with an emission peak at 640 nm. Figure 2 also shows that the probes for HBV, HCV1 and HCV3, contrary to their intended design, produce clusters in their unbound hairpin configuration (blue solid lines). These clusters have different peak emission (570 nm (HBV), 650 nm (HCV1), 630 nm (HCV3)), indicating that a different cluster is produced in each case. Despite producing AgNCs in their 'off' state, it should be noted that these particular hairpins can still serve as fluorescent turn-on probes by appropriate choice of excitation and detection wavelength and produce relatively low background and high signal enhancement for samples containing target (Figure 2c-d). However, this behavior is not universal because the three remaining target sequences (HCV1, HCV2 and HCV4) fail to produce clusters after binding target and cannot function as fluorescent probes.

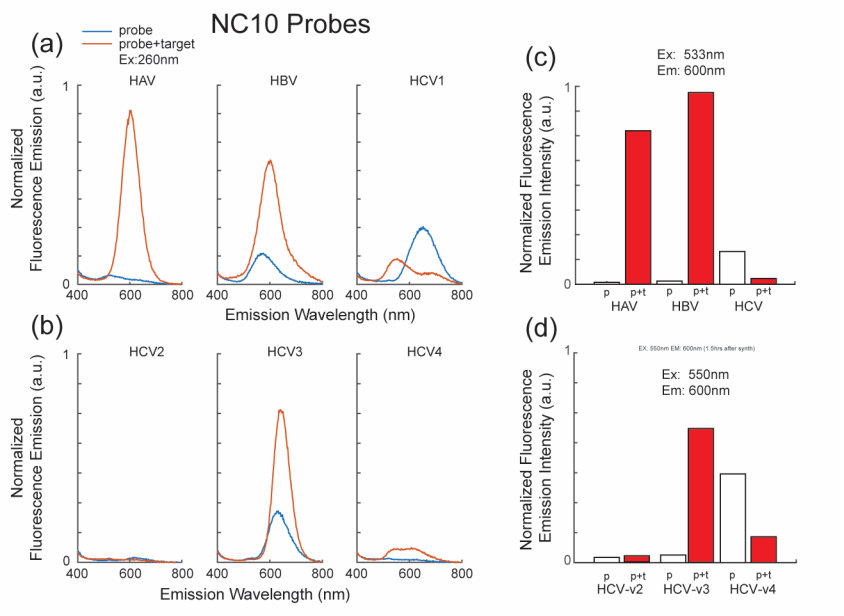

Figure 4-2 Fluorescence emission of NC12 MB-AgNC probes. (a)-(b) Fluorescence emission spectra of samples containing probes both with (blue) and without (red) target DNA under 260 nm illuminaiton. (c)-(d) Fluorescence emission intensity of NC12 probes under peak visible excitation illumination. Only HAV, HBV and HCV1 exhibit low background and high fluorescence enhancement when binding target.

The variation between AgNCs produced by the different NC12 probes points to a dependence of cluster formation on bases contained within the target binding sequence. Perturbations to bases nearby a cluster forming domain are known to influence cluster formation and fluorescence.[36] Although leveraged for sensing in other probe designs,[30,37] this behavior would prevent the hairpin probe from being easily modified for arbitrary target sequence. To determine whether adjacent bases influenced cluster formation in the hairpin probes, we created probe variants (NC12-4T) that include a 4 thymidine sequence as a spacer between the AgNC and binding domains to disrupt any synergistic capacity for the two to stabilize a cluster together. We chose thymidine for its negligible affinity for silver ions,[15,19,56] making it an excellent candidate for bisecting two portions of the probe sequence

without directly altering the stoichiometry between the bases and silver ions and provide roughly a nanometer separation[99] between the bases contained in the two different regions. After the addition of AgNO3 and reduction, all of the NC12-4T probes failed to produce significant fluorescence regardless of whether target DNA was present (Figure 3), including the probe for the original HBV target, confirming that the 12-base AgNC domain relies on the recruitment of bases in the binding region to stabilize a cluster. This behavior is surprising considering that previous reports show this 12-base sequence stabilizes a cluster on its own.[13] Despite using the same buffer conditions as our current work, the sequence produced yellow clusters exhibiting fluorescence excitation and emission peaks at 475 nm and 540 nm respectively, a 60 nm shift compared to the NC12 HBV probe. A possible explanation for this discrepancy is that the 12-base sequence produces yellow clusters via the formation of a homodimer, a common phenomenon for AgNCs stabilized using strands containing fewer than 16 bases.[16,17,43] Dimerization is likely inhibited when the 12-base sequence is incorporated into the large NC12 hairpin probe at lower concentrations, preventing formation of the yellow clusters. Additionally, this 12-base sequence appears in an aptamer probe design that produces strong red fluorescence emission at 630 nm only after a conformational change puts it in close proximity to a G-rich sequence,[27] further supporting the notion that additional bases are required to produce a viable AgNC.

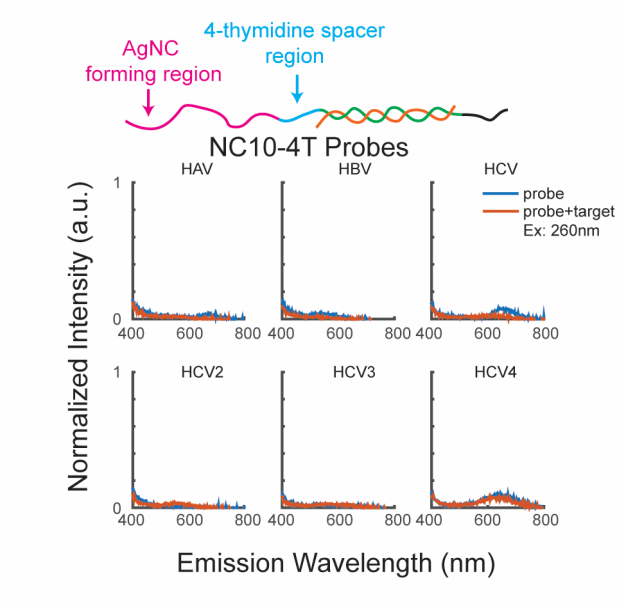

Figure 4-3 Fluorescence of NC12 probes containing a 4T spacer sequence between AgNC domain and binding domain. Introducing this spacer caused all probes to fail to generate a AgNC bother before and after binding target.

An ideal AgNC hairpin probe would be universal, allowing for easy swapping of binding domains, while providing a consistent, ratiometric signal by producing clusters with different fluorescence emissions in its hairpin and bound states. To achieve this, we redesigned the sequences contained within the AgNC formation and 'blocking' domains of the previous hairpin design (herby referred to as NC22). We replaced the 12-base AgNC domain of the original NC12 probe with a 22-base sequence. This sequence was previously shown to produce a bright red emissive cluster even when incorporated into larger DNA structures using a 4 thymidine linker,[100,101] making it a logical candidate for our universal probe. Choosing a longer domain sequence also means that it could contain a subdomain capable of forming a different cluster when hybridized to the blocking domain in the stem, providing a ratiometric signal. We also increased the length of the 'blocking' domain from 7 to 10 bases.

We did this for two reasons: i) a 10 base stretch incorporates more of the C and G bases in the AgNC domain to minimize unwanted clusters, and ii) the resulting ratio of loop length to stem length is more consistent with those of optimized molecular beacons previously reported to improve hairpin stability.[102] Increasing the 'blocking' domain to 22 bases so that it completely hybridizes with the AgNC domain would both inhibit the hairpin from binding target as well as eliminating the chance of forming a cluster for a ratiometric signal. We also removed 5 bases from the 3' end of the target-binding domain to reduce overall probe length, thereby decreasing the cost and increasing the chemical yield of the DNA synthesis. This did not inhibit the probes from binding to their original targets.

Because the blocking domain is shorter than the AgNC domain, there are many locations along the AgNC domain that it can hybridize. To explore what effects the 'blocking' domain sequence has on probe behavior, we create 3 different versions of our NC22 probe, each with a 'blocking' domain complementary to a different portion of the AgNC domain. The three variants, shown schematically in Figure 4, are labeled as 5'-block, mid-block and 3'-block to indicate the region of the AgNC domain blocked in the hairpin state. Using an HCV1 binding domain (which failed to produce a cluster bearing probe using the original NC12 design), we measured the fluorescence of AgNCs produced by each version of the NC22 probe with and without added target. Each version of the NC22 probe produces an AgNC with the same red fluorescence peaked at 640 nm when bound to target but exhibited different fluorescence behavior in the absence of target (Figure 4). The 5'-block design forms AgNCs with bright red emission of similar spectra and intensity regardless of whether target DNA was present, therefore a poor probe candidate. The mid-block design exhibits a fluorescence enhancement

in the presence of target, providing a 'turn-on' signal to indicate target binding. Lastly, the 3'-block design leaves exposed a subdomain that forms AgNCs that emit strong green fluorescence in the hairpin state, which is easily distinguished from the red fluorescence produced in its bound state. The intensities from these two fluorescence channels can provide a ratiometric signal to indicate relative amounts of both bound and unbound probe, leading to improved sensitivity, quantitation and reduced environmental variability.

The ability of the NC22 design to harbor a different AgNCs in its hairpin state (Figure 5a) is a result of the bases left unpaired in the NC22 sequence. In its hairpin state, 12 bases are left unpaired on the 5' end: TTCCCACCCACC. Excluding the first two T's, this 10-base sequence is a subsequence of several 16 base sequences previously shown to stabilize fluorescent silver nanoclusters, albeit with near infrared emission.[17,103,104] However, mass spectrometry revealed these clusters formed from homodimers of these strands, which could account for the significant spectral difference.[17] The NC22 hairpin produces higher energy clusters likely because it does not recruit additional bases through dimerization. The NC22 probe is less likely to dimerize given the lower concentrations used as well as possible steric effects related to the other domains of the probe. Other factors that could contribute to this discrepancy are differences in buffering salts (Na+, PO4-, PO3- vs. NH4+, OAc-) and stoichiometry. Conversely, when the full 22-base sequence is available after binding, the probe produces clusters with similar excitation and emission to those demonstrated by Schultz *et al.*[17]

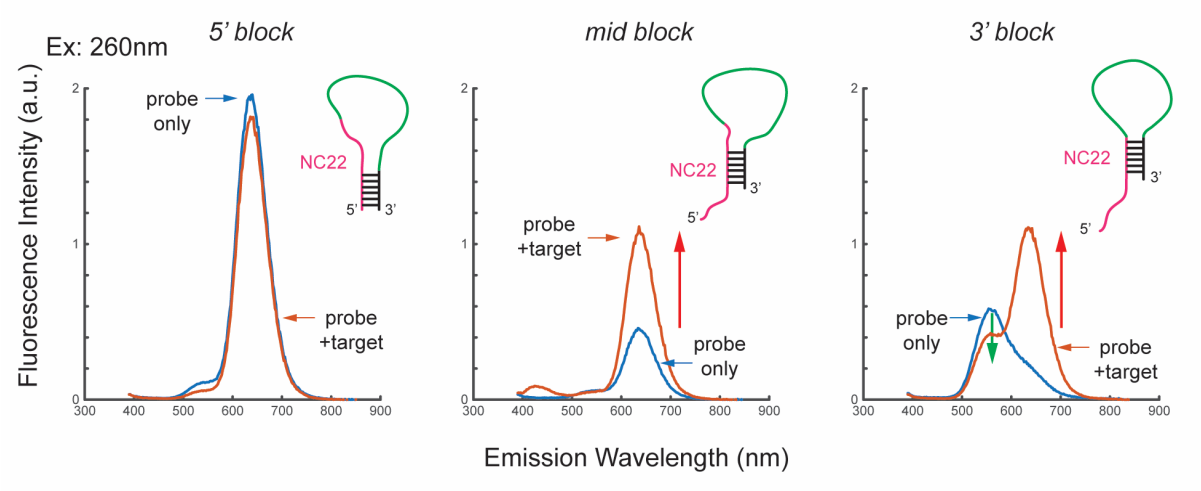

Figure 4-4 Fluorescence emission behavior of NC22 probes with blocking domains complementary to different regions of the AgNC formation domain. Samples were excited using 260 nm illumination.

We assessed the use of the 3'-block NC22 design as a ratiometric detection strategy and quantified the sensitivity of the probe by exposure to different concentrations of target DNA. Ratiometric fluorescence was obtained by on-peak excitation and fluorescence collection for the two distinct cluster channels. As target concentration increases (Figure 5a), fluorescence intensity from green clusters decreases, corresponding to fewer probes remaining in the hairpin conformation. Conversely, fluorescence intensity from red clusters increases, corresponding to a greater proportion of probes hybridizing to target DNA. Figure 5b shows ratiometric fluorescence emission ($F_R/[F_R+F_G]$) for the HCV1 probe is a linear relationship of probe to target DNA concentration. This ratiometric fluorescence emission provides a self-calibrating metric to measure target DNA concentration from 400 nM to 4 μm using 4 μM of probe. Using a lower concentration of probe (150 nM, Figure 4c), target concentrations ranging from 9.4 nM to 150 nM are easily detected with a calculated limit of detection

($3\sigma_{STD,noise}$) of 8.9 nM, which is comparable to the detection limit of typical fluorophore-quencher based molecular beacons.[105,106]

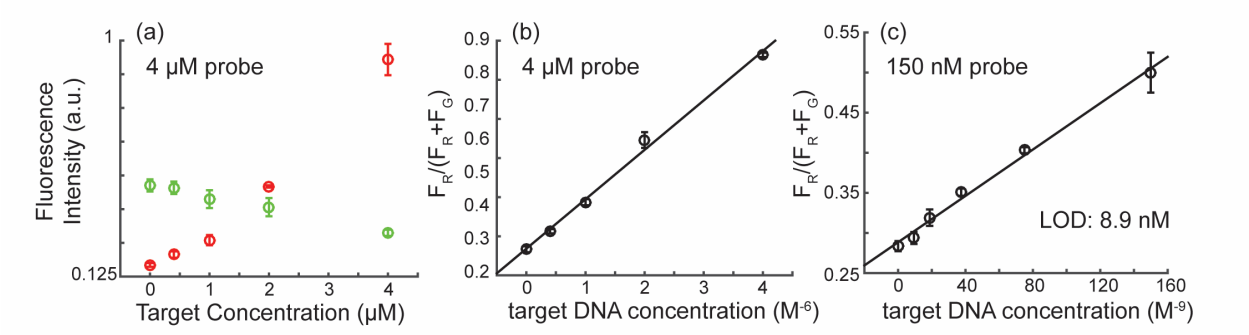

Figure 4-5 (a) Green and red fluorescence emission versus target concentration for NC22 probe for HCV1 target. Error bars indicate the standard deviation of three separate samples. (b),(c) Ratiometric fluorescence emission is sensitive (8.9 nM LOD) and linear.

An additional benefit of using a ratiometric measurement is that quantification of target DNA concentration can be made independent of time. Silver nanoclusters stabilized by DNA are often incubated for potentially hours after reduction to allow for cluster formation.[96,107] Figure 6a shows fluorescence intensity of both the green (hairpin) and red (target-bound) AgNCs stabilized by our HCV1 probe increases by an order of magnitude over 12 hours after chemical reduction as the nanoclusters mature. In addition, some silver nanoclusters are known to oxidize over time, with consequent changes in emission spectrum and/or intensity,[51] further complicating a quantitative measurement. For probes that rely on generating AgNCs,[34,96] the reaction needs to equilibrate before a quantitative measurement can be made. Our ratiometric probe eliminates this complication and allows for immediate fluorescence quantification. Ratiometric fluorescence varies by less than 0.2% from its mean

over the course of 12 hours (Figure 6b). Additionally, fluorescence onset occurs almost immediately.

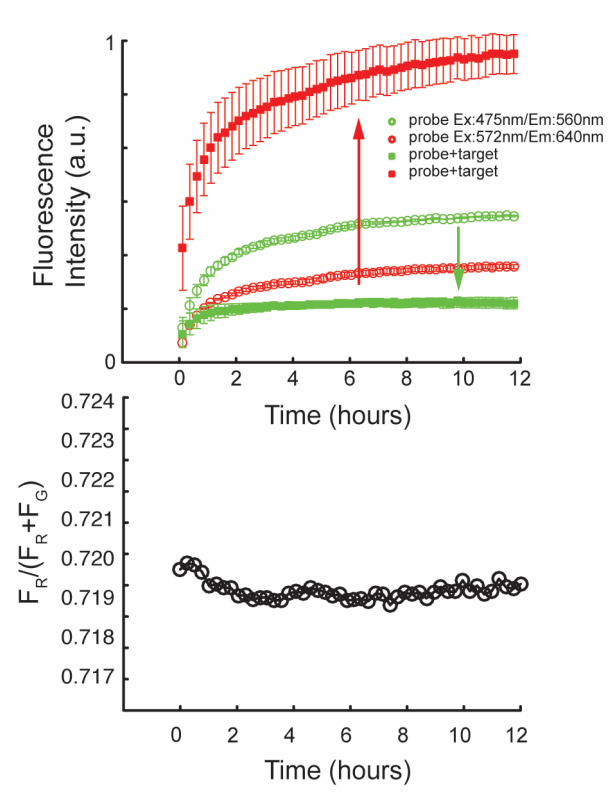

Figure 4-6 (a) Fluorescence intensity of HCV1 probe measured over time after reduction. Fluorescence intensity of the peak red and green emission increases as the clusters form over 12 hours. (b) The ratiometric fluorescence of the probe+target remains constant over time, with a variation of 0.2% from the mean, allowing for quantification within minutes.

Having confirmed the ratiometric capabilities of our new design, we next determined whether the NC22 probe produces a consistent cluster for the different target sequences previously tested using the NC12 probes. Figure 7 shows fluorescence excitation and emission scans of 3'-block NC22 probes containing binding domains for HAV, HBV and HCV1 target sequences. Each NC22 probe produces clusters with the same peak wavelength regardless of the sequence in the binding region both before and after binding target. In its

hairpin form, each 3'-block NC22 probe produces predominantly green emitting fluorescent AgNCs with a peak excitation of 475 nm and peak emission of 550 nm. In its bound form, with an equimolar amount of respective target, the probes produce red emitting AgNCs with peak excitation at 572 nm and emission at 640 nm, accompanied by a decrease in the green fluorescence. We observe similar behavior for NC22 probes containing binding domains for the additional HCV target sequences (see appendix Figure IV-1), showing that it works for all of the binding sequences we tested using the NC12 probes.

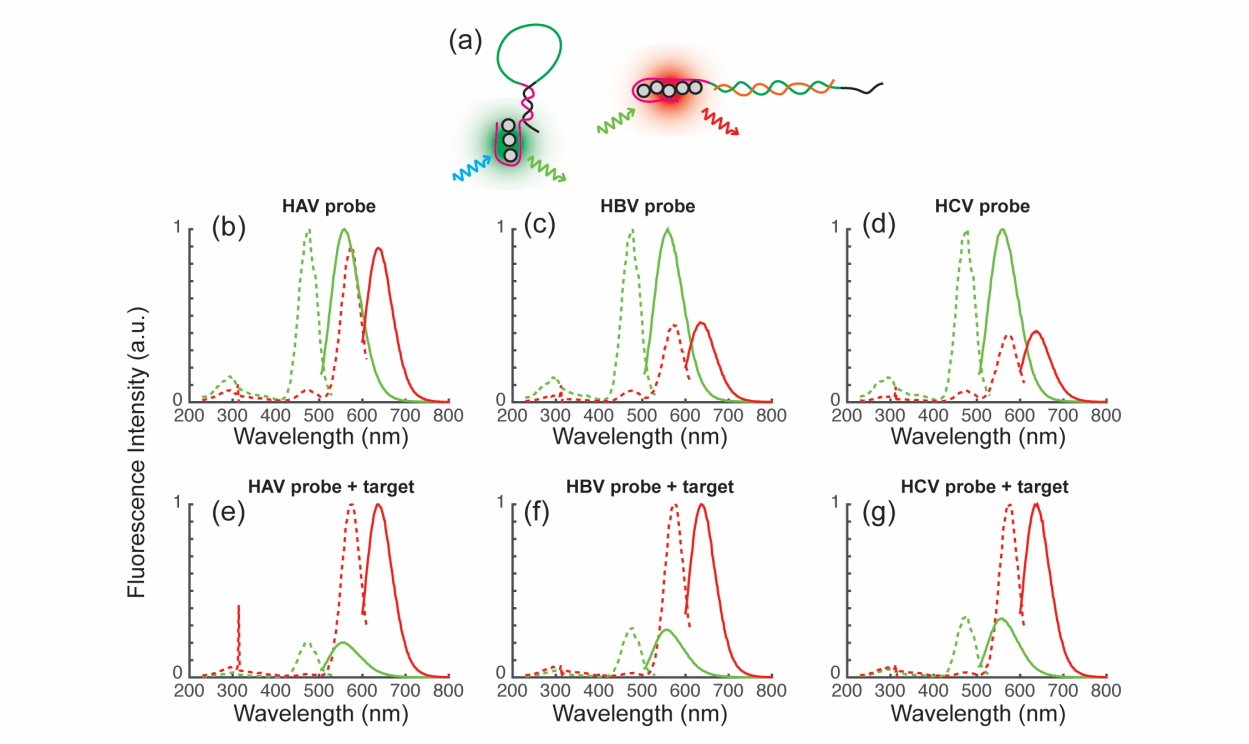

Figure 4-7 (a) Schematic representation of the ratiometric AgNC DNA probe. (b)-(d) Excitation (dotted line) and emission (solid line) spectra for different AgNC DNA probes in their hairpin state. Each contains a different binding domain. (e)-(f) Excitation and emission spectra for each AgNC DNA probe after binding target. Green fluorescence decreases while red fluorescence emission increases in the presence of target.

The robustness of the NC22 domain suggests our probe design might adapt to a diverse array of biologically and clinically relevant targets of different lengths. Figure 8a shows the fluorescence emission of an NC22 probe designed to bind the DNA analog of miRNA182, a miRNA whose targets, regulation and expression are relevant to various cancers, neurological disorders, as well as sepsis.[108–111] Additionally, we can design the probes to discriminate mutations with high specificity. A probe designed to bind to the *HRAS* gene containing a single base mutation associated with a bladder cancer[112,113] easily discriminates

between mutant and wild-type targets in a mixture with a discrimination factor ($[F_{red,mut}-F_{red,background}]/[F_{red,wt}-F_{red,background}]$) of 23.45 (Figure 8b).

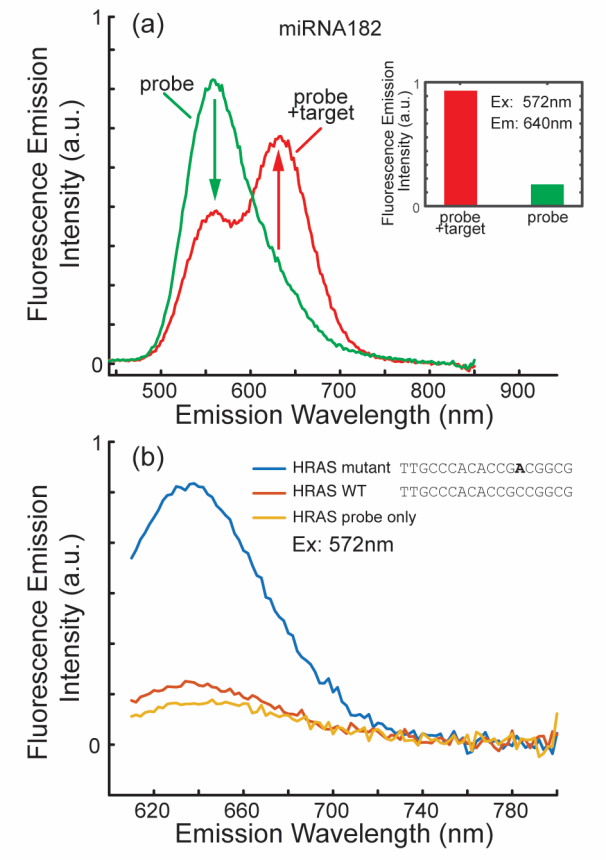

Figure 4-8 (a) Fluorescence emission of an NC22 probe for a DNA target of miRNA182 under 260nm excitation. (b) Fluorescence emission of an NC22 probe selective for the mutant form of the *HRAS* gene.

Although our design improves upon previous AgNC hairpin probes, they still suffer from drawbacks common to many AgNC based sensors. AgNC synthesis is highly susceptible to variations in buffer composition and pH, which potentially limits the range of environments in which it can be used as an assay. Also, because synthesis is performed after probe binding, it is not amenable to real time monitoring of target production, such as PCR amplification

products. This may also limit its applications for *in vivo* monitoring of target concentration. However, for one-shot, target quantification in controlled *in vitro* conditions, our probe provides a robust, low-cost and viable alternative to MBs.

Materials and Methods

Preparation of silver nanoclusters

Probe and target DNA strands were purchased from Integrated DNA Technologies, Inc. (Coralville, IA, USA) with standard desalting and rehydrated with 18.2 MOhm cm deionized water (DI, MilliQ, Millipore) and stored at 100-500 μM at –20° C. Sodium phosphate buffer was prepared as a 10x stock at 200 mM at pH 7.5 by combining solutions of sodium phosphate monobasic and sodium phosphate dibasic (Fisher Scientific, ACS certified) in MQ DI. pH was measured using an Oakton pH 11 series meter with dual junction electrode. Silver nitrate (Sigma Ultra) and sodium borohydride pellets (Aldrich, 99.99%) were purchased from Sigma Aldrich.

AgNC generation using NC12 probes was adapted from[34,96] and prepared as follows: frozen DNA stocks were allowed to thaw at room temperature followed by vortexing. 3 μL of 500 μM probe was combined with 32.2 μL of 20 mM sodium phosphate buffer. Probe and buffer were heated to 90° C for 5 minutes and then snap cooled in an ice bath. 3 μL of 500 μM target (or 3 μL of DI water for target-less control samples) was added to probe and buffer samples, vortexed and allowed to incubate at room temperature for 1 hour in the dark. An addition of 0.9 μL of 10mM $AgNO_3$ to each sample was followed by a 20 minute

incubation at room temperature in the dark before chemical reduction using 4.5 μL of 2 mM $NaBH_4$ in 0.1 mM NaOH and vortexing. After reduction, samples were storage at room temperature in the dark until fluorescence characterization. The final concentrations were 34.4 μM DNA, 206 μM $AgNO_3$ and 206 μM $NaBH_4$ ([DNA probe]:[AgNO3]:[NaHB4] = 1:6:6).

AgNC generation using NC22 probes was adapted from[100] and prepared as follows: frozen DNA stocks were allowed to thaw at room temperature followed by vortexing. 1.5 μL of 500 μM probe was combined with 31.88 μL of 20 mM sodium phosphate buffer. Probe and buffer were heated to 90° C for 5 minutes and then snap cooled in an ice bath. 1.5 μL of 500 μM target (or 1.5 μL of DI water for target-less control samples) was added to probe and buffer samples, vortexed and allowed to incubate at room temperature for 1 hour in the dark. An addition of 0.75 μL of 10mM $AgNO_3$ to each sample was followed by a 20 minute incubation at room temperature in the dark before chemical reduction using 1.875 μL of 2 mM $NaBH_4$ in 0.1 mM NaOH and vortexing. After reduction, samples were storage at room temperature in the dark until fluorescence characterization. The final concentrations were 20 μM DNA probe, 200 μM $AgNO_3$ and 100 μM $NaBH_4$ ([DNA probe]:[AgNO3]:[NaHB4] = 1:10:5). We obtained similar results using a modified procedure that maintained the same concentration ratios (10 μL of 10 μM probe, 10 μL of 10 μM target, 20 μL of 20 mM buffer, 5 μL of 0.2 mM AgNO3, 5 μL of 0.1 mM NaBH4). For sensitivity measurements, the final concentration of AgNO3 and NaBH4 were scaled with concentration of probe (4 μM or 150 μM) to maintain the same concentration ratios. In the presence of 5x excess of target DNA, probe samples failed to produce a fluorescent signal, presumably due to competition between

probe and target for Ag^{+}. For probes designed for the *HRAS* gene target, we included 7 mM citric acid and 2 mM magnesium acetate and raised incubation and reaction temperatures to 30° C to improve discrimination between mutant and wildtype targets.

Fluorescence spectroscopy

Fluorescence excitation and emission spectra and intensities were obtained using a Tecan infinite 200Pro plate reader with Tecan i-control software (Tecan Group Ltd.) between 1 and 5 hours after chemical reduction of samples. The step size and bandwidth were set to 2 nm and 20 nm for emission scans, and for 5 nm and 5-10 nm for excitation scans and were performed using Top Mode. The gain was kept constant for characterization experiments (105 for 260 nm scans and 75 for visible excitation). For sensitivity measurements, the gain was optimized for the samples containing the highest concentration of target and then held constant for remaining samples. For time series fluorescence data, the 384 well plates (black, clear-flat bottom, Part 3540, Corning, Inc.) were covered with transparent tape and measured using Bottom Mode. Empty wells were also processed to check for autofluorescence of the wellplate and tape. Peak excitation and emission wavelengths were obtained by fitting Gaussian distributions using Matlab (The Mathworks, Inc.).

Conclusions

We demonstrate a rational design for a universal, label-free DNA probe that generates spectrally distinct AgNCs in its bound and unbound states. We find that hairpin DNA probes previously shown to generate fluorescent AgNCs upon binding target behave unpredictably for different targets, limiting their effective use. This behavior is due to the recruitment of

bases from the binding domain for cluster formation. Through optimization of the stem portion of the hairpin DNA, the probe produces a green emitting AgNCs in its hairpin state, and a red emitting AgNC after binding to its respective target. We find that the design provides a consistent and robust ratiometric signal regardless of the choice of binding sequence incorporated into the loop portion of the hairpin, a significant improvement over previously demonstrated designs. The ratiometric signal is constant through time, allowing for rapid quantification of target DNA concentration within minutes and can serve as a low-cost alternative to common molecular beacons for rapid DNA detection.

Chapter 5

Additional applications and characterization of DNA-AgNCs – Preliminary Studies

Fundamental understanding of DNA-AgNCs formation and its dependence on strand sequence is still in its infancy,[20] as is the potential for applications. In this final chapter, preliminary projects and results are presented to motivate future research directions. First, preliminary work using DNA-AgNCs as fluorescent sensors to detect the neurotransmitter dopamine is presented. Second, changes in the optical and conformational properties of AgNCs when T substitution mutations are placed in different regions of the template sequence are reported. Finally, we present preliminary microfluidic capillary electrophoresis data showing changes in conformational heterogeneity of a dye labeled template after addition of $AgNO_3$ and chemical reduction.

DNA-AgNCs as sensitive and specific probes for the detection of dopamine

The results of Chapter 2 highlight the inherent sensitivity of AgNC fluorescence on perturbations made to the template sequence. This sensitivity has enabled the use of DNA-AgNCs as novel sensors for a variety of molecules that interact directly with the DNA stabilizing strand, e.g. DNA detection, single nucleotide polymorphism detection,[23,114] as well as metal ions and other molecules that interact with either the DNA backbone, bases or the silver core.[115] These properties make DNA-stabilized AgNCs ideal candidates for

developing novel optical sensors for biologically relevant small molecules, such as neurotransmitters.

Neurotransmitters (NTs) are a class of small molecules used throughout the nervous system for signaling pathways and are critical to brain function. The relative concentrations and regulation of neurotransmitters within the brain are important for understanding and detecting a number of neurological and neurodegenerative disorders including depression and Parkinson's.[116] While electrochemical methods provide sensitive detection of neurotransmitter uptake and release *in vitro*,[117] the need to place electrodes near cells of interest greatly limits its application for analyzing neurotransmitter release and uptake deep within the brain, which is necessary for *in vivo* studies. For this reason, less invasive spectroscopic methods are necessary for studying neurotransmitters within the brain in real time. Specific binding and fluorescence sensing of neurotransmitters using optically active nanomaterials is an emerging and promising approach towards *in vivo* methods.[118–120]

To evaluate the potential for using DNA-AgNCs to sense specific neurotransmitters, we screened a library of 8 neurotransmitters and 6 different DNA-AgNCs. The specific AgNC template sequences used were those from literature that were readily available at the time. Figure 5-1a shows the emission spectra of 4 of the DNA-AgNCs prepared in 20 mM sodium phosphate buffer (pH 7.5). Strand 2 and 3 exhibited similar fluorescence emission to Strand 1 and were omitted from the plot for clarity. To determine whether neurotransmitters disrupt AgNC fluorescence, we investigated two approaches: adding neurotransmitters to samples containing pre-formed fluorescent DNA AgNCs (Method 1); and adding the neurotransmitters to DNA solutions prior to the formation of the AgNCs (Method 2). We

expect that interactions between the NTs and DNA-AgNCs using either of these methods will lead to either enhancement or quenching of fluorescence, represented schematically in Figure 5-1b.

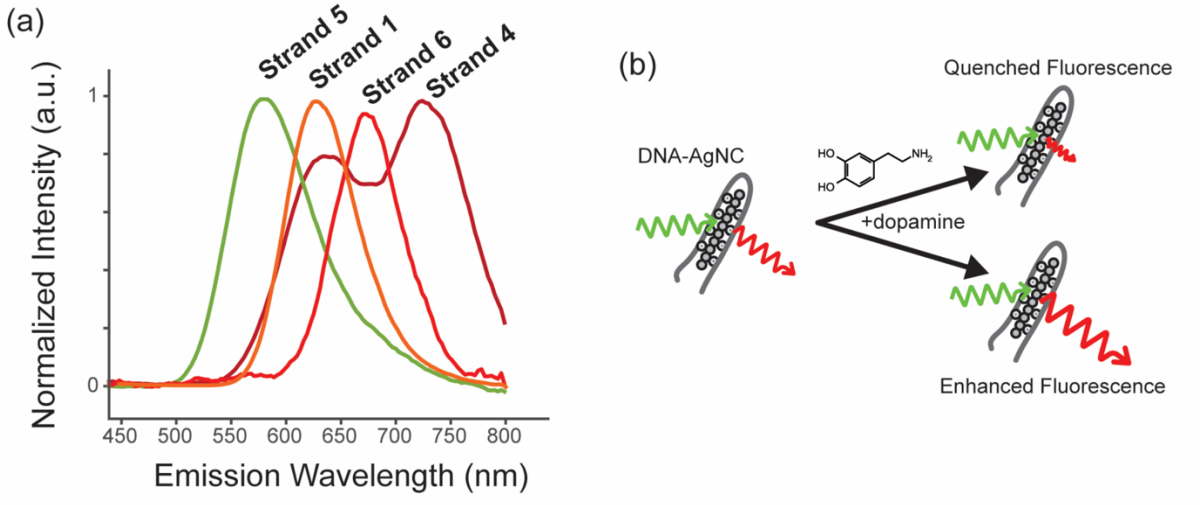

Figure 5-1 (a) Fluorescence emission spectra for AgNCs prepared using the different DNA strands used in this study. AgNCs were prepared in sodium phosphate buffer at pH 7.5 and excited using 260 nm light. (b) Schematic representation of the effect of dopamine on cluster fluorescence. We find that depending on conditions, dopamine either quenches or enhances fluorescence emission of DNA-AgNC samples.

Figure 5-2 shows the relative change in fluorescence, $(F-F_0)/F_0$, for each DNA-AgNC in the presence of each neurotransmitter added either before or after cluster synthesis, all performed in sodium phosphate buffer (pH 7.5). When the neurotransmitters were added to each strand prior to synthesis, we found that dopamine strongly and selectively quenched the fluorescence of the AgNCs formed using Strands 1, 2 and 3, while enhancing the fluorescence only of those generated by Strand 4. When added after cluster synthesis, dopamine selectively quenched the fluorescence of AgNCs generated by Strands 2, 3, and 5. AgNCs generated using Strand 4 exhibited a moderate fluorescence enhancement in the

presence of epinephrine. In these cases, the other NTs either had a negligible or contrasting effect on AgNC fluorescence compared to dopamine, which demonstrates its specificity.

The relative intensity change ($[F-F_0]/F_0$) for the AgNCs in the presence of NTs (Figure 5-2a,b) were calculated by measuring the peak emission at peak excitation (Figure 5-1) for each specific cluster in the absence of NTs (F_0) and then measuring the fluorescence for the same wavelengths in the presence of NTs (F). For this reason, if the NTs induced a chromatic shift in fluorescence excitation or emission, the fluorescence emission of the cluster would decrease and provide a greater differential signal. This was found to be the base in at least several cases. For example, Figure 5-2c shows that addition of dopamine to Strand 5 AgNCs both decreases fluorescence by approximately 75% and induces a shift in peak emission from 600 nm to 560nm under 260 nm illumination. Figure 5-2d shows the same sample, but excitation and detection wavelengths are fixed at the peaks for the unperturbed Strand 5 AgNC. The change in fluorescence is reflected by a nearly 2 order of magnitude decrease in fluorescence emission at these wavelengths.

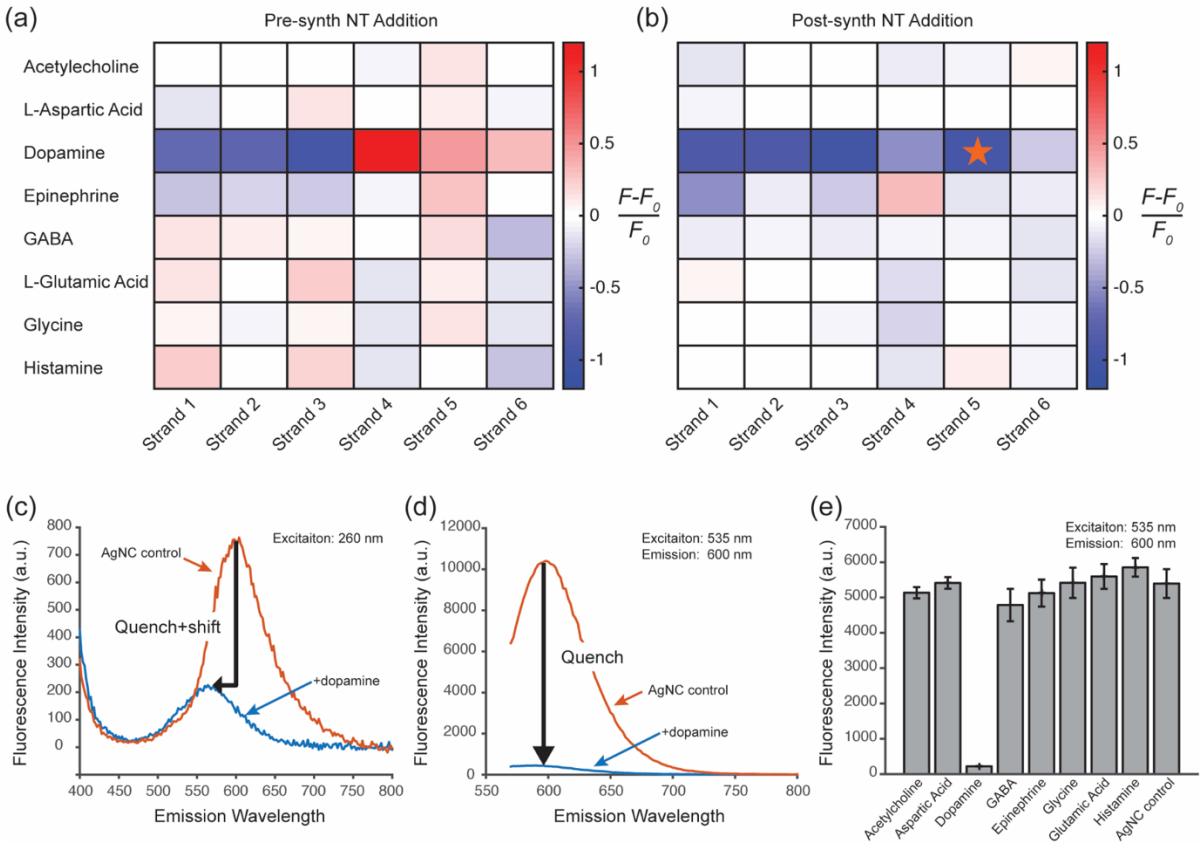

Figure 5-2 Relative fluorescence intensity changes for DNA-AgNCs in the presence of different NTs added prior to (a) or after (b) cluster synthesis. The star indicates the NT and Strand # combination shown in (c) and (d). (c) UV illumination of samples with and without dopamine showing a change in intensity and peak wavelength. (d) Exciting on peak shows that fluorescence emission is quenched by an order of magnitude in the presence of dopamine. (e) AgNCs stabilized using Strand 5 excited at peak in the presence of different NTs added after synthesis. Error bars indicate the standard deviation of n=3 replicate experiments.

To test further the selectivity of DNA-AgNCs for NTs, we compared the fluorescence of AgNCs generated by Strand 4, which we found to be specifically and strongly quenched by dopamine, to samples containing structural homologues of dopamine and species known to interfere with dopamine binding: DOPAC, l-DOPA, l-tyrosine, l-tryptophan, phenylalanine and urica acid.[118,121] Figure 5-3 shows the emission intensity of samples containing Strand 4 AgNCs mixed with different potential interfering compounds, along with dopamine and a

control containing only Strand 4 AgNCs in buffer. None of the compounds produced a significant fluorescence response, indicating a highly specific interaction between dopamine and the DNA-AgNC when added before or after synthesis.

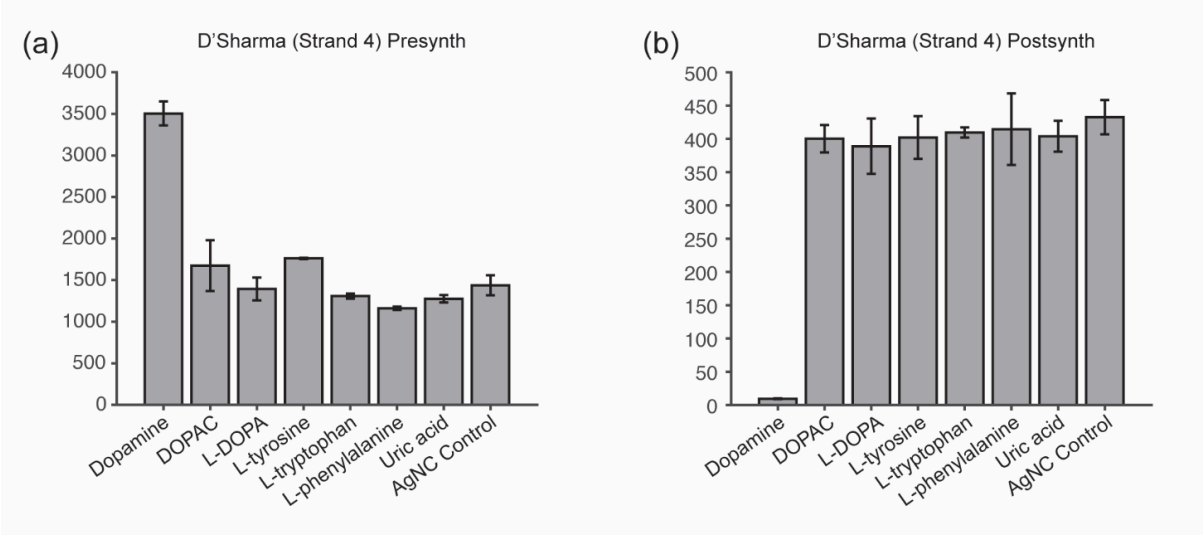

Figure 5-3 Fluorescence response of Strand 4 AgNCs in the presence of dopamine along with structural homologues and binding competitors for dopamine. Only dopamine is shown to significantly enhance (when added prior to synthesis) or quench (when added after synthesis) fluorescence. Fluorescence emission was recorded at a wavelength of 610 nm using 520 nm excitation.

Although the above results show that dopamine selectively enhances or quenches cluster fluorescence in sodium phosphate buffer, the precise mechanism is unclear. Strands 4, 5 and 6 exhibited opposite responses to dopamine depending on whether it was added before or after synthesis. Enhanced fluorescence was observed when adding dopamine prior, while we observed quenched fluorescence when adding dopamine after the addition of silver and reduction with borohydride. This may suggest that the dopamine is interacting directly with

the DNA, rather than binding with Ag^{+} or Ag^{0} and skewing the AgNC reaction stoichiometry. If the latter were the case, we would expect universal quenching of fluorescence when dopamine is added in excess prior to synthesis. Therefore, the dopamine is likely binding to or reacting with the DNA. This could result in a conformational change, or a chemical modification to the bases, that affects the strand's efficacy to stabilize a cluster, or perturb the fluorescence of a cluster that has already formed. Interactions between dopamine and DNA have been previously observed to produce adducts and cleavage, which would dramatically alter cluster fluorescence and stability.[120,122–124]

The changes in AgNC fluorescence we observe with dopamine are not universal to catecholamines, as we see dissimilar or no response with epinephrine and the dopamine derivatives. This suggests that the terminal amine plays a critical role in the responses we observe. Future experiments comparing the AgNC fluorescence response in the presence of catechol and propylamine or other derivatives may be necessary to determine the details of binding.

A possible explanation for the specificity we observe is that the DNA adopts a particular conformation that binds dopamine, akin to a DNA aptamer.[125] However, the similarity in fluorescence response observed for strands with substantially different sequences makes it unlikely that they adopt similar conformations. Further characterization using NMR and circular dichroism spectroscopy would be necessary to better understand how the interaction between dopamine and these DNA sequences influences cluster fluorescence.

This preliminary work shows the potential for specific detection of dopamine using DNA stabilized AgNCs, but further work is necessary to completely evaluate their efficacy in real-

world applications. For example, we must quantify the sensitivity and the dynamic range of the fluorescence response to determine whether biologically relevant concentrations and changes can be detected efficiently. Furthermore, reversibility of binding is also an important requirement, especially for developing real-time fluorescent sensors for monitoring neurotransmitter levels *in vivo*. One method to test whether the observed AgNC fluorescence responses are due to an irreversible reaction or whether it can be modulated over time is to use a flow cell using tethered AgNCs and washing through different concentrations of dopamine.

Materials and Methods

Chemicals were purchased from Sigma Aldrich (St. Louis, MO, USA) unless otherwise noted. Dopamine hydrochloride (Sigma), Acetylcholine chloride (≥99% TLC), Histamine dihydrochloride (≥99.0% (AT)), γ-Aminobutyric acid (GABA) (BioXtra, ≥99% (Sigma)), L-Aspartic Acid (reagent grade, ≥98% (HPLC)), Glycine (from non-animal source, meets EP, JP, USP testing specifications, suitable for cell culture, ≥98.5%), Epinephrine hydrochloride (Sigma), L-Glutamic acid (*ReagentPlus*®, ≥99% (HPLC)), Uric acid (≥99%, crystalline (Sigma)), 3,4-Dihydroxy-L-phenylalanine (L-DOPA) (≥98% (TLC) (Sigma)), L-tryptophan (reagent grade, ≥98% (HPLC) (Sigma-Aldrich)), L-Tyrosine (BioUltra, ≥99.0% (NT) (Sigma)), Homovanillic acid (Fluorimetric reagent), 3,4-Dihydroxyphenylacetic acid (DOPAC) (98% (Aldrich)), L-Phenylalanine (reagent grade, ≥98% (Sigma-Aldrich)), (−)-Norepinephrine (≥98%, crystalline (Sigma)). Solutions were prepared as 10 mM to 100 mM aqueous stock solutions at 4°C.

Silver nitrate (Sigma Ultra), Sodium borohydride (Aldrich 99.99%, pellets) and sodium hydroxide (Fisher Scientific, Certified ACS, pellets) solutions were prepared fresh for AgNC synthesis.

DNA oligos purchased from Integrated DNA Technologies, Inc. (Coralville, IA, USA), were hydrated with MilliQ deionized water (DI), and stored at -20°C in stock concentrations of between 100 μM and 1 mM. Sodium phosphate buffer was prepared at a pH of 7.3 and concentration of 200mM by titrating solutions of sodium phosphate monobasic and sodium phosphate dibasic (Fisher Scientific, Waltham, MA, USA).

Strand 1: CGTGTCCCCCCCCGATTTTTATCGGCCCCCCACACG [126]

Strand 2: CGTGACTGTACCCCCCCCCCCCTACAGTCACG [126]

Strand 3: GCACAGGCTACCCCCCCCCCCCTAGCCTGTGC [126]

Strand 4: ACCCGAACCTGGGCTACCACCCTTAATCCCC [127]

Strand 5: GGGTTAGGGTCCCCCCACCCTTACCC [45]

Strand 6: TTCACCGCTTTTGCCTTTTGGGGACGGATA [17]

Solutions containing DNA were prepared by combining 25 μL of a 100 μM solution of DNA with 50 μL of 20 mM sodium phosphate buffer and then heated at 90 °C for 5 min. The solution was then snap cooled by running the sample tube under cool DI water for ten to twenty seconds.

For **Method 1**, 12.5 μL of 1.6 mM silver nitrate was added to the DNA solution, and allowed to incubate in the dark for ten to twenty minutes. Then, 12.5 μL of freshly prepared 0.8 mM sodium borohydride diluted in 100 μM sodium hydroxide was added to the solution and vortexed. The solution was allowed to react in the dark for sixteen to twenty hours at

4°C. Lastly, 10 µL samples of the DNA AgNCs were placed in a 384-well plate(Product #3821BC, Corning, Inc.) and combined with 10 µL of a 100 µM neurotransmitter solution or DI water as a control. Each sample was prepared in triplicate. The well plate was stored at 4°C until measurements were taken.

For **Method 2**, after annealing DNA solutions, instead of adding silver nitrate, 50 µL of 100 µM solutions of each neurotransmitter (or DI) were added to individual DNA and buffer solutions, and allowed to incubate for fifteen to twenty minutes at room temperature. 12.5 µL of 0.16 mM silver nitrate was then added to each sample. Next, 12.5 µL of freshly prepared 0.8 mM sodium borohydride diluted in 100 µM sodium hydroxide was added to the solution and vortexed. The solutions were left to incubate at 4°C for two hours. Finally, 20 uL of each DNA-AgNC/neurotransmitter solution was placed into wells in a 90-well microplate, which was stored at 4°C until measurements were taken.

Fluorescence excitation and emission spectra and intensities were obtained using a Tecan infinite 200Pro plate reader with Tecan i-control software (Tecan Group Ltd.). Samples where measured between 1 and 5 hours after chemical reduction or after addition of NTs. The step size and bandwidth were set to 2 nm and 20 nm for emission scans, and for 5 nm and 5-10 nm for excitation scans and were performed using Top Mode. The gain was kept constant for characterization experiments (105 for 260 nm scans and 75 for visible excitation). Empty wells were also processed to check for autofluorescence of the wellplate and tape.

Point mutations within common sequence motifs disrupt DNA-stabilized AgNC fluorescence and potentially conformation

Despite the numerous applications that demonstrate the utility of AgNCs,[21,22,24,25,30,36,37] the inability to correlate a given DNA sequence with its ability to stabilize a cluster, or the photophysical properties of a resulting cluster severely limits designing new template strands. Template strand discovery is typically done by modifying or concatenating previously discovered sequences, or just choosing arbitrary sequences that are C- and G-rich.[30] A better understanding of the relationship between DNA sequence and the photophysical properties of the AgNCs they stabilize could eventually lead to robust methods for tailoring their properties to particular applications. Below, we look into the possibility of Ag^+-mediated DNA conformations and their relationship to template sequence and cluster generation.

Until recently, the general rule for generating AgNC template sequences was that they need to be rich in C and G bases. However, a more precise approach was developed by applying machine learning algorithms to fluorescence data collected from AgNCs synthesized from hundreds of 10 base template strands.[20] This statistical approach revealed a set of subsequences, termed bright motifs, that are found to be common in template sequences that stabilize bright AgNCs, as well as dark motifs, which were common to poor template sequences. Biasing random template sequence generation to include bright motifs and exclude dark motifs was found to significantly improve the likelihood of generating a silver nanocluster compared to selecting sequences purely at random.[20] However, despite this improvement, the precise role that these motifs play in cluster formation remains a mystery.

One possibility is that these motifs are related to stable structures adopted by the DNA template, stabilized by Ag^{+}-mediated, non-Watson-Crick base pairing.[128] To investigate this, we systematically study a particular template sequence known to stabilize a bright, stable fluorescent cluster,[16,17] and compared their photophysical and structural differences. In this preliminary work, we used 4 different mutants of the 30 base sequence, RS, that contain a single T substitution (Table 5-1). Two of the T substitutions replace Cs and two replace Gs. Using fluorescence spectroscopy, microfluidic capillary electrophoresis, polyacrylamide gel electrophoresis and circular dichroism spectroscopy, we compare the fluorescence characteristics and conformation of the resulting DNA-AgNCs and discuss how this may relate to the presence of sequence motifs.

Table 5-1 DNA sequence of the original RS cluster strand and the 4 mutants which contain T substitutions at different points along the sequence.

RS_original	TTCACCGCTTTTGCCTTTTGGGGACGGATA
RSmut4	TTCAC**T**GCTTTTGCCTTTTGGGGACGGATA
RSmut12	TTCACCGCTTTTG**T**CTTTTGGGGACGGATA
RSmut19	TTCACCGCTTTTGCCTTTTG**T**GGACGGATA
RSmut25	TTCACCGCTTTTGCCTTTTGGGGACG**T**ATA

The RS and RS mutant strand sequences are outlined in Table 2. Each mutant contains a single T base substitution in a different region of the sequence.

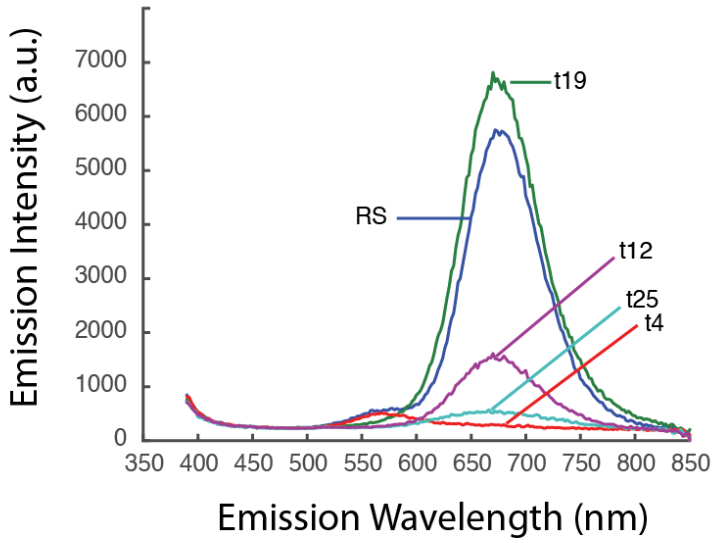

Figure 5-4 Fluorescence emission of AgNCs under 260 nm excitation generated using RS and RS mutant templates in NaOAc buffer, pH 4.8.

The fluorescence emission of the resulting AgNCs produced by each mutant strand after performing a standard AgNC synthesis in sodium acetate buffer (pH 4.8) is shown in Figure 5-4. A stoichiometry of 1:12.5:6.25 for DNA:AgNO3:NaBH4 yielded comparable relative fluorescence intensities to a 1:8:8 synthesis (Appendix, Figure V-1). The clusters generated by the RS strand have a peak excitation wavelength centered at 600 nm and peak emission at 674 nm. Of the mutant strands, mutT19, T25 and T12 exhibit fluorescence emission with similar peak wavelengths but different intensities. mutT19 samples have a 10% higher fluorescence emission intensity, while the mutT12 and T25 strands are both dimmer, roughly 75% and 95% respectively. The mutT4 strand is 95% dimmer as well as having a peak emission wavelength that is shifted to 560 nm. Similar trends in intensity are observed when synthesis is performed in neutral buffer, NH_4OAc pH 7.0, but are accompanied by shifts in peak wavelength (Appendix Figure

Figure V-2). In NH_4OAc buffer, mut19 and mut25 both have a peak emission at 662 nm, while mutT12 has a peak emission at 636 nm. Of the two mutations that most dramatically disrupted cluster formation, one was a CsubT while the other was a GsubT, meaning that the substituted base identity in itself is not indicative of cluster disruption. These differences in fluorescence observed for the clusters generated by the mutant template strands could be the result of differences in i) cluster composition (number of Ag^0 or Ag^+), ii) quantum yield, iii) chemical stability or iv) differences in interactions due to relative arrangement to the nucleobases, i.e. DNA conformational changes. These results show that bases at particular locations within the sequence play a more critical role in cluster formation than others.

One possible method we could use to predict which bases are critical to cluster formation by analyzing the RS template sequence in terms of data-mined motif subsequences.[20] Comparison of motifs common to the brightest 10% of templates strands sequences from the previous study[20] to the RS sequence reveal two domains within the RS sequence that contain bright motifs (Figure 5-5). The subT mutations that most dramatically affect cluster formation (mut4, mut25) fall within these two motif domains, suggesting that the particular bases contained within these domains are critical for cluster formation and stability. In particular, these bases could be the critical binding sites for Ag^+ that drive cluster formation.

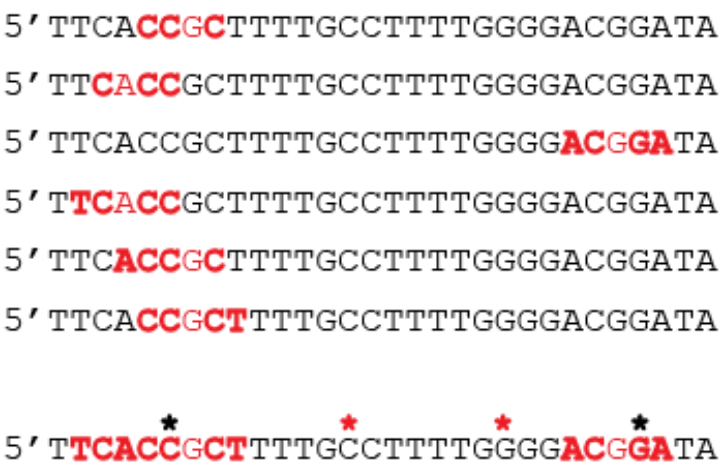

Figure 5-5 RS template sequence with bright motif sequences highlighted in red. A non-bold character indicates a wildcard base contained within the motif. The final template sequence identifies (in red) every base in the RS sequence that is contained within any identified motif. Stars indicate locations of subT mutations of the mutant templates that produced clusters with high fluorescence (red) or poor fluorescence (black).

The presence of two distinct motif domains may also hint at the overall structure of the DNA surrounding the clusters produced by the RS, mut19 and mut12 templates. The two domains are located on opposite ends of the 30 base sequence but could come within close contact if the strand were to fold over onto itself. This stem-loop conformation is readily adopted by self-complementary DNA strands discussed in Chapter 2. Although in this case the two domains are not self complementary, the presence of Ag^{+} could stabilize this stem-loop-like structure through non-Waston-Crick base pairing[49] and provide the necessary DNA conformation for cluster formation. The bases contained within the loop are mostly T's, which provide flexibility, but the C's and G's present can still play minor roles in cluster formation, which we see in the case of our mut12 and mut19 templates sequences. To determine the validity of the hypothesis that permutations in the motif domains disrupts the

folded conformation necessary for cluster formation, analyses of the conformation of the RS and mutant templates were performed using a variety of methods.

As discussed in Chapter 2, microfluidic capillary electrophoresis can be employed to study differences in strand conformations. The difference in electrophoretic mobility between DNA in a globular versus a folded state is easily resolved by similar methods involving capillary electrophoresis.[129] Using the MCE methods outlined in Chapter 2, the electrophoretic mobility of each strand in the presence of Ag^+ was measured alongside an internal standard composed of a poly-dT10, each labeled with a fluorescent dye molecule. Representative electropherograms are shown in the appendix Figure V-3. The electropherograms reveal that the RS strand exhibits two distinct conformations in the presence of silver, but this is not shared by the mut19 or mut12 strands, that also stabilize bright clusters. The mobility shift relative to the internal standard is plotted versus the resulting cluster intensity for each template strand in Figure 5-6. The relative mobilities do not reveal any correlation between the RS templates and the bright mutant templates (mut19, mut12) that would indicate a shared conformation or charge density that is significantly different than the dim mutants (mut25, mut4). However, these results could potentially be due to intrinsic incompatibility of this system with MCE. The DNA and Ag+ are oppositely charged which could significantly deplete Ag+ concentration around the DNA and potentially destabilize any Ag+ mediated conformation. Further work needs to be done to tailor the MCE protocol to this particular system.

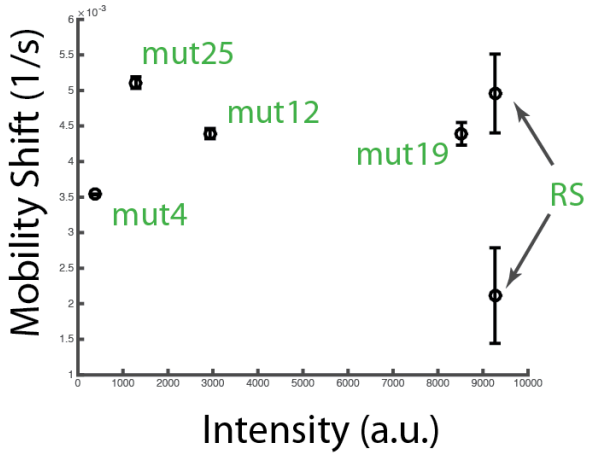

Figure 5-6 Mobility shift relative to internal poly-dT10 standard for each template sequence as a function of the resulting cluster intensity. Two distinct species were resolved for the RS template and were assigned the same intensity value for comparison. Error bars indicate the standard deviation of mobility shift from 3-8 separation experiments.

An additional technique for resolving conformational differences between ssDNA is polyacrylamide gel electrophoresis (PAGE).[130] A gel shift assay performed using off the shelf components and procedures reveals that slight mobility differences exist between the template strands when $AgNO_3$ is added to each sample. Similar to the results from MCE experiments, the RS template had the highest mobility (although the secondary peak resolved using MCE was not resolved by PAGE), which strongly indicates a more compact structure relative to the globular conformation adopted by the poly-dT30 in the adjacent line. The relative mobilities of the mutant strands as measured by PAGE were inconsistent with the mobilities measured by MCE (RS>T12>m4/m25>m19) and did not reveal any relationship between mobility and their capacity to produce bright AgNCs. However, as with MCE, the high electric fields employed using this technique may separate the Ag^+ from the DNA and disrupt its conformation and further work will be needed to better evaluate this approach.

Also, there are many parameters that can be further optimized in order for PAGE to resolve conformational differences between single stranded DNA, including gel density, running buffer type and concentration, temperature, glycerol content in gel and in sample among others.[131]

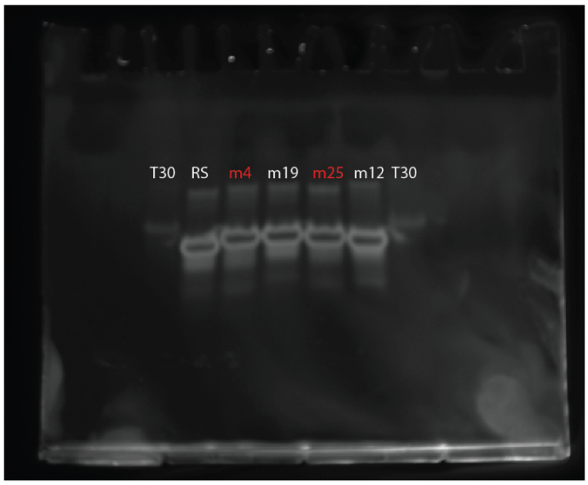

Figure 5-7 PAGE gel shift assay of RS and mutant templates in the presence of Ag^{+}. Red indicates templates that fail to produce bright AgNCs.

Lastly, we evaluate circular dichroism spectroscopy as a potential method to infer conformational differences between the template strands. One of the benefits of using CD spectroscopy is that data can be obtained for samples in their native environment, in this case, buffer and $AgNO_3$. Therefore, unlike MCE and PAGE, we do not expect that this technique imparts any changes to the sample. CD spectra for the difference template strands are shown in Figure 5-8. The RS template exhibits a distinctive negative peak near 280 nm, but this is not shared with any of the other template strands, including those that produce bright AgNCs. However, high noise below 270 nm make it difficult to make even qualitative

comparisons. Longer integration times for the measurements would be needed to improve the data quality. Additionally, the weaker peak intensities compared to a sample containing purified AgNCs generated using the RS template suggests a higher conformational heterogeneity in the unpurified samples. Further work using post-synthesis and purified samples may improve the spectral quality and reveal spectral differences that could relate to conformational differences between the templates.

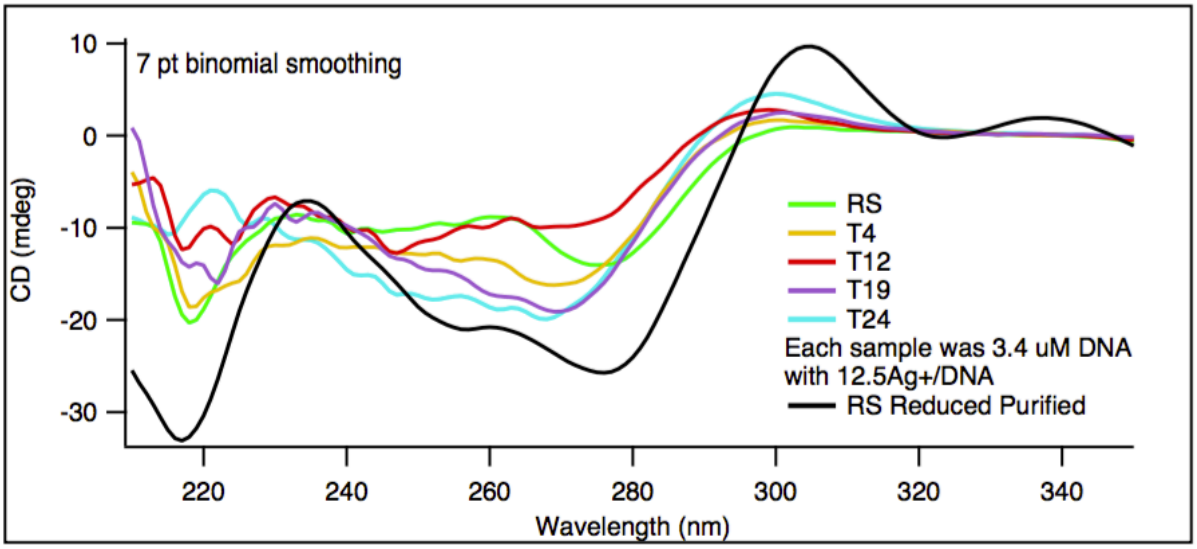

Figure 5-8 CD spectra of RS and mutant templates in the presence of AgNO3 and buffer. The black line shows the spectra for a sample of reduced AgNCs generated by the RS template that have been purified using high performance liquid chromatography.[128] Data courtesy of Steven Swasey.

This preliminary work highlights the use of sequence motifs in analyzing the effect point mutations have on a DNA templates propensity to stabilize bright AgNCs. Although we hypothesize that the motifs play a critical role in stabilizing a preferred DNA conformation, our initial approaches using MCE, PAGE shift assay and CD spectroscopy do not provide supporting evidence. However, we suggest potential optimizations for each approach that

would provide a better means to evaluate the usefulness of each technique for analyzing the Ag^+ mediated conformations of AgNC template DNA strands. Continued work investigating the relationship between sequence and structure of AgNC DNA templates will be of great importance to the future of the AgNC community and is critical for improving their design, synthesis and applications.

Materials and Methods

Synthetic DNA oligos were purchased from Integrated DNA Technologies, Inc. (Coralville, Iowa, USA) with standard desalting, with exception of dye labeled strands containing a 5′ modified Alexafluor488, which were purified by HPLC. DNA strands were rehydrated using 18.2 MΩ cm de-ionized water (DI, MilliQ, Millipore), stored at 100–500 μM at −20 °C and thawed at room temperature as needed. Ammonium acetate and sodium acetate (trihydrate) buffers were prepared from 10× stocks at a concentration of 200 mM (Fisher Scientific, ACS certified grade). Sodium acetate buffer was titrated using glacial acetic acid to pH 4.8. pH was verified using an Oakton pH 11 series meter and dual junction electrode.

AgNC-DNA probe solutions were prepared by combining 32.2 μL of 20 mM buffer with 3 μL of 500 μM DNA probe and 3 μL of 500 μM DNA target (or 3μM of DI for target-free samples) and then placed in a dry block at 90 °C for 5 min and then quenched in an ice bath. To prepare fluorescent clusters, 0.9 μL of 10 mM silver nitrate (Sigma Ultra) was added to the samples and were left for 20 min at room temperature in the dark. Lastly, 4.5 μL of freshly prepared 2 mM sodium borohydride (Aldrich 99.99%, pellets) was added to each sample and vortexed before incubating at room temperature in the dark for 2–5 hours until

fluorescence measurements were performed. The relative concentrations of each reagent were adjusted for samples prepared using different stoichiometry of DNA:$AgNO_3$:$NaBH_4$, e.g. 1:12.5:6.25 and 1:8:8.

Fluorescence spectroscopy was performed between 2-5 hours after synthesis as well as overnight (~12 hours) using a Tecan infinite m200Pro as described in detail in the experimental methods section of Chapter 3. CD spectroscopy was performed by Steven Swasey and the details of the methods are published elsewhere.[49,128] MCE methods are outlined in the methods section of Chapter 2. PAGE was performed using a Bio-Rad mini-PROTEAN Tetra Cell and 15% Precast TBE Gel with1 2 wells. 2 μM DNA template strand was combined with 250 μM $AgNO_3$ and then diluted by 5X with buffer followed by 2X with 25% glycerol. The reservoirs were filled with 0.5X TBE buffer (Bio-Rad) and run at 60 V for 95 minutes in an ice bath. The gel was removed and stained with 1X SYBR Gold (Thermo Fisher) in 0.5X TBE buffer for 40 minutes followed by a rinse with TBE buffer. The gel was imaged using a UV transilluminator box and digital camera.

Microfluidic capillary electrophoresis reveals changes in conformational heterogeneity of template strand after silver nanocluster formation

In Chapter 2, we showed that there were conformational differences between AgNCs formed using poly-dC hairpins containing varied stem sequences. In addition, we found conformational heterogeneity between clusters formed by a particular template sequence. To extend this work, we explore the conformational heterogeneity of the template strand before and after AgNC synthesis. To do this, we performed the electrophoretic separations as outlined in Chapter 2, but this time labeling a template strand (12C-hp10-T10) with fluorescent dye (an Alexafluor488), whose fluorescence we can distinguish from the AgNC by using an appropriate filter set. Labeling the template strand allows us to detect all the DNA present in a sample, instead of just the portion that stabilizes a fluorescent AgNC, both before and after synthesis of the cluster.

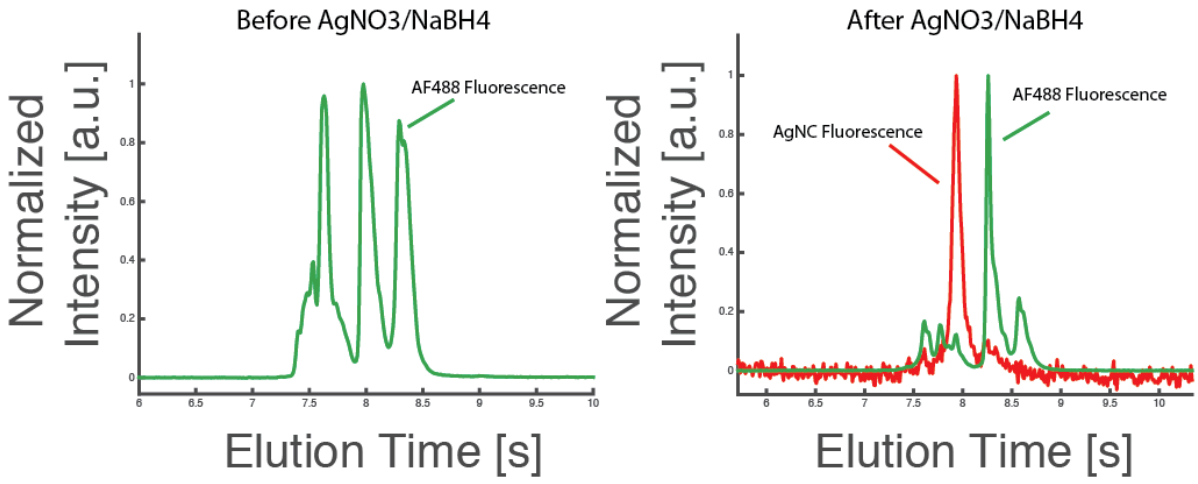

Figure 5-9 Microfluidic electropherograms of dye-labeled template strand 12C-hp10-T10 before (left) and after (right) addition of $AgNO_3$ and chemical reduction to form AgNCs in NaOAc buffer, pH 4.8.

Figure 5-9 shows electropherograms of microfluidic separations performed on the dye labeled template 12C-hp10-T10 introduced in Chapter 2. On the left, where the separation was performed before addition of $AgNO_3$, the electropherogram contains three distinct peaks, indicating the presence of three distinct conformations with relatively equal abundance. This is surprising considering that free-energy models predict a single abundant hairpin species.[66] After adding $AgNO_3$ and $NaBH_4$ to form AgNCs, the separation profile changed dramatically, shown in the right panel of Figure 5-9. Although there are still multiple species present, indicated by the different peaks, the abundance of a lower mobility species is dominant over the others. By switching filter sets to interrogate the DNA-AgNCs, we find a single dominant peak for the cluster generated by the 12C-hp10-T10 template, in agreement with the results of Chapter 2. By performing sequential separations and alternating between the two filter sets, we confirm that the mobility did not change appreciably over time and the

separation profiles measured from the two channels can be directly compared. We find that the AgNC peak has a higher electrophoretic mobility that the dominant DNA template species, consistent with the notion that the DNA-AgNCs are highly compact. Performing the same experiments in a different buffer (NH_4OAc, pH 7.0), also revealed multiple resolved species but different in number and relative abundance (see Appendix), showing that buffer composition has a significant effect on template strand conformation as well as AgNC formation.

Further work and optimization needs to be done to improve repeatability of these separation experiments, as preliminary experiments found variation in the absolute abundance and number of species when measured on different days. This could indicate a sensitivity to handling of the DNA and AgNCs, or in separation conditions such as temperature fluctuations and channel surface conditions. Optimization of the sieving matrix polymer and surface coatings could both improve repeatability as well separation resolution.

Although the precise nature of the different species revealed by MCE remains unknown, these preliminary results highlight the potential this method has for exploring the conformations of template DNA and the role it may have in AgNC formation. Moving forward, similar experiments could be performed to characterize conformational differences between the stem mutant template strands from Chapter 2 prior to synthesis. This information could potentially provide insight into the differences observed between the AgNCs they stabilize and perhaps provide clues into the precise nature of the relationship between template sequence and cluster fluorescence.

Chapter 6

Future Directions

Moving forward, the two main directions of research involving DNA-AgNCs will likely be i) optimizing their photophysical properties through improved template sequence generation, and ii) devising new applications, particularly probes and sensors for biomedical applications. Another, although perhaps smaller, field of research involving DNA-AgNCs may focus more on applications of DNA-AgNCs for self-assembled nanoscale systems for fundamental studies related to nanoscale photonics.[101]

The preliminary work presented here shows progress towards better understanding the sequence dependence on cluster formation and could eventually be used to design better DNA templates. Of particular interest for biological applications is the development of DNA-AgNCs with excitations and emissions in the infrared (IR), which can readily travel through tissue. DNA-AgNCs with emissions in the near IR have already been demonstrated,[75,103,132] and are usually stabilized by template strands greater than 20 bases long or through dimerization of multiple template strands. This is not surprising given that IR emitting clusters would contain more Ag^0, which would require more Ag^+ binding sites in its template sequence.[16,17] However, longer template sequences have an exponentially larger sequence space, which could make finding particular template sequences infeasible by random search using a well-plate level throughput. Biasing sequence selection towards the inclusion of data-mined motifs will provide a significant advantage,[20] but higher throughput methods will still be necessary to screen larger libraries containing longer template sequences.

One promising high-throughput approach has been developed previously for screening libraries for DNA aptamers.[133] This method takes a DNA template library of ssDNA that can range from 20-100 bases, including a common primer sequence, and segregates each strand into separate water in oil emulsions using an emulsifier, though a microfluidic droplet generator could provide similar functionality.[134] Each droplet also contains the reagents necessary to perform PCR amplification as well as a microbead covered in covalently attached forward primer DNA. The template is amplified and the resulting dsDNA coats the microbead. The emulsion is then broken and washed to remove reagents and denature the dsDNA on the bead surface, leaving a library of microbeads, each containing 10^5 copies of a library template ssDNA on its surface. This bead library could then be subjected to a AgNC synthesis, which would form AgNCs on the surface of beads containing viable template strands. These AgNC coated beads have the potential to emit enough fluorescence to sort via a custom fluorescence activated cell sorter (FACS) that could be retrofitted with UV excitation along with a visible-IR sensitive detector. Viable DNA-AgNCs could then be sorted based on spectra or intensity and later processed and sequenced to reveal the template sequence. In addition to serving as a discovery platform for template sequences, the large amount of data potentially obtained using this method could serve as a much larger dataset for machine learning and bioinformatics algorithms to obtain more statistically relevant information regarding sequence motifs or sequence-spectra relationships.

The discovery of IR emitting DNA-AgNCs would provide a tremendous boon for biologically relevant sensors and could be incorporated into the ratiometric probe design presented here. Additionally, future work can look into substituting the loop region of the

hairpin probe design to accommodate aptamer sequences for specific, ratiometric detection of small molecules, proteins and peptides, expanding the relevancy of our adaptable DNA-AgNC probe design. Another future modification to the probes we present here could be developing a means to pre-synthesize the clusters onto probes that would then undergo a shift in emission wavelength after binding target. This would enable reversible and time resolved binding, similar to NanoCluster Beacons,[32,97] for use in RT-qPCR or for real-time cellular imaging, expanding the host of applications where DNA-AgNCs can serve as functional, low-cost, and viable alternatives to organic dyes.

References

1. Zheng, J., Nicovich, P. R. & Dickson, R. M. Highly fluorescent noble-metal quantum dots. *Annu. Rev. Phys. Chem.* **58,** 409–31 (2007).

2. Kreibig, U. & Vollmer, M. *Optical Properties of Metal Clusters*. **25,** (Springer Berlin Heidelberg, 1995).

3. Jain, P. K., Huang, X., El-Sayed, I. H. & El-Sayed, M. A. Noble Metals on the Nanoscale: Optical and Photothermal Properties and Some Applications in Imaging, Sensing, Biology, and Medicine. *Acc. Chem. Res.* **41,** 1578–1586 (2008).

4. Rabin, I. *et al.* Absorption and fluorescence spectra of Ar-matrix-isolated Ag3 clusters. *Chem. Phys. Lett.* **320,** 59–64 (2000).

5. Félix, C. *et al.* Ag8 fluorescence in argon. *Phys. Rev. Lett.* **86,** 2992–5 (2001).

6. Harbich, W., Fedrigo, S., Buttet, J. & Lindsay, D. M. Optical spectroscopy on size selected gold clusters deposited in rare gas matrices. *Zeitschrift f*[illegible]*r Phys. D Atoms, Mol. Clust.* **19,** 157–159 (1991).

7. Peyser, L. A., Vinson, A. E., Bartko, A. P. & Dickson, R. M. Photoactivated fluorescence from individual silver nanoclusters. *Science* **291,** 103–6 (2001).

8. Zheng, J. & Dickson, R. M. Individual Water-Soluble Dendrimer-Encapsulated Silver Nanodot Fluorescence. *J. Am. Chem. Soc.* **124,** 13982–13983 (2002).

9. Zheng, J., Petty, J. T. & Dickson, R. M. High quantum yield blue emission from water-soluble Au8 nanodots. *J. Am. Chem. Soc.* **125,** 7780–1 (2003).

10. Schmid, G. *et al.* Current and future applications of nanoclusters. *Chem. Soc. Rev.* **28,** 179–185 (1999).

11. Shang, L., Dong, S. & Nienhaus, G. U. Ultra-small fluorescent metal nanoclusters: Synthesis and biological applications. *Nano Today* **6,** 401–418 (2011).

12. Petty, J. T., Zheng, J., Hud, N. V & Dickson, R. M. DNA-templated Ag nanocluster formation. *J. Am. Chem. Soc.* **126,** 5207–12 (2004).

13. Richards, C. I. *et al.* Oligonucleotide-stabilized Ag nanocluster fluorophores. *J. Am. Chem. Soc.* **130,** 5038–9 (2008).

14. Alberts, B. *et al. Molecular Biology of the Cell, 5th Edition*. (Garland Science, 2002). at <http://www.ncbi.nlm.nih.gov/books/NBK21054/>

15. Shukla, S. & Sastry, M. Probing differential Ag+-nucleobase interactions with isothermal titration calorimetry (ITC): Towards patterned DNA metallization. *Nanoscale* **1,** 122–7 (2009).

16. Schultz, D. & Gwinn, E. G. Silver atom and strand numbers in fluorescent and dark Ag:DNAs. *Chem. Commun. (Camb).* **48,** 5748–50 (2012).

17. Schultz, D. *et al.* Evidence for Rod-Shaped DNA-Stabilized Silver Nanocluster Emitters. *Adv. Mater.* **25,** 2797–2803 (2013).

18. Gwinn, E. G., Schultz, D. E., Copp, S. M. & Swasey, S. M. DNA-Protected Silver Clusters for Nanophotonics. *Nanomaterials* **5,** 180–207 (2015).

19. Gwinn, E. G., O'Neill, P., Guerrero, A. J., Bouwmeester, D. & Fygenson, D. K. Sequence-Dependent Fluorescence of DNA-Hosted Silver Nanoclusters. *Adv. Mater.* **20,** 279–283 (2008).

20. Copp, S. M., Bogdanov, P., Debord, M., Singh, A. & Gwinn, E. Base motif recognition and design of DNA templates for fluorescent silver clusters by machine learning. *Adv. Mater.* **26,** 5839–45 (2014).

21. Choi, S., Yu, J., Patel, S. A., Tzeng, Y.-L. & Dickson, R. M. Tailoring silver nanodots for intracellular staining. *Photochem. Photobiol. Sci.* **10,** 109–15 (2011).

22. Choi, S., Dickson, R. M. & Yu, J. Developing luminescent silver nanodots for biological applications. *Chem. Soc. Rev.* **41,** 1867–91 (2012).

23. Obliosca, J. M., Liu, C. & Yeh, H.-C. Fluorescent silver nanoclusters as DNA probes.

Nanoscale **5,** 8443–61 (2013).

24. Guo, W., Yuan, J. & Wang, E. Oligonucleotide-stabilized Ag nanoclusters as novel fluorescence probes for the highly selective and sensitive detection of the Hg2+ ion. *Chem. Commun. (Camb).* 3395–7 (2009). doi:10.1039/b821518a

25. Lan, G.-Y., Huang, C.-C. & Chang, H.-T. Silver nanoclusters as fluorescent probes for selective and sensitive detection of copper ions. *Chem. Commun. (Camb).* **46,** 1257–9 (2010).

26. Chen, W.-Y., Lan, G.-Y. & Chang, H.-T. Use of fluorescent DNA-templated gold/silver nanoclusters for the detection of sulfide ions. *Anal. Chem.* **83,** 9450–5 (2011).

27. Li, J., Zhong, X., Zhang, H., Le, X. C. & Zhu, J.-J. Binding-induced fluorescence turn-on assay using aptamer-functionalized silver nanocluster DNA probes. *Anal. Chem.* **84,** 5170–4 (2012).

28. Sharma, J., Yeh, H.-C., Yoo, H., Werner, J. H. & Martinez, J. S. Silver nanocluster aptamers: in situ generation of intrinsically fluorescent recognition ligands for protein detection. *Chem. Commun. (Camb).* **47,** 2294–6 (2011).

29. Li, J. *et al.* Aptamer-functionalized silver nanoclusters-mediated cell type-specific siRNA delivery and tracking. *Chem. Sci.* (2013). doi:10.1039/c3sc51538a

30. Shah, P. *et al.* Design Aspects of Bright Red Emissive Silver Nanoclusters/DNA Probes for MicroRNA Detection. *ACS Nano* **6,** 8803–14 (2012).

31. Shah, P. *et al.* In-solution multiplex miRNA detection using DNA-templated silver nanocluster probes. *Analyst* **139,** 2158–66 (2014).

32. Yeh, H.-C., Sharma, J., Han, J. J., Martinez, J. S. & Werner, J. H. A DNA--silver nanocluster probe that fluoresces upon hybridization. *Nano Lett.* **10,** 3106–10 (2010).

33. Ma, J.-L., Yin, B.-C. & Ye, B.-C. A novel linear molecular beacon based on DNA-scaffolded silver nanocluster for DNA detection via exonuclease III-assisted cyclic amplification. *RSC Adv.* **5,** 65437–65443 (2015).

34. Xiao, Y., Wu, Z., Wong, K.-Y. & Liu, Z. Hairpin DNA probes based on target-induced in situ generation of luminescent silver nanoclusters. *Chem. Commun. (Camb).* **50,** 4849–4852 (2014).

35. Petty, J. T. *et al.* Optical sensing by transforming chromophoric silver clusters in DNA nanoreactors. *Anal. Chem.* **84,** 356–64 (2012).

36. Guo, W., Yuan, J., Dong, Q. & Wang, E. Highly sequence-dependent formation of fluorescent silver nanoclusters in hybridized DNA duplexes for single nucleotide mutation identification. *J. Am. Chem. Soc.* **132,** 932–4 (2010).

37. Yeh, H.-C. *et al.* A Fluorescence Light-Up Ag Nanocluster Probe That Discriminates Single-Nucleotide Variants by Emission Color. *J. Am. Chem. Soc.* **134,** 11550–8 (2012).

38. Jin, R. Quantum sized, thiolate-protected gold nanoclusters. *Nanoscale* **2,** 343–62 (2010).

39. Garzón, I. L. *et al.* Lowest Energy Structures of Gold Nanoclusters. *Phys. Rev. Lett.* **81,** 1600–1603 (1998).

40. Michaelian, K., Rendón, N. & Garzón, I. L. Structure and energetics of Ni, Ag, and Au nanoclusters. *Phys. Rev. B* **60,** 2000–2010 (1999).

41. Sharma, J., Yeh, H.-C., Yoo, H., Werner, J. H. & Martinez, J. S. A complementary palette of fluorescent silver nanoclusters. *Chem. Commun. (Camb).* **46,** 3280–2 (2010).

42. Chen, W., Lan, G. & Chang, H. Use of Fluorescent DNA-Templated Gold/Silver Nanoclusters for the Detection of Sulfide Ions. *Anal. Chem.* **83,** 9450–9455 (2011).

43. Copp, S. M. *et al.* Magic Numbers in DNA-Stabilized Fluorescent Silver Clusters Lead to Magic Colors. *J. Phys. Chem. Lett.* **5,** 959–963 (2014).

44. Sengupta, B. *et al.* DNA Templates for Fluorescent Silver Clusters and I-Motif Folding. *J. Phys. Chem. C* **113,** 19518–19524 (2009).

45. Li, T., Zhang, L., Ai, J., Dong, S. & Wang, E. Ion-Tuned DNA / Ag Fluorescent Nanoclusters as Versatile Logic Gates. *ACS Nano* 6334–6338 (2011). at

<http://pubs.acs.org/doi/abs/10.1021/nn201407h>

46. Fu, Y. *et al.* Silver Nanomaterials Regulated by Structural Competition of G-/C-Rich Oligonucleotides. *J. Phys. Chem. C* **115,** 10370–10379 (2011).

47. Li, W. *et al.* Effects of polymorphic DNA on the fluorescent properties of silver nanoclusters. *Photochem. Photobiol. Sci.* **12,** 1864–72 (2013).

48. Ono, A. *et al.* Specific interactions between silver(I) ions and cytosine-cytosine pairs in DNA duplexes. *Chem. Commun. (Camb).* 4825–7 (2008). doi:10.1039/b808686a

49. Swasey, S. M., Leal, L. E., Lopez-Acevedo, O., Pavlovich, J. & Gwinn, E. G. Silver (I) as DNA glue: Ag(+)-mediated guanine pairing revealed by removing Watson-Crick constraints. *Sci. Rep.* **5,** 10163 (2015).

50. Morishita, K., MacLean, J. L., Liu, B., Jiang, H. & Liu, J. Correlation of photobleaching, oxidation and metal induced fluorescence quenching of DNA-templated silver nanoclusters. *Nanoscale* **5,** 2840–9 (2013).

51. O'Neill, P., Velasquez, L., Dunn, D., Gwinn, E. & Fygenson, D. K. Hairpins with Poly-C Loops Stabilize Four Types of Fluorescent Agn:DNA. *J. Phys. Chem. C* **113,** 4229–4233 (2009).

52. Driehorst, T., O'Neill, P., Goodwin, P. M., Pennathur, S. & Fygenson, D. K. Distinct conformations of DNA-stabilized fluorescent silver nanoclusters revealed by electrophoretic mobility and diffusivity measurements. *Langmuir* **27,** 8923–33 (2011).

53. Bharadwaj, R., Santiago, J. G. & Mohammadi, B. Design and optimization of on-chip capillary electrophoresis. *Electrophoresis* **23,** 2729–44 (2002).

54. Gao, Q. & Yeung, E. S. A Matrix for DNA Separation: Genotyping and Sequencing Using Poly(vinylpyrrolidone) Solution in Uncoated Capillaries. *Anal. Chem.* **70,** 1382–1388 (1998).

55. Milanova, D., Chambers, R. D., Bahga, S. S. & Santiago, J. G. Electrophoretic mobility measurements of fluorescent dyes using on-chip capillary electrophoresis. *Electrophoresis* **32,** 3286–94 (2011).

56. Soto-Verdugo, V., Metiu, H. & Gwinn, E. The properties of small Ag clusters bound to DNA bases. *J. Chem. Phys.* **132,** 195102 (2010).

57. O'Neill, P., Gwinn, E. & Fygenson, D. K. UV Excitation of DNA-Stabilized Ag-Cluster Fluorescence via the DNA Bases. *J. Phys. Chem. C* **115,** 24061–24066 (2011).

58. Jacobson, S. C., Hergenroder, R., Koutny, L. B. & Ramsey, J. M. High-Speed Separations on a Microchip. *Anal. Chem.* **66,** 1114–1118 (1994).

59. Meagher, R. J. *et al.* End-labeled free-solution electrophoresis of DNA. *Electrophoresis* **26,** 331–50 (2005).

60. Williamson, J. R. G-quartet structures in telomeric DNA. *Annu. Rev. Biophys. Biomol. Struct.* **23,** 703–30 (1994).

61. Arakawa, H., Nakashiro, S., Maeda, M. & Tsuji, A. Analysis of single-strand DNA conformation polymorphism by capillary electrophoresis. *J. Chromatogr. A* **722,** 359–368 (1996).

62. Luckey, J. A. & Smith, L. M. A model for the mobility of single-stranded DNA in capillary gel electrophoresis. *Electrophoresis* **14,** 492–501 (1993).

63. Russell, A. J., Del Bonis-O'Donnell, J. T., Wynne, T. M., Napoli, M. T. & Pennathur, S. Separation behavior of short single- and double-stranded DNA in 1 micron and 100 nm glass channels. *Electrophoresis* **35,** 412–8 (2014).

64. Rohozinski, J., Hancock, J. M. & Keniry, M. A. Polycytosine regions contained in DNA hairpin loops interact via a four-stranded, parallel structure similar to the i-motif. *Nucleic Acids Res.* **22,** 4653–4659 (1994).

65. Kypr, J., Kejnovská, I., Renciuk, D. & Vorlícková, M. Circular dichroism and conformational polymorphism of DNA. *Nucleic Acids Res.* **37,** 1713–25 (2009).

66. Zuker, M. Mfold web server for nucleic acid folding and hybridization prediction. *Nucleic Acids Res.* **31,** 3406–3415 (2003).

67. Nikolova, E. N. *et al.* Transient Hoogsteen base pairs in canonical duplex DNA. *Nature* **470,** 498–502 (2011).

68. Manabe, T., Chen, N., Terabe, S., Yohda, M. & Endo, I. Effects of linear polyacrylamide concentrations and applied voltages on the separation of oligonucleotides and DNA sequencing fragments by capillary electrophoresis. *Anal. Chem.* **66,** 4243–52 (1994).

69. Rogacs, A. & Santiago, J. G. Temperature Effects on Electrophoresis. *Anal. Chem.* **85,** 5103–5113 (2013).

70. Khurana, T. K. & Santiago, J. G. Detection of Nonfluorescent Analytes Using Fluorescent Mobility Markers. *Anal. Chem.* **80,** 279–286 (2008).

71. Kolpashchikov, D. M. Binary probes for nucleic acid analysis. *Chem. Rev.* **110,** 4709–23 (2010).

72. Tan, W., Wang, K. & Drake, T. J. Molecular beacons. *Curr. Opin. Chem. Biol.* **8,** 547–53 (2004).

73. Tyagi, S. & Kramer, F. R. Molecular beacons: probes that fluoresce upon hybridization. *Nat. Biotechnol.* **14,** 303–8 (1996).

74. Wu, C. S. *et al.* Engineering molecular beacons for intracellular imaging. *Int. J. Mol. Imaging* **2012,** 501579 (2012).

75. Petty, J. T., Sengupta, B., Story, S. P. & Degtyareva, N. N. DNA sensing by amplifying the number of near-infrared emitting, oligonucleotide-encapsulated silver clusters. *Anal. Chem.* **83,** 5957–64 (2011).

76. Petty, J. T., Story, S. P., Hsiang, J.-C. & Dickson, R. M. DNA-Templated Molecular Silver Fluorophores. *J. Phys. Chem. Lett.* **4,** 1148–1155 (2013).

77. Lee, S. Y., Hairul Bahara, N. H., Choong, Y. S., Lim, T. S. & Tye, G. J. DNA fluorescence shift sensor: A rapid method for the detection of DNA hybridization using silver nanoclusters. *J. Colloid Interface Sci.* **433,** 183–8 (2014).

78. Vet, J. A. M. *et al.* Multiplex detection of four pathogenic retroviruses using molecular beacons. *Proc. Natl. Acad. Sci.* **96,** 6394–6399 (1999).

79. Marras, S. A. E., Russell Kramer, F. & Tyagi, S. Multiplex detection of single-nucleotide variations using molecular beacons. *Genet. Anal. Biomol. Eng.* **14,** 151–156 (1999).

80. Gardner, S. N., Kuczmarski, T. A., Vitalis, E. A. & Slezak, T. R. Limitations of TaqMan PCR for Detecting Divergent Viral Pathogens Illustrated by Hepatitis A, B, C, and E Viruses and Human Immunodeficiency Virus. *J. Clin. Microbiol.* **41,** 2417–2427 (2003).

81. Carneiro, J. S. *et al.* 5' UTR of hepatitis A virus RNA: mutations in the 5'-most pyrimidine-rich tract reduce its ability to direct internal initiation of translation. *J. Gen. Virol.* **76,** 1189–1196 (1995).

82. Moretti, F. *et al.* The hepatitis C virus 5'UTR genomic region remains highly conserved under HAART: a 4- to 8-year longitudinal study from HCV/HIV co-infected patients. *AIDS Res. Hum. Retroviruses* **26,** 527–32 (2010).

83. Jothikumar, N., Cromeans, T. L., Sobsey, M. D. & Robertson, B. H. Development and evaluation of a broadly reactive TaqMan assay for rapid detection of hepatitis A virus. *Appl. Environ. Microbiol.* **71,** 3359–63 (2005).

84. Germer, J. J., Rys, P. N., Thorvilson, J. N. & Persing, D. H. Determination of Hepatitis C Virus Genotype by Direct Sequence Analysis of Products Generated with the Amplicor HCV Test. *J. Clin. Microbiol.* **37,** 2625–2630 (1999).

85. Markham, N. R. & Zuker, M. DINAMelt web server for nucleic acid melting prediction. *Nucleic Acids Res.* **33,** W577–W581 (2005).

86. Markham, N. R. & Zuker, M. UNAFold: software for nucleic acid folding and hybridization. *Methods Mol. Biol.* **453,** 3–31 (2008).

87. Wang, Y. *et al.* Silver ions-mediated conformational switch: facile design of structure-controllable nucleic acid probes. *Anal. Chem.* **82,** 6607–12 (2010).

88. Del Bonis-O'Donnell, J., Fygenson, D. K. & Pennathur, S. Tuning the mobility of fluorescent, DNA-templated, silver nanoclusters for electrophoretic separations in microchannels. in *17th Inernational Conf. Miniaturized Syst. Chem. Life Sci.* W.169i (2013).

89. Krylov, S. N. & Berezovski, M. Non-equilibrium capillary electrophoresis of equilibrium mixtures-appreciation of kinetics in capillary electrophoresis. *Analyst* **128,** 571–575 (2003).

90. Bercovici, M. *et al.* Rapid detection of urinary tract infections using isotachophoresis and molecular beacons. *Anal. Chem.* **83,** 4110–7 (2011).

91. Bahga, S. S., Chambers, R. D. & Santiago, J. G. Coupled isotachophoretic preconcentration and electrophoretic separation using bidirectional isotachophoresis. *Anal. Chem.* **83,** 6154–62 (2011).

92. Zadeh, J. N. *et al.* NUPACK: Analysis and design of nucleic acid systems. *J. Comput. Chem.* **32,** 170–3 (2011).

93. Wang, K. *et al.* Molecular engineering of DNA: molecular beacons. *Angew. Chem. Int. Ed. Engl.* **48,** 856–70 (2009).

94. Kolpashchikov, D. M. An elegant biosensor molecular beacon probe: challenges and recent solutions. *Scientifica (Cairo).* **2012,** 928783 (2012).

95. Ma, D.-L. *et al.* Label-free luminescent oligonucleotide-based probes. *Chem. Soc. Rev.* **42,** 3427–40 (2013).

96. Del Bonis-O'Donnell, J. T., Fygenson, D. K. & Pennathur, S. Fluorescent silver nanocluster DNA probes for multiplexed detection using microfluidic capillary electrophoresis. *Analyst* **140,** 1609–1615 (2015).

97. Obliosca, J. M. *et al.* A complementary palette of NanoCluster Beacons. *ACS Nano* **8,** 10150–60 (2014).

98. Tyagi, S., Marras, S. A. & Kramer, F. R. Wavelength-shifting molecular beacons. *Nat. Biotechnol.* **18,** 1191–6 (2000).

99. Mills, J. B., Vacano, E. & Hagerman, P. J. Flexibility of single-stranded DNA: use of gapped duplex helices to determine the persistence lengths of poly(dT) and poly(dA). *J. Mol. Biol.* **285,** 245–57 (1999).

100. Schultz, D. *et al.* Dual-Color Nanoscale Assemblies of Structurally Stable, Few-Atom

Silver Clusters, As Reported by Fluorescence Resonance Energy Transfer. *ACS Nano* (2013). doi:10.1021/nn4033097

101. Copp, S. M., Schultz, D. E., Swasey, S. & Gwinn, E. G. Atomically precise arrays of fluorescent silver clusters: a modular approach for metal cluster photonics on DNA nanostructures. *ACS Nano* **9,** 2303–10 (2015).

102. Tsourkas, A., Behlke, M. A., Rose, S. D. & Bao, G. Hybridization kinetics and thermodynamics of molecular beacons. *Nucleic Acids Res.* **31,** 1319–30 (2003).

103. Petty, J. T. *et al.* DNA Encapsulation of Ten Silver Atoms Produces a Bright, Modulatable, Near Infrared-Emitting Cluster. *J. Phys. Chem. Lett.* **1,** 2524–2529 (2010).

104. Petty, J. T. *et al.* Optically enhanced, near-IR, silver cluster emission altered by single base changes in the DNA template. *J. Phys. Chem. B* **115,** 7996–8003 (2011).

105. Liu, X. & Tan, W. A Fiber-Optic Evanescent Wave DNA Biosensor Based on Novel Molecular Beacons. *Anal. Chem.* **71,** 5054–5059 (1999).

106. Zuo, X., Xia, F., Xiao, Y. & Plaxco, K. W. Sensitive and selective amplified fluorescence DNA detection based on exonuclease III-aided target recycling. *J. Am. Chem. Soc.* **132,** 1816–8 (2010).

107. Ritchie, C. M. *et al.* Ag Nanocluster Formation Using a Cytosine Oligonucleotide Template. *J. Phys. Chem. C. Nanomater. Interfaces* **111,** 175–181 (2007).

108. Hanke, M. *et al.* A robust methodology to study urine microRNA as tumor marker: microRNA-126 and microRNA-182 are related to urinary bladder cancer. *Urol. Oncol.* **28,** 655–61 (2010).

109. Essandoh, K. & Fan, G.-C. Role of extracellular and intracellular microRNAs in sepsis. *Biochim. Biophys. Acta* **1842,** 2155–2162 (2014).

110. Maes, O. C., Chertkow, H. M., Wang, E. & Schipper, H. M. MicroRNA: Implications for Alzheimer Disease and other Human CNS Disorders. *Curr. Genomics* **10,** 154–68 (2009).

111. Kong, Y. W., Ferland-McCollough, D., Jackson, T. J. & Bushell, M. microRNAs in cancer management. *Lancet. Oncol.* **13,** e249–58 (2012).

112. Reddy, E. P., Reynolds, R. K., Santos, E. & Barbacid, M. A point mutation is responsible for the acquisition of transforming properties by the T24 human bladder carcinoma oncogene. *Nature* **300,** 149–152 (1982).

113. Franzini, R. M. & Kool, E. T. 7-Azidomethoxy-coumarins as profluorophores for templated nucleic acid detection. *Chembiochem* **9,** 2981–8 (2008).

114. Liu, J. DNA-stabilized, fluorescent, metal nanoclusters for biosensor development. *TrAC Trends Anal. Chem.* **58,** 99–111 (2014).

115. Latorre, A. & Somoza, Á. DNA-mediated silver nanoclusters: synthesis, properties and applications. *Chembiochem* **13,** 951–8 (2012).

116. Höglinger, G. U. *et al.* Dopamine depletion impairs precursor cell proliferation in Parkinson disease. *Nat. Neurosci.* **7,** 726–35 (2004).

117. Adams, K. L., Puchades, M. & Ewing, A. G. In Vitro Electrochemistry of Biological Systems. *Annu. Rev. Anal. Chem. (Palo Alto. Calif).* **1,** 329 (2008).

118. Kruss, S. *et al.* Neurotransmitter detection using corona phase molecular recognition on fluorescent single-walled carbon nanotube sensors. *J. Am. Chem. Soc.* **136,** 713–724 (2014).

119. Wang, H.-B., Zhang, H.-D., Chen, Y., Huang, K.-J. & Liu, Y.-M. A label-free and ultrasensitive fluorescent sensor for dopamine detection based on double-stranded DNA templated copper nanoparticles. *Sensors Actuators B Chem.* **220,** 146–153 (2015).

120. Lin, Y. *et al.* Silver nanoprobe for sensitive and selective colorimetric detection of dopamine via robust Ag-catechol interaction. *Chem. Commun. (Camb).* **47,** 1181–3 (2011).

121. Wightman, R. M., May, L. J. & Michael, A. C. Detection of Dopamine Dynamics in the Brain. *Anal. Chem.* **60,** 769A–793A (1988).

122. LIU, J., WANG, Z.-H., LUO, G.-A., LI, Q.-W. & SUN, H.-W. The Interaction of DNA with Dopamine by Spectroscopic and Electrochemical Methods. *Anal. Sci.* **18,** 751–755 (2002).

123. Lévay, G. & Bodell, W. J. Detection of dopamine DNA adducts: potential role in Parkinson's disease. *Carcinogenesis* **14,** 1241–1245 (1993).

124. Zahid, M. *et al.* Formation of dopamine quinone-DNA adducts and their potential role in the etiology of Parkinson's disease. *IUBMB Life* **63,** 1087–93 (2011).

125. Hermann, T. Adaptive Recognition by Nucleic Acid Aptamers. *Science (80-.).* **287,** 820–825 (2000).

126. Del Bonis-O'Donnell, J. T., Pennathur, S. & Fygenson, D. K. Changes in spectra and conformation of hairpin DNA-stabilized silver nanoclusters induced by stem sequence perturbations. *Langmuir* (2015). doi:10.1021/acs.langmuir.5b03934

127. Sharma, J. *et al.* A DNA-templated fluorescent silver nanocluster with enhanced stability. *Nanoscale* **4,** 4107–10 (2012).

128. Swasey, S. M. *et al.* Chiral electronic transitions in fluorescent silver clusters stabilized by DNA. *ACS Nano* **8,** 6883–92 (2014).

129. Stellwagen, E., Abdulla, A., Dong, Q. & Stellwagen, N. C. Electrophoretic mobility is a reporter of hairpin structure in single-stranded DNA oligomers. *Biochemistry* **46,** 10931–41 (2007).

130. Hongyo, T., Buzard, G. S., Calvert, R. J. & Weghorst, C. M. 'Cold SSCP': a simple, rapid and non-radioactive method for optimized single-strand conformation polymorphism analyses. *Nucleic Acids Res.* **21,** 3637–3642 (1993).

131. Spinardi, L., Mazars, R. & Theillet, C. Protocols for an improved detection of point mutations by SSCP. *Nucleic Acids Res.* **19,** 4009 (1991).

132. Hooley, E. N., Paolucci, V., Liao, Z., Carro Temboury, M. R. & Vosch, T. Single-Molecule Characterization of Near-Infrared-Emitting Silver Nanoclusters. *Adv. Opt. Mater.* n/a–n/a (2015). doi:10.1002/adom.201500048

133. Wang, J. *et al.* Particle Display: A Quantitative Screening Method for Generating High-Affinity Aptamers. *Angew. Chemie* **126,** 4896–4901 (2014).

134. Kumaresan, P., Yang, C. J., Cronier, S. a, Blazej, R. G. & Mathies, R. a. High-throughput single copy DNA amplification and cell analysis in engineered nanoliter droplets. *Anal. Chem.* **80,** 3522–9 (2008).

135. Sengupta, B. *et al.* Base-Directed Formation of Fluorescent Silver Clusters. *J. Phys. Chem. C* **112,** 18776–18782 (2008).

136. Ganguly, S. & Kundu, K. K. Protonation/deprotonation energetics of uracil, thymine, and cytosine in water from e.m.f./spectrophotometric measurements. *Can. J. Chem.* **72,** 1120–1126 (1994).

137. Mie, G. Articles on the optical characteristics of turbid tubes, especially colloidal metal solutions. *Ann. Phys* **25,** 377–445 (1908).

138. Doremus, R. H. Optical Properties of Small Silver Particles. *J. Chem. Phys.* **42,** 414 (1965).

139. Tinland, B., Pluen, A., Sturm, J., Weill, G. & Sadron-cnrs-universite, I. C. Persistence Length of Single-Stranded DNA. *Macromolecules* **30,** 5763–5765 (1997).

Appendix I Supplementary Information for Chapter 1

No additional information is provided for Chapter 1.

Appendix II Supplementary Information for Chapter 2

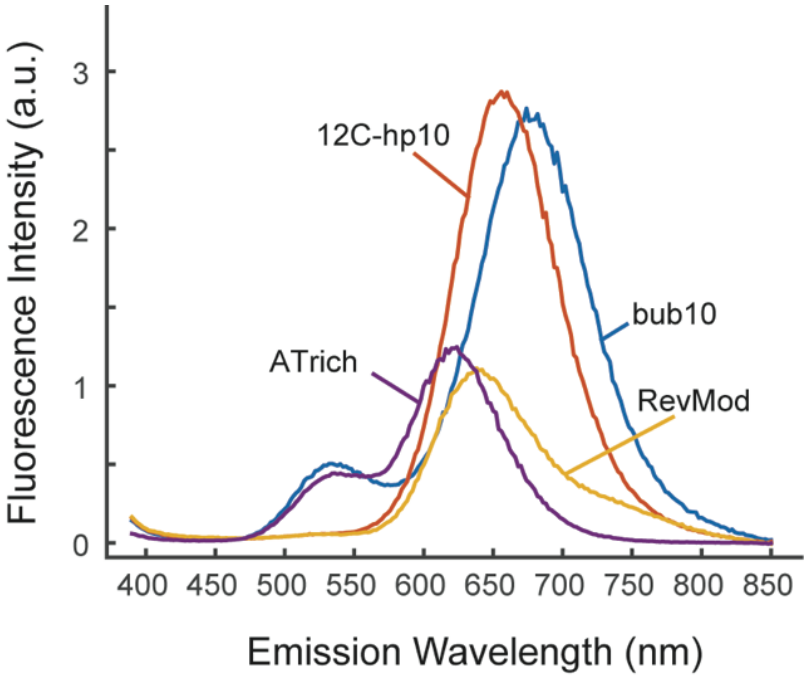

Figure II-1 Fluorescence emission of clusters generated by 12C-hp10, RevMod, ATrich and bub10 under 260 nm illumination.

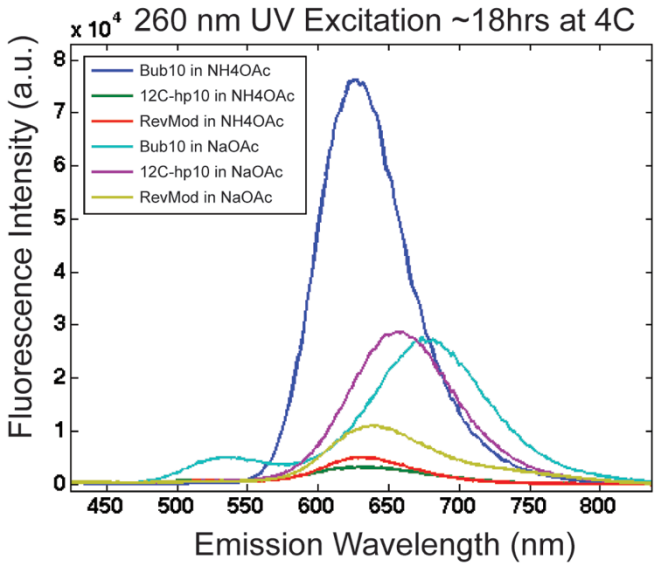

Figure II-2 Fluorescence emission of 12C-hp10, RevMod and Bub10 AgNCs in two different buffer solutions.

Bub10 produced an exceptionally bright and stable cluster when synthesized in 10mM ammonium acetate (NH_4OAc) buffer at pH 7 (Figure S1). Bub10 samples prepared in NH_4OAc were stable for weeks when stored at 4° C, compared to only 48 hours for clusters produced in NaOAc at pH 4.8. The 12C-hp10 and RevMod both exhibited lower fluorescence emission intensity and shifts in peak emission wavelength when synthesized in NH_4OAc compared to NaOAc.

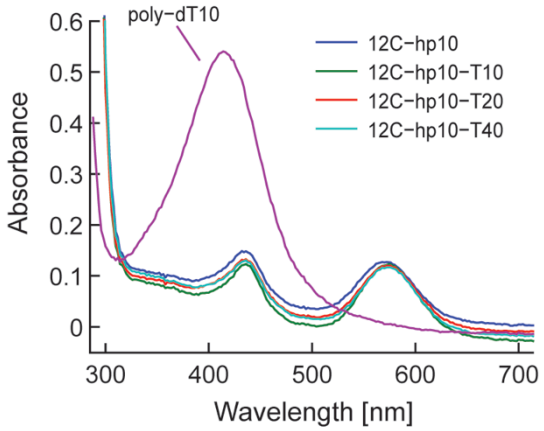

Figure II-3 Absorbance of AgNC samples containing 12C-hp10, T#, and poly-dT10. All species had an absorbance maximum at 574 nm, corresponding to the visible excitation maximum for their 655 nm emission. Another peak in absorbance, at 435 nm, could indicate a weakly emitting or non-radiating AgNC, or the presence of colloidal silver. Synthesis with poly-dT10 alone also produces a large absorbance peak in the vicinity of 400 nm.

In contrast to the other stem variations, the poly-dT variants produced clusters with fluorescence emission identical to the original 12C-hp10 DNA strand (Figure I-1a), indicating that the addition of thymine to the 3' end did not influence the cluster formation or its final fluorescent properties. Inertness of the poly-dT region with respect to DNA AgNC fluorescence is consistent with previous studies (albeit performed in neutral pH) that found thymine-rich strands do not yield fluorescent clusters.[19] Fluorescent clusters can be stabilized by poly-dT_{12} under basic conditions,[135] but under neutral conditions and at the acidic pH used in our study, thymine is expected to be fully protonated and not amenable to silver binding.[19,56,136]

Similarity in absorbance between AgNCs synthesized with 12C-hp10 and the poly-dT variants further confirms that the emitting species are the same (Figure II-1). Absorbance peaks at 574 nm correspond to the excitation maximum fluorescence emission of the AgNC. Although the absorbance peak at 435 nm has no corresponding peak in the excitation spectrum, such a

peak might indicate the presence of a weak- or non-emitting AgNC, or to scattering of colloidal silver particles.[137,138] Accordingly, a synthesis performed using a DNA strand composed only of thymidine (poly-dT10) also produced no detectable fluorescence emission (Chpater 2: Figure 2b), and a strong absorbance centered at 410 nm (Figure II-3).

Modified Ogston Sieving Curve Fit:

Our data was fit to the functional form for modified Ogston sieving proposed by Luckey et *el*.[62] The model has been used to describe the transport of DNA through capillaries containing entangled polymer networks of comparable concentration to that used in the current work. Also, the model takes into account electric field effects which play a role in transport, particularly at the high field strengths used here. Transport is governed by the following equation:

$$\log \mu = \log \mu^0 - \alpha \lambda C N \left[1 + [a_1 E]^{\frac{1}{4}} N^{\frac{3}{2}}\right]^{-1}$$

where μ is the apparent mobility through the gel, μ^0 is the free solution mobility of DNA, C is the concentration of gel, E is the electric field strength, λ is the constant relating the radius of gyration, R_g, of the DNA to the number of nucleotides, N, and lastly, α and a_1 are constants. Luckey *et al.* showed that $a_1$was well estimated as 2.76×10^{-22} m/V and was independent of DNA length and electric field strength for a comparable range of values. We fit this relationship to our data by non-linear least square minimization (MATLAB fit()) using α and μ^0 as fitting paramters. λ was estimated as 0.04 nm using $R_g = \left(\frac{1}{3}\right) pL = \lambda N$, where L is the DNA contour length, and $p=40$ Å, the persistence length for ssDNA.[139]

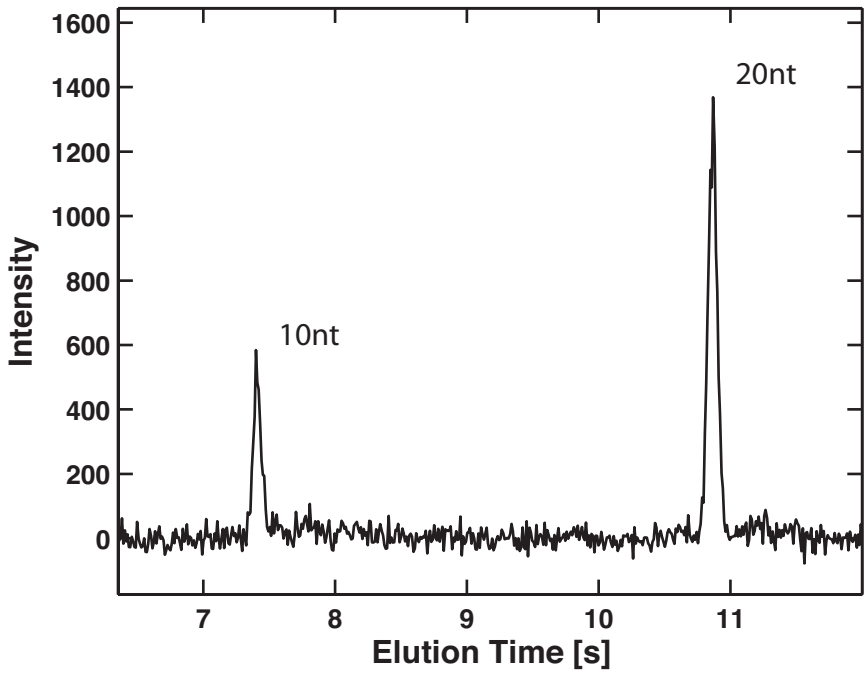

Figure II-4 Electropherogram depicting the separation of 10 base ssDNA and 20 base ssDNA. The mobility of the 20 base ssDNA is reduced to nearly 50% of the 10 base ssDNA. The separations were run at the same conditions as those outlined in the manuscript. The DNA sequences used were AAGAGGAGGG for the 10 base and AAGAGGAGGGAAGAGGAGGG for the 20 base and contained a 6-FAM on the 5' end.

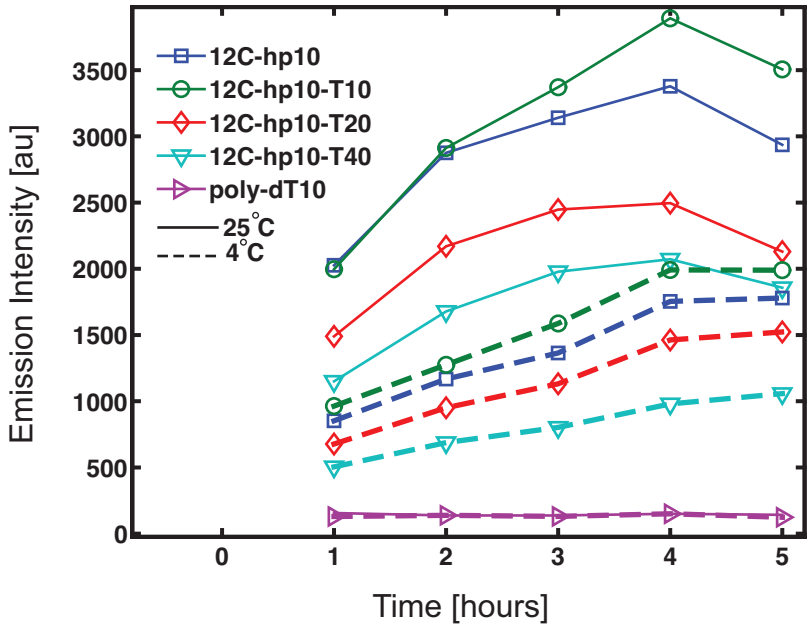

Figure II-5 Peak emission (650 nm) intensity of 12C-hp10 AgNCs over time following reduction and incubated at different temperatures. Samples were excited using 260 nm light.

Fluorescence intensity of silver nanoclusters resulting from the 12C-hp10 strand and its poly-dT variants exhibited a weak dependence on incubation temperature after chemical reduction. Fluorescence intensity peaks 4 hours after reduction, regardless of incubation temperature, but samples kept at ambient room temperature (~25° C) resulted in samples that were roughly twice as bright. Variation in absolute intensity between samples is due to a combination of pipetting uncertainty and increased number of poly-dT absorbing strongly in the UV and not contributing to fluorescence emission of clusters.

Appendix III Supplementary Information for Chapter 3

Table III-1 Sequences for AgNC-DNA probes and targets listed from 5' to 3'. Underlined regions indicate the target binding sequence. Upstream of the underlined sequence is the AgNC stabilizing region. Downstream of the underlined sequence is the blocking sequence and poly-dT mobility modifying region.

HBV-probe	CCCTTAATCCCCTACCACATCATCCATATAACTGAAAGCCAAGGGGATT
HBV-target	TTGGCTTTCAGTTATATGGATGATGTGGTA
HAV-probe	CCCTTAATCCCCGAATTAATATTTACAAGCAAAACAAAGGAAGGGGATT
HAV-target	TTCCTTTGTTTTGCTTGTAAATATTAATTC
HCV-probe	CCCTTAATCCCCGCACCCTGTCAGGCAGTCACTCTCGAGCACGGGGATT
HCV-target	GTGCTCGAGAGTGACTGCCTGATAGGGTGC
HAV-probe-20T	CCCTTAATCCCCGAATTAATATTTACAAGCAAAACAAAGGAAGGGGATTT20
HCV-probe-10T	CCCTTAATCCCCGCACCCTGTCAGGCAGTCACTCTCGAGCACGGGGATTT10

Table III-2 List of probe and target sequences from 5’ to 3’ for HCV that did not produce viable probes. Underlined regions indicate the target binding sequence. Upstream of the underlined sequence is the AgNC stabilizing region. Downstream of the underlined sequence is the blocking sequence and poly-dT mobility modifying region.

HCV-probe2	CCCTTAATCCCCTCACAGGGGAGTGATTCATGGTGGAGTGTCGGGGATT
HCV-target2	GACACTCCACCATGAATCACTCCCCTGTGA
HCV-probe3	CCCTTAATCCCCTTTCTGCCGTGAAACATGGCTAGACGCTTTGGGGATT
HCV-target3	AAAGCGTCTAGCCATGTTTCACGGCAGAAA
HCV-probe4	CCCTTAATCCCCTCATGGTGCACGGTCTACGAGACCTCCCGGGGGGATT
HCV-target4	CCGGGAGGTCTCGTAGACCGTGCACCATGA

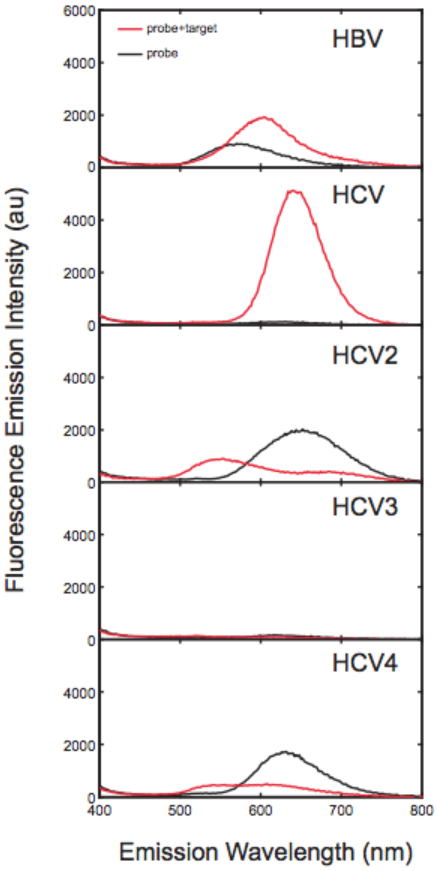

Figure III-1 Emission spectra of the different HCV probe sequences under 260 nm excitation with and without corresponding target DNA. HCV2, HCV3 and HCV4 sequences did not produce viable probes. The HBV and HCV probes used in the manuscript are included in the first 2 panels for reference.

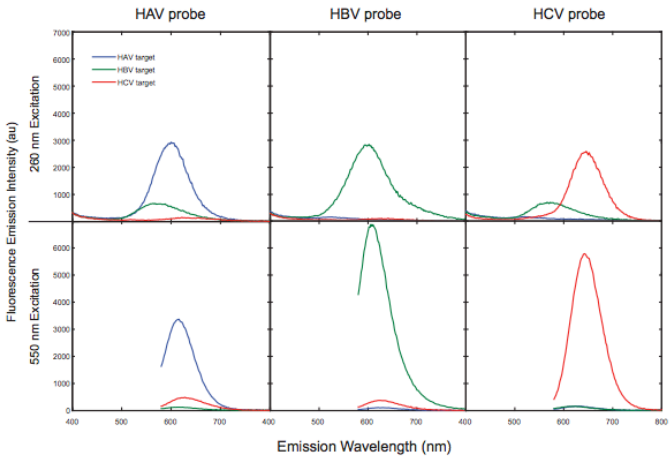

Figure III-2 Emission spectra of each probe in the presence of all three different DNA targets. Top row shows emission at 260 nm excitation. Bottom row shows emission at 550 nm excitation. Each probe shows bright fluorescence in the presence of its complementary target and weak to no fluorescence when in the presence of mismatched target. Excitation at 550 nm further minimizes any fluorescent emission from probes with mismatched targets.

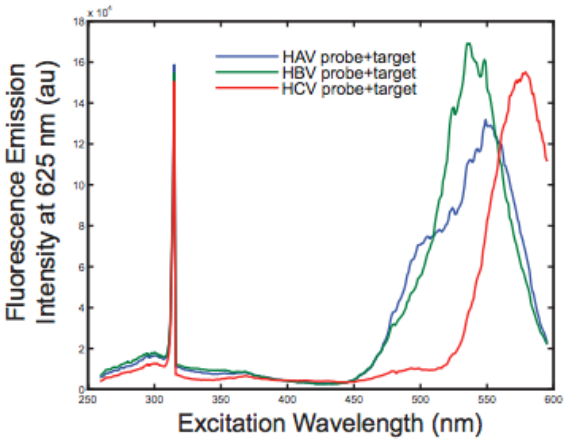

Figure III-3 Fluorescence excitation scan of AgNC-DNA probes for HAV, HBV and HCV in the presence of their respective target DNA. The detector is set to an emission wavelength of 625 nm. The large spike near 312 nm is an artifact related to a harmonic of the detector wavelength, 625 nm. These spectra show that excitation at 550 nm produces approximately equal emission for each probe.

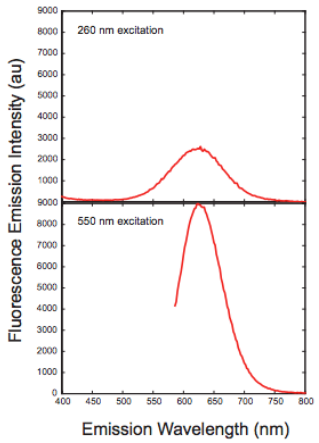

Figure III-4 Fluorescence emission intensity of a mixture of AgNC-DNA probes for HAV, HBV and HCV with a mixture of all three targets. The top plot shows fluorescence emission of the mixture under 260 nm excitation. The bottom plot shows fluorescence emission under 550 nm excitation. The emission spectra appears to be the sum of each probe's emission spectra with a peak at 625 nm, which falls between the peak emissions of the individual probes.

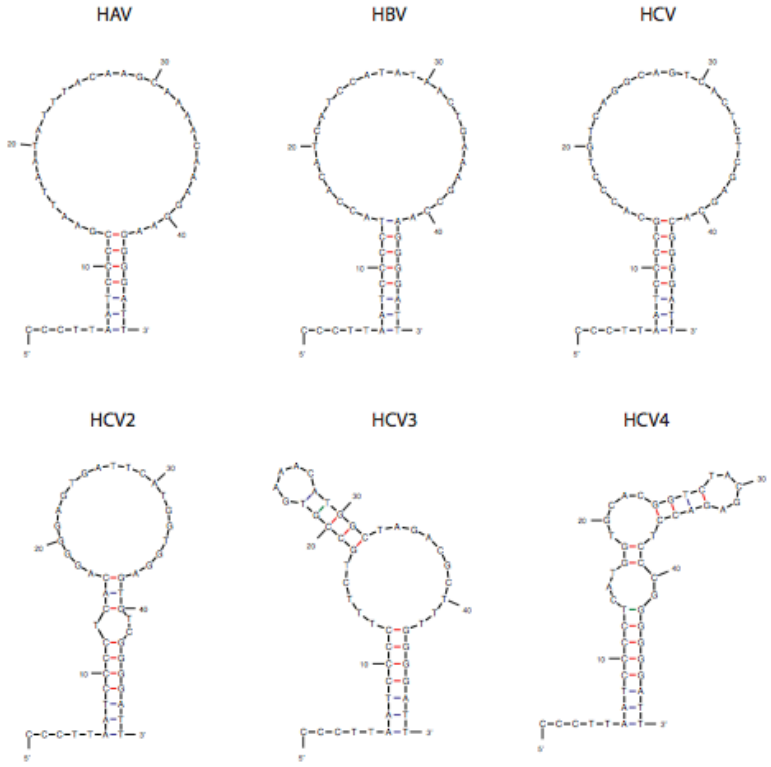

Figure III-5 Predicted lowest free energy secondary structures of the native probes generated using the DINAMelt Web Server tool "Two-state Folding"(http://mfold.rna.albany.edu/?q=DINAMelt/software). The conditions set for the calculations were: [Na+]=20 mM, Temperature=25◦ C and [DNA]=15 µM

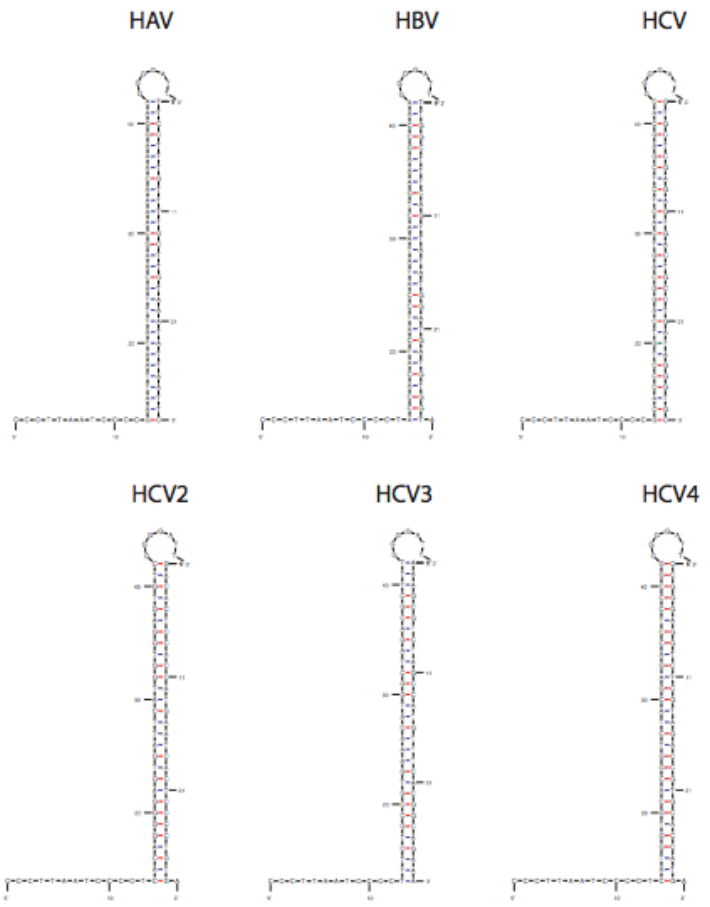

Figure III-6 Predicted lowest free energy secondary structures of the probe-target complexes generated using the DINAMelt Web Server tool "Two State melting (hybridization)"(http://mfold.rna.albany.edu/?q=DINAMelt/software). The conditions set for the calculations were: [Na+]=20 mM, Temperature=25◦ C and [DNA]=15 µM.

HBV	ΔG = -4.2	ΔH = -62.5	ΔS = -195.4	T_m= 46.7° C
HAV	ΔG = -3.4	ΔH = -57.1	ΔS = -180.0	T_m= 44.0° C
HCV	ΔG = -5.6	ΔH = -65.4	ΔS = -200.6	T_m= 52.9° C
HCV2	ΔG = -4.7	ΔH = -79.7	ΔS = -251.7	T_m= 43.5° C
HCV3	ΔG = -3.9	ΔH = -93.0	ΔS = -298.9	T_m= 37.9° C
HCV4	ΔG = -4.0	ΔH = -108.7	ΔS = -351.1	T_m= 36.5° C
HBV+target	ΔG = -30.1	ΔH = -228.0	ΔS = -663.8	T_m= 57.9° C
HAV+target	ΔG = -26.3	ΔH = -231.7	ΔS = -689.0	T_m= 51.5° C
HCV+target	ΔG = -34.4	ΔH = -234.3	ΔS = -670.6	T_m= 63.8° C
HCV2+target	ΔG = -34.3	ΔH = -234.1	ΔS = -670.1	T_m= 63.7° C
HCV3+target	ΔG = -34.9	ΔH = -240.4	ΔS = -689.3	T_m= 63.5° C
HCV4+target	ΔG = -38.5	ΔH = -246.0	ΔS = -696.1	T_m= 68.1° C

Figure III-7 Thermodynamic parameters for probes in their native state and bound to target calculated using the DINAMelt Web Server tools ”Two-state Folding” and ”Two State melting (hybridization)”(http://mfold.rna.albany.edu/?q=DINAMelt/software)[2, 1]. The conditions set for the calculations were: [Na+]=20 mM, Temperature=25 C and [DNA]=15 µM. Free energy and enthalpy are in kcal/mol; entropy is in e.u. (cal/mol/K).

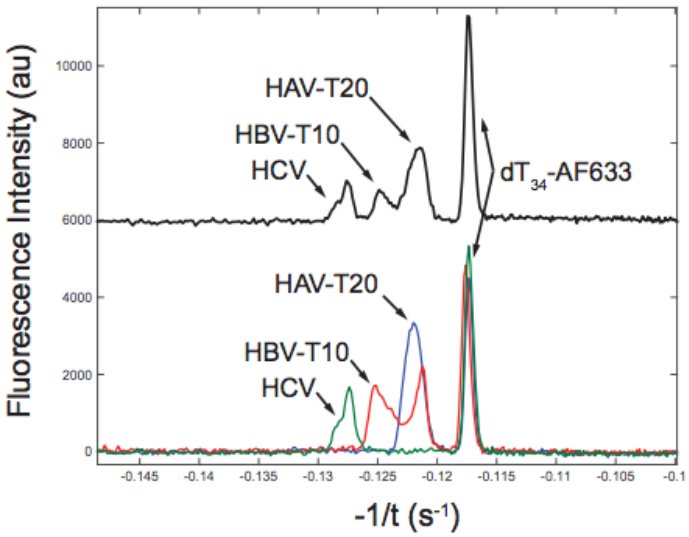

Figure III-8 mCE separation of a sample mixture containing probe+target for HAV-T20, HBV-T10, HCV and a poly-dT34 reference peak with an Alexafluor633 tag. The HBV-T10 probe+target complex produces two elution peaks indicating that there are two stable conformations that yield similar AgNCs. However, improved separation resolution is necessary to separate the secondary HBV-T10 peak and the HAV-T20 and eliminate a false-positive for HAV target in the presence of HBV target.

Appendix IV Supplementary Information for Chapter 4

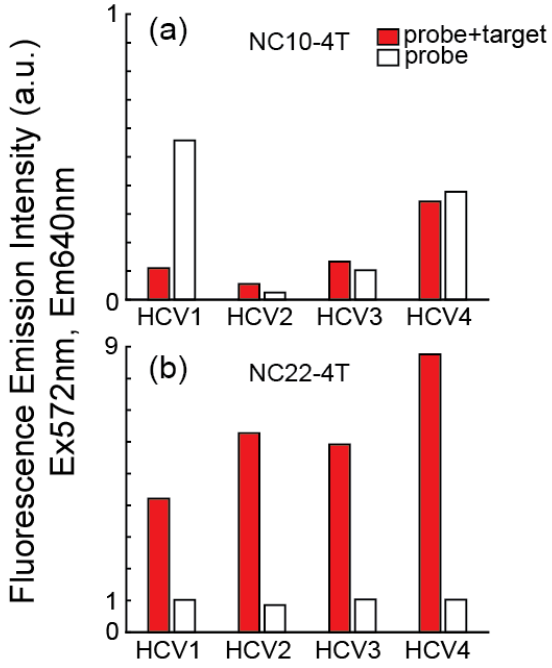

Figure IV-1 Fluorescence emission intensity of probes designed for targets HCV1, HCV2, HCV3, and HCV4. (a) NC10-4T versions of the probe fail to produce in increase in fluorescence signal intensity in the presence of target. Additionally, each produces a different level of fluorescence intensity in its hairpin state. (b) The NC22-4T version of the hairpin probe consistently exhibits fluorescence enhancement of red fluorescence emission in the presence of target.

Table IV-1. Target DNA sequences

HCV1	GACACTCCACCATGAATCACTCCCCTGTGA
HCV2	AAAGCGTCTAGCCATGTTTCACGGCAGAAA
HCV3	GTGCTCGAGAGTGACTGCCTGATAGGGTGC
HCV4	CCGGGAGGTCTCGTAGACCGTGCACCATGA
HAV	TTCCTTTGTTTTGCTTGTAAATATTAATTC
HBV	TTGGCTTTCAGTTATATGGATGATGTGGTA
miR182	TTTGGCAATGGTAGAACTCACACT

HrasMUT	TTGCCCACACCGACGGCG
HrasWT	TTGCCCACACCGCCGGCG

Table IV-2. NC22 Probes

HCV1	TTCCCACCCACCCCGGCCCGTTTTTTTCACAGGGGAGTGATTCATGGTGGAAACGGGCCGG
HCV2	TTCCCACCCACCCCGGCCCGTTTTTTTTTCTGCCGTGAAACATGGCTAGACAACGGGCCGG
HCV3	TTCCCACCCACCCCGGCCCGTTTTTTGCACCCTGTCAGGCAGTCACTCTCGAACGGGCCGG
HCV4	TTCCCACCCACCCCGGCCCGTTTTTTTCATGGTGCACGGTCTACGAGACCTAACGGGCCGG
mr182	TTCCCACCCACCCCGGCCCGTTTTTTAGTGTGAGTTCTACCATTGCCAAAAACGGGCCGG
HrasMUT	TTCCCACCCACCCCGGCCCGTTTTTTCGCCGTCGGTGTGGGCAAAACGGGCCGG
HAV	TTCCCACCCACCCCGGCCCGTTTTTTGAATTAATATTTACAAGCAAAACAAAACGGGCCGG
HBV	TTCCCACCCACCCCGGCCCGTTTTTTTACCACATCATCCATATAACTGAAAGCCAAAACGGGCCGG

Table IV-3. NC12 Probes

HCV1	CCCTTAATCCCCTCACAGGGGAGTGATTCATGGTGGAGTGTCGGGGATT
HCV2	CCCTTAATCCCCTTTCTGCCGTGAAACATGGCTAGACGCTTTGGGGATT
HCV4	CCCTTAATCCCCTCATGGTGCACGGTCTACGAGACCTCCCGGGGGGATT
HAV	CCCTTAATCCCCGAATTAATATTTACAAGCAAAACAAAGGAAGGGGATT
HBV	CCCTTAATCCCCTACCACATCATCCATATAACTGAAAGCCAAGGGGATT

Table IV-4. NC12-4T Probes

HCV1	CCCTTAATCCCCTTTTTCACAGGGGAGTGATTCATGGTGGAGTGTCGGGGATT
HCV2	CCCTTAATCCCCTTTTTTTCTGCCGTGAAACATGGCTAGACGCTTTGGGGATT
HCV3	CCCTTAATCCCCTTTTGCACCCTATCAGGCAGTCACTCTCGAGCACGGGGATT
HCV4	CCCTTAATCCCCTTTTTCATGGTGCACGGTCTACGAGACCTCCCGGGGGGATT
HAV	CCCTTAATCCCCTTTTGAATTAATATTTACAAGCAAAACAAAGGAAGGGGATT
HBV	CCCTTAATCCCCTTTTTACCACATCATCCATATAACTGAAAGCCAAGGGGATT

Appendix V Supplementary Information for Chapter 5

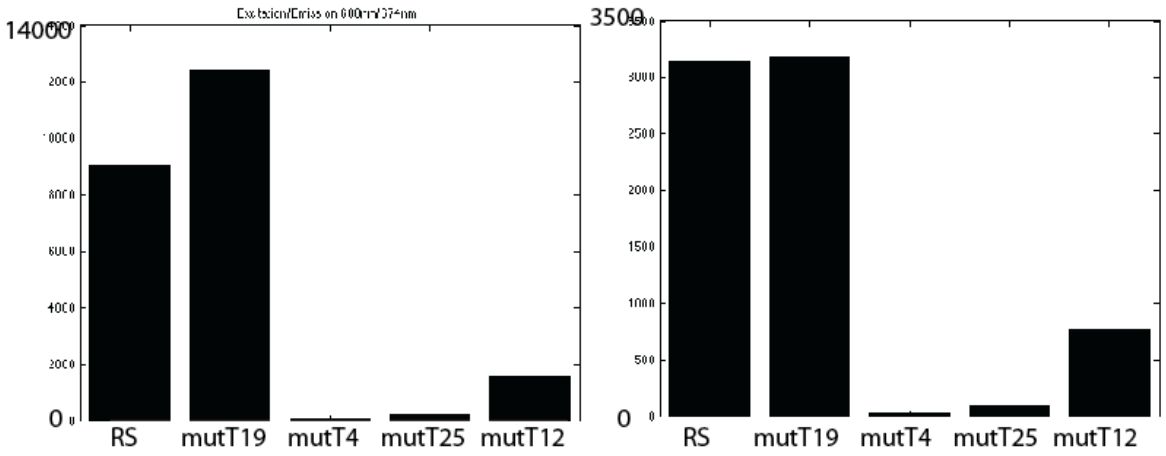

Figure V-1 Peak emission intensity (674 nm) of AgNCs generated using RS and RS mutant strands (Excitation wavelength: 600 nm). Left: 1:12.5:6.25, Right 1:8:8 (DNA:AgNO3:NaBH4). Synthesis performed in NaOAc buffer, pH 4.8.

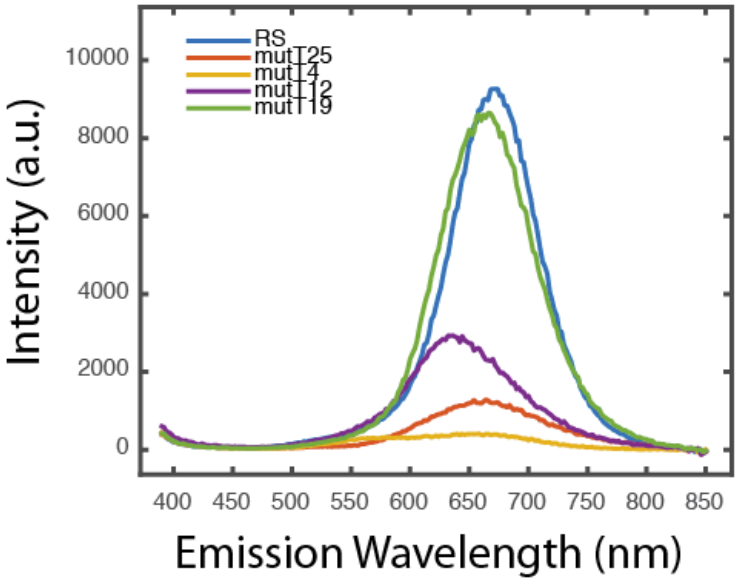

Figure V-2 Fluorescence emission of clusters stabilized by template strands RS and mutants synthesized in NH_4OAc buffer at pH 4.8. Sample excitation: 260 nm.

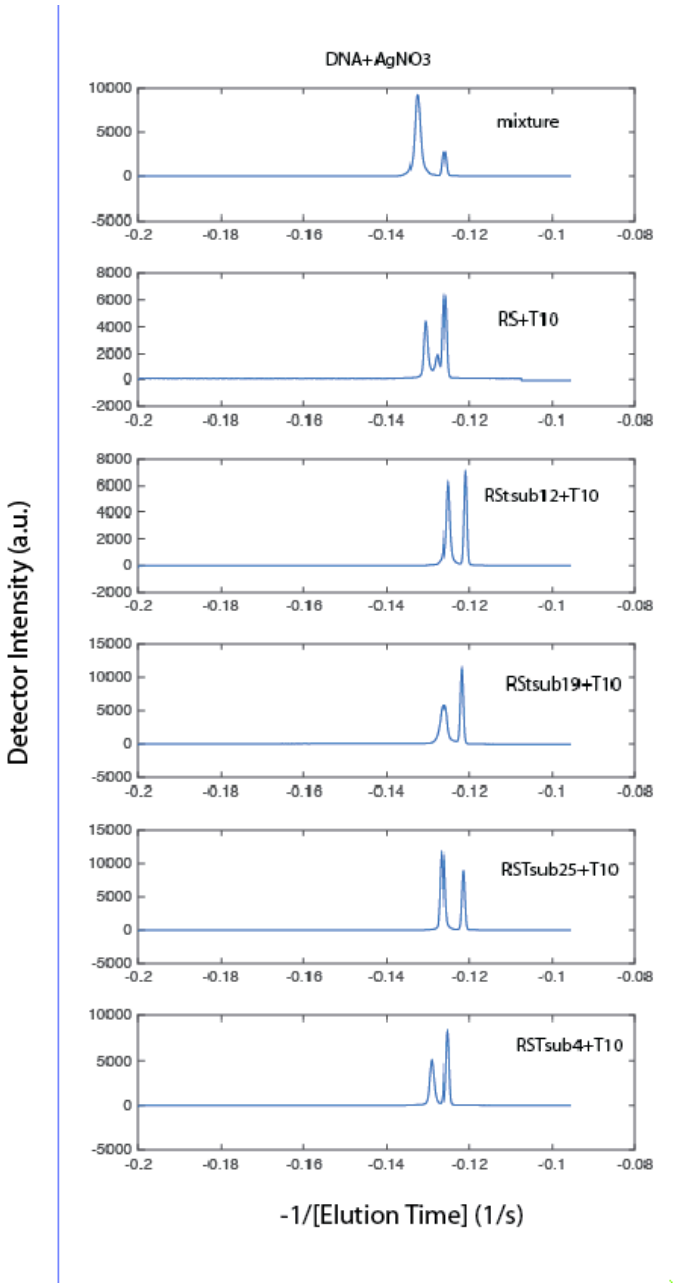

Figure V-3 Representative electropherograms of RS and mutant template DNA strands and a poly-dT10 internal standard in the presence of Ag+.

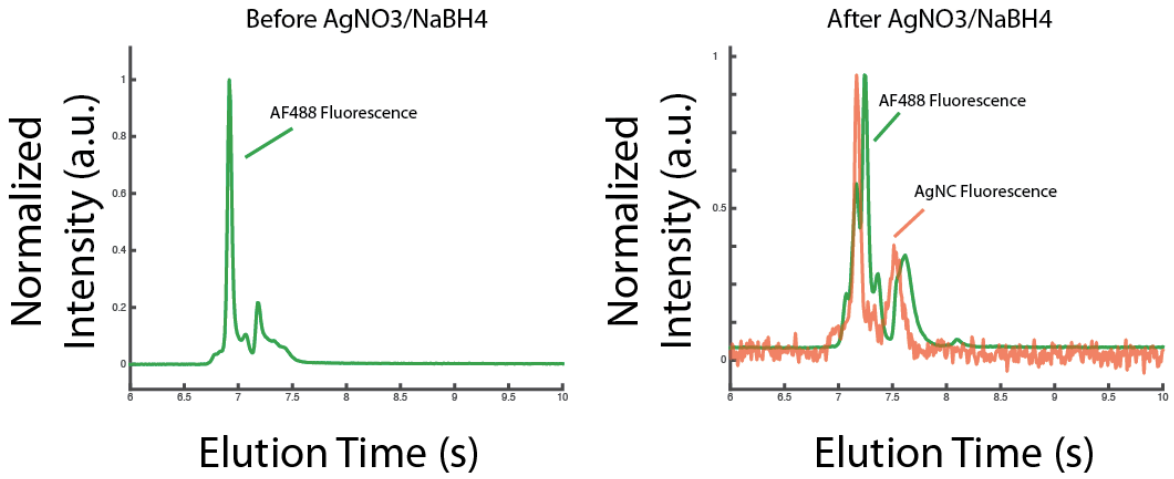

Figure V-4 Microfluidic electropherograms of dye-labeled template strand 12C-hp10-T10 before (left) and after (right) addition of $AgNO_3$ and chemical reduction to form AgNCs in NH_4OAc buffer, pH 7.0.